Deciphering the Quaternary sedimentary and neotectonic history of a loess-paleosol sequence from Langenlois (Lower Austria) by optically stimulated luminescence (OSL) dating

Master's thesis

Submitted to the
Leopold-Franzens-Universität Innsbruck
Faculty of Geo- and Atmospheric Sciences

For the degree of
Master of Science

Fabian Auer

Supervisor:
Ass. Prof. Dr. Michael Meyer
Department of Geology
Innsbruck, 18.06.2021

universität innsbruck

Eidesstattliche Erklärung

Ich erkläre hiermit an Eides statt durch meine eigenhändige Unterschrift, dass ich die vorliegende Arbeit selbständig verfasst und keine anderen als die angegebenen Quellen und Hilfsmittel verwendet habe. Alle Stellen, die wörtlich oder inhaltlich den angegebenen Quellen entnommen wurden, sind als solche kenntlich gemacht.

Die vorliegende Arbeit wurde bisher in gleicher oder ähnlicher Form noch nicht als Magister-/Master-/Diplomarbeit/Dissertation eingereicht.

18.06.2021	
Datum	Unterschrift

Acknowledgments

OSL sample preparation and dating was conducted by the study author at the University of Innsbruck under supervision of Ass. Prof. Michael Meyer. Mineralogical, sedimentological, and geochemical analyses were performed in the laboratories at the Geological Survey of Austria in Vienna under the coordination of Reinhard Roetzel.

I am grateful to Michael Meyer for supervising this thesis, his assistance, and infinite patience. I appreciate the collaboration and discussion with Reinhard Roetzel and Kurt Decker. Sincere thanks are given to Kornelia Pellegrini for her assistance in the OSL laboratory. Fam. Nidetzky and Steininger are acknowledged for the access to the study site and the logistic support. Finally, I want to express my deepest gratitude to my parents for supporting me throughout the entire duration of my study.

Abstract

Loess-paleosol sequences are abundant in the Krems-Langenlois region due to its lee-sided position behind a crystalline spur on the south-eastern margin of the Bohemian massif. These terrestrial sediment sequences form a high-resolution archive of Quaternary climate and environmental change. In the “wine-world Loisium” (a vine tastery with a vine cellar and Hotel complex) in the town of Langenlois in Lower Austria, three sedimentary outcrops showing fluvial and aeolian sediments with intercalated fragments of paleosols are investigated and an Optically Stimulated Luminescence (OSL) chronology is established based on the blue OSL quartz signal. The outcrops reveal (i) fluvial gravels at the base that could not be OSL dated but were lithostratigraphically correlated with the Early Pleistocene Hochstrassberg Danube terrace, followed by (ii) fluvial sands that were OSL dated to the Marine Isotope Stage (MIS) 6a, which are overlain by (iii) a loess-paleosol sequence. Eight OSL ages from this loess-paleosol sequence constrain three main periods of loess deposition: from ~48-50 ka (early MIS 3), from ~30-36 ka (late MIS 3) and from ~21 ka, i.e. the Last local Glacial Maximum. Slabs of a paleosol embedded in the loess due to post-depositional disturbance, document at least one period of warmer and more humid climatic conditions during the early MIS 3. The sequences further reveal a hiatus suggestive of regional incision between ~55 and 106 ka in the Krems-Langenlois area. Landscape instability and erosion is also indicated in similar aged sedimentary sequences of other study sites in the Krems-Langenlois area. A striking feature in outcrops of the “wine-world Loisium” is the occurrence of numerous high-angle normal faults. These were recorded in the basal (Early Pleistocene) gravels that were litho-stratigraphically correlated with the Hochstrassberg Danube terrace, as well as in the MIS 6 and MIS 3 sedimentary units, suggestive of repeated tectonic activity during the Quaternary. The youngest set of normal faults cuts the late MIS 3 units and is overlain by the tectonically undisturbed LGM unit and thus constrains the youngest evidence for seismic activity in the outcrops of the “wine-world Loisium” to >21 ka. No detailed analyses of the fault kinematics were conducted in the course of this study, but the overall orientation of these faults (dip direction northwest to southwest) strongly suggests that they are part of the NE-SW striking sinistral Diendorf strike-slip fault system. It is suggested that the splitting of the Diendorf fault ~9 km north-east of the study site creates a transtensional strike-slip regime that in turn causes a pull-apart basin in the Langenlois area to form. Such a localized pull-apart basin would reconcile the faulting pattern observed in the “wine-world Loisium” with the supra-regional tectonic setting.

Table of Contents

1. Introduction

In the circum-alpine area Quaternary climate changes and landscape evolution are often chronicled in sedimentary sequences such as fluvial sediment successions (e.g. Miall, 1977; Cordier et al., 2017) or loess-paleosol sequences (e.g. Fink & Kukla, 1977; Pye, 1995). In order to understand the underlying environmental system and its dependency on the magnitude and frequency of quaternary climate fluctuations, detailed sedimentological investigations and a precise and accurate chronology are essential (e.g. Thiel et al., 2011; Rixhon et al., 2017). Loess sequences in particular are a high-resolution archive for environmental and climatic changes due to the relatively high accumulation rate of this type of aeolian deposit (Frechen et al., 2003). In mid-latitude Europe, loess is related to glacial periods, and formed in periglacial, sparsely vegetated areas where fine-grained material was produced by frost weathering, glacial abrasion, fluvial erosion and subsequent deflation, mainly from barren proglacial outwash plains and river valleys (Pecsi & Richter, 1996; Van Husen and Reitner, 2011; Van Husen 2000;). Deflation was driven by the strong and prevailing westerlies during glacial periods, and deposition of the resulting mineral dust preferentially occurred in the form of thick loess sequences particularly in topographic lee sided positions (Meyer and Kottmeier, 1989; Van Husen and Reitner, 2011). Loess weathers relatively fast, thus is prone to pedogenesis, particularly during warm, humid interglacials and interstadials, when chemical weathering is intensified (Pecsi & Richter, 1996; Van Husen and Reitner, 2011). These environmental processes can result in loess-paleosol sequences reflecting the alternation of dry and arid tundra or cold steppe environment with prevailing loess accumulation, interrupted by more humid and milder intervals with prevailing pedogenesis (Pye, 1995; Fink and Kukla, 1977; Thiel et al., 2011; Terhorst et al., 2014; Nigst et al., 2014; Kohfeld and Harrison, 2003; Stevens et al., 2018).

Loess-paleosol sequences in Austria have been studied for decades (e.g. Götzinger, 1936; Brandtner, 1954; Fink, 1954, 1976; Terhorst et al., 2011; Nigst et al., 2014; Sprafke, 2016). The area of Krems-Langenlois in Lower Austria (Fig. 1A and 1B) is of particular interest for geoscientists and archaeologists alike, because here thick loess-paleosol sequences have accumulated in a topographic wind sheltered position, and these deposits are frequently associated with archaeological finds, such as an Upper Paleolithic double infant burial at Wachtberg (Einwögerer et al., 2006) or a Venus statuette in Stratzing (Neugebauer-Maresch, 1989). Furthermore, several studies were conducted on loess-paleosol sequences in the wider Krems area in order to reconstruct the paleoenvironmental evolution of that region during the Pleistocene (Smolíková, 2003; Fladerer et al., 2005; Smolíková and Havliček, 2007; Haslinger et al., 2009; Thiel et al. 2011a, b, c). However, until relatively recently, correlation of distant profiles and establishing a reliable absolute loess stratigraphy was difficult due to a lack of suitable dating methods.

With the invention of optically stimulated luminescence (OSL) dating (Huntley et al., 1985) and subsequent methodological and instrumental improvements (e.g. Murray and Wintle, 2000; BØtter-Jensen et al., 1999, 2003; Buylaert et al., 2012), OSL dating became a powerful geochronological tool in loess research. OSL dating determines the time since the last exposure of sedimentary mineral grains to daylight (Aitken, 1998; Huntley et al., 1985). When sediment grains get buried, natural ionizing irradiation causes electrons getting trapped in meta-stable traps that are associated with defects within the crystal lattices of these grains. Upon stimulation with light, these meta-stable traps are emptied, and the electrons can recombine with holes at luminescence centres. The release of energy during this recombination process occurs in form of photons, and the number of photons is

proportional to the rate of natural ionizing irradiation and thus to burial time. For an accurate OSL age sufficient daylight exposure before sediment burial is crucial in order to empty (or bleach) all electron traps and reset the OSL clock properly. Sufficient daylight exposure is provided during aeolian transport, making loess a suitable sediment for this dating technique (Roberts, 2008). OSL dating has the advantage of stimulating more rapidly discharging traps compared to the initially used TL method and reduces the risk of partial bleaching (Roberts, 2008). However, OSL dating of quartz has the limitation of a datable age range of up to ~150 ka. IRSL signals of feldspar have a much higher saturation dose and can be utilized to expand the limit to >300 ka (Thiel et al., 2011b).

One of the first luminescence dating studies of loess in Austria was undertaken by Wallner et al. (1990), who used the thermoluminescence method (TL), i.e. a precursor technique to OSL dating (Aitken, 1998; Huntley et al., 1985). In the region of Krems, TL dating was applied to loess by Noll et al. (1994) and Zöller et al. (1994) and more recently, OSL dating was applied for dating the loess-paleosol sequence that also encompassed an Upper Paleolithic archaeological site that contained a Gravettian double infant burial on the Wachtberg in Krems (Lomax et al., 2014). Thiel et al. (2011a, b, c) investigated loess profiles using the infrared spectrum (IRSL) for stimulating feldspar, including one site in Langenlois and one site in Stratzing, both villages situated in the wider Krems area (Fig. 1B).

This study aims to combine both, the potential of fluvial and loess-paleosol sequences as paleoenvironmental archives and utilizes OSL dating to provide a geochronological framework and to enable correlation of sedimentary units on a regional scale. A 12-meter thick sedimentary sequence composed of fluvial sediments, loess and intercalated paleosols and situated in and adjacent to the so-called wine-world Loisium (i.e. a renowned complex of vine cellars with an integrated wine-shop and associated hotel) in Langenlois (Fig. 1C) was investigated. Three outcrops were analysed in total: two minor outcrops are located in the Loisium cellar complex, while the third (major) outcrop was exposed only temporarily during construction work adjacent to the Loisium. Samples for sedimentological, mineralogical and geochemical analyses and for OSL dating were collected in order to correlate the loess-paleosol layers of the Loisium with loess-paleosol sequences from the wider Langenlois and Krems region.

The initial purpose of this study of contributing to the paleoenvironmental research in the Krems-Langenlois area was expanded by the aspect of neotectonic activity, because numerous faults were encountered within the investigated sediment successions during fieldwork. Normal faults within quaternary sediments in the area of Langenlois were already described by Piffl (1959), who documented continuous downward displacement of fluvial gravels, but this author did not undertake a closer examination of these structures and the underlying tectonic processes and its kinematics. The current thesis places the faults encountered at the Loisium wine-world, as well as those of Piffl (1959) in relation to each other and argues that both set of faults are kinematically linked to the Diendorf fault (DDF), a sinistral strike-slip fault trending NE-SW in the area of Langenlois. Recent seismic activity along the DDF was reported by Figdor & Scheidegger (1977), who also related damages on buildings and subsidence in Platt, a town ~30 km NE of Langenlois, to ongoing tectonic activity of the DDF. Roetzel (1996) also suggested quaternary activity of the DDF based on geological mapping of the Langenlois region (i.e. tertiary sediments and quaternary loess units were faulted along the DDF on the mapping scale). Neotectonic investigations and OSL dating have already been successfully combined in the central Vienna Basin in eastern Lower Austria in order to determine the age and slip rates of Quaternary faults in the Vienna basin (Weissl et al., 2017; Hintersberger et al., 2017). For the DDF no

such attempt has been undertaken so far. This study describes newly discovered neotectonic structures in Langenlois and provides OSL-ages for the faulted sediment layers and thus – for the first time – numerically constrains the timing of neotectonic activity along the DDF.

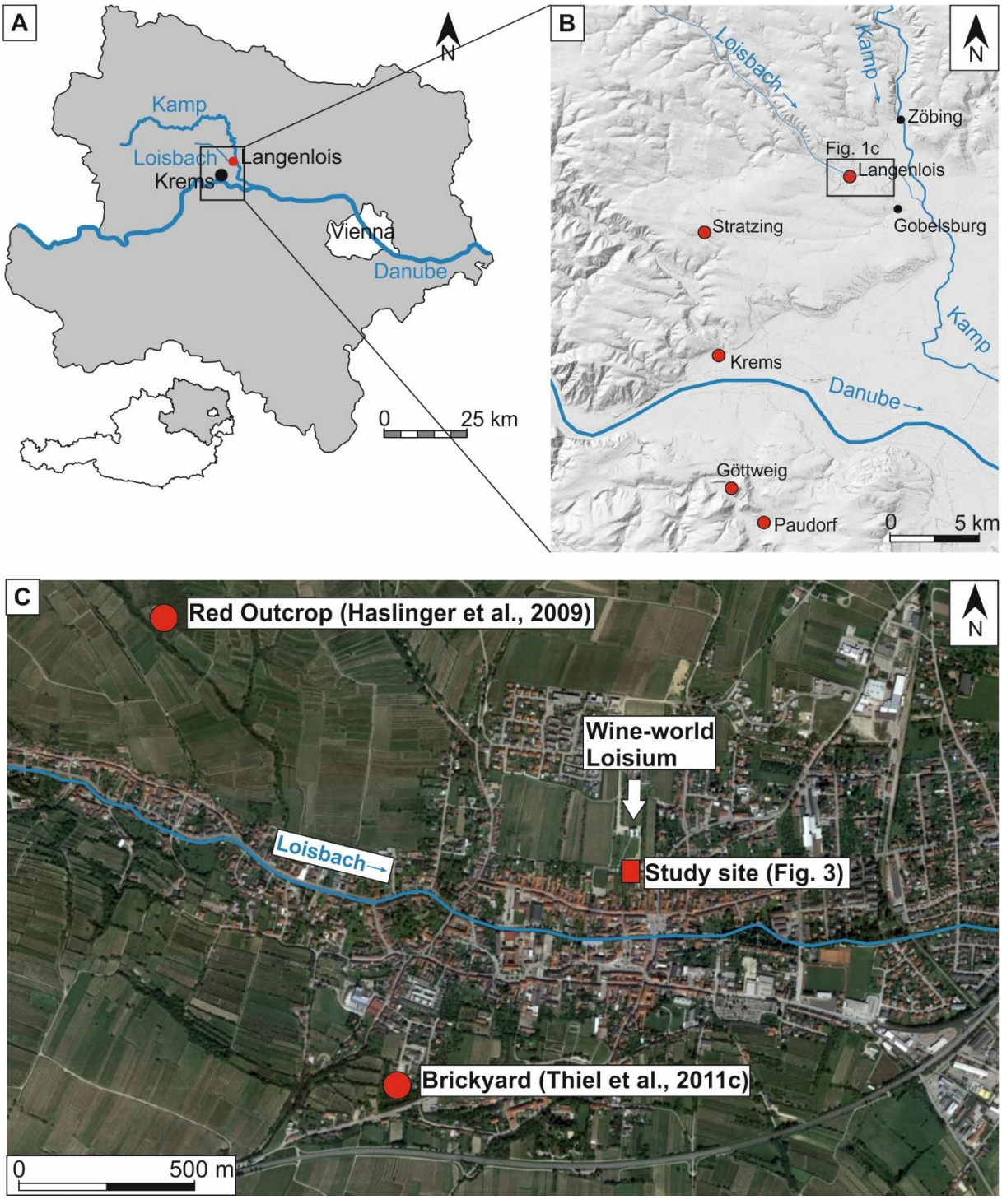

Fig. 1: Overview of the study site. **A:** Lower Austria with Langenlois (red dot). **B:** Digital terrain model of the area of Krems with towns referred to in the text and previously OSL-dated loess sites (red dots): Langenlois: this study; Thiel et al., 2011c; Stratzing: Thiel et al., 2011a; Paudorf: Thiel et al., 2011b; Göttweig: Zöller et al., 1994; Thiel et al, 2011b; Krems: Lomax et al., 2014. **C:** Langenlois with the study site (for exact position of investigated sedimentary logs see Fig. 3B) with the wine-world Loisium to its north and the position of the brickyard with the sediment succession dated by Thiel et al. (2011c). Details see text.

2. Regional geologic and tectonic setting

The study area is situated in Lower Austria ~9 km north-east of Krems, in the town of Langenlois (Fig. 1). Langenlois lies at the outlet of the Kamp valley, i.e. where the Kamp river joins the alluvial plain of the Danube. To the north and west Langenlois is encompassed by crystalline rocks of the Bohemian massif (Fig. 2). The Bohemian massif formed during the Variscan orogenesis and in the area of Langenlois is composed of amphibolite and paragneiss with minor occurrences of quartzite, serpentinite and marble (Fuchs et al., 1984).

Three km north-east of the study area near the village Zöbing am Kamp, the DDF is cutting through the Bohemian massif and subsequently submerges towards southwest under the tertiary molasse sediments and the overlying quaternary fluvial deposits of the Danube River and its tributaries and re-appears southwest of Krems (Schnabel et al., 2002; Fig. 2). East of Zöbing am Kamp, a tectonic horse with the sediments of the Zöbing formation is preserved in between branches of the DDF (Vasicek & Steininger, 1999; Fig. 2). The Zöbing formation represents the remanents of the Upper Palaeozoic sediment cover of the Bohemian massif and is composed of silt and sandstones, conglomerates, and limestones. These sediments were originally deposited in an extensional graben system that formed during a late variscian extensional phase of the orogeny, probably during a time when the DDF was already active (e.g. Boskovice Furrow; Steininger, 1999; Schnabel et al., 2002). Further to the northeast (i.e. outside of the field of view of Fig. 2) the DDF continues as linear geological structure and juxtaposes Variscan crystalline rocks against tertiary sediments (Roetzel, 1996).

The tectonic and kinematic history of the DDF is long and potentially complex and starts during the variscan orogenesis already. Together with the Vitis fault, the Rodel fault and other minor faults, the DDF comprise a set of NE-SW striking transform-faults within the Austrian Bohemian massif, with a preferentially sinistral strike-slip kinematic throughout its entire history (Höck, 1999). Wallbrecher et al. (1993) demonstrated that the DDF originally developed as a ductile fault at a relatively late stage of the variscian orogenesis through $^{40}Ar/^{39}Ar$ dating of mica. Ages from Rb-Sr dating of muscovite indicate a brittle reactivation of the DDF within the upper crust during the alpine orogenesis (Wallbrecher et al., 1993). Post-alpine reactivation of the fault system occurred as brittle deformation (Wallbrecher et al., 1993). Quaternary tectonic and even historic activity of the DDF has been documented by Roetzel (1996) and Figdor & Scheidegger (1977), respectively. Variscan ductile and alpine to post-alpine brittle faulting show a constant principal stress field with the major principal stress (s1) acting NS and the minor principle stress (s3) acting EW (Wallbrecher et al., 1993). Joint measurements in loess in the Langenlois area show similar stress field during the Quaternary (Figdor & Scheidegger, 1977) and these structural observations might be linked to neotectnoic activity of the DDF. Figdor & Scheidegger (1977) calculated a total left lateral displacement of ~40 km along the DDF within the Bohemian massif using gravimetric measurements and correlating positive Bouguer anomalies. Furthermore, Steinhauser et al. (1987) suggested that the DDF is responsible for a vertical and stepwise displacement geometry of the crystalline rocks of more than 100 m to the east of the fault based on borehole logging and seismic measurements.

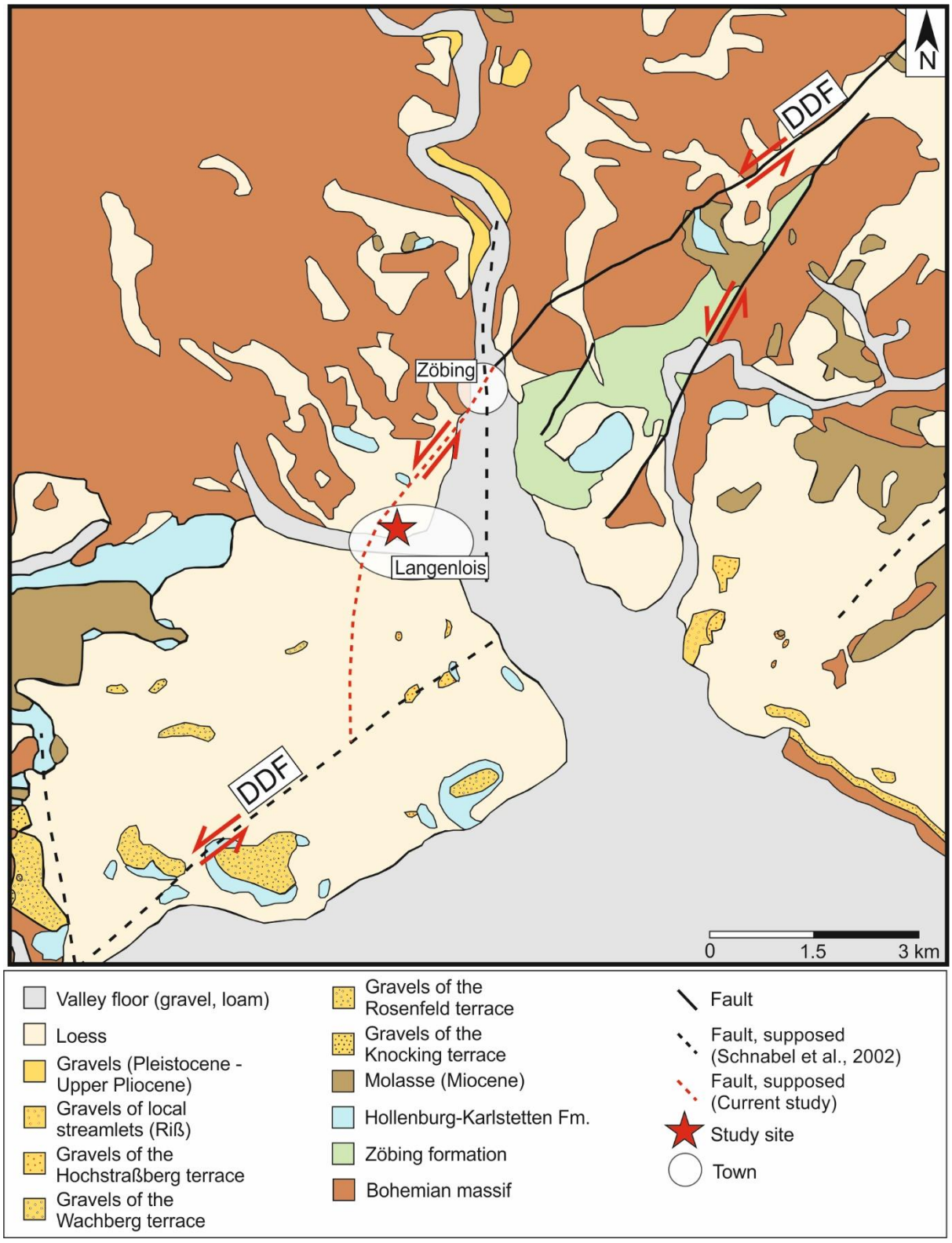

Fig. 2: Overview of the study site. **A:** Lower Austria with Langenlois (red dot). **B:** Digital terrain model of the area of Krems with towns referred to in the text and previously OSL-dated loess sites (red dots): Langenlois: this study; Thiel et al., 2011c; Stratzing: Thiel et al., 2011a; Paudorf: Thiel et al., 2011b; Göttweig: Zöller et al., 1994; Thiel et al, 2011b; Krems: Lomax et al., 2014. **C:** Langenlois with the study site (for exact position of investigated sedimentary logs see Fig. 3B) with the wine-world Loisium to its north and the position of the brickyard with the sediment succession dated by Thiel et al. (2011c). Details see text.

Another geologically relevant unit within the Langenlois area is the Hollenburg-Karlstetten formation. This formation has been deposited on top of the Bohemian massif during the Miocene and is composed of conglomerates, sands, and marls (Schnabel et al., 2002). These clastic sediments were transported from the Northern Calcareous Alps by an alpine river (Paleo-Traisen) into the Badenian Molasse-sea that expanded in the Langenlois area ca. 15 Ma ago (Fuchs, 1972). Sediments of the Hollenburg-Karlstetten formation are exposed in between Langenlois and the town of Lengenfeld (10 km west of Langenlois) and near the town Rohrendorf (6 km south of Langenlois) where small layer-bounded karst caves within the Hollenburg-Karlstetten formation exist (Knobloch, 1980). Minor occurrences of the Hollenburg-Karlstetten formation also exist north of Langenlois on the local hill tops of the Schilterner Berg and Heiligenstein (Fig. 2).

During the Pliocene and Pleistocene fluvial deposition and erosion were the main land shaping processes within the confluence area of the rivers Danube and Kamp. Fuchs et al. (1984) differentiate several terrace levels in the relatively broad confluence area, which are indicated in the geological map of Fig. 2. These terrace levels and their relative elevation above the modern Danube are: the Lehen terrace (25-30 m), the Hochstraßberg terrace (45 m), the Wachberg terrace (75-80 m), the Rosenfeld terrace (105 m) and the Knocking terrace (130 m). The ages generally ascribed to these terraces range from the Middle Pleistocene (Lehen terrace, Mindel) to the late Pliocene /oldest Pleistocene (Knocking terrace; Fuchs et al., 1984). No numerical ages exist for these terraces, but a biostratigraphic age constraint is available for the Rosenfeld terrace. A molar tooth of the species *Elephas planifrons* (*meridionalis*) has been retrieved from the Rosenfeld terrace, allowing an assignment of this terrace level to the late Pliocene/early Pleistocene (Grill, 1957). In the surrounding of Langenlois, gravels of the Hochstraßberg terrace are exposed and were described by Piffl (1959), who termed this terrace level Gobelsburger level (after a village situated 1 km southeast of Langenlois). In the terrace outcrops around Gobelsburg Piffl (1959) recognized a 5 m thick sequence composed of crystalline gravels with a brown sand matrix and intercalated layers with manganese crusted components. This fluvial sequence is overlain by cryoturbated and normal-faulted loess and the terrace level was assigned by Piffl (1959) to the early Pleistocene based on its morpho-stratigraphic position. A further occurrence of the Hochstraßberg terrace sediments is documented at the base of the former brickyard "Hammerer" in Langenlois, situated ~900 m southwest of the current study site. In this brickyard fluvial gravels are overlain by sand with intercalated silty-clayey layers (Piffl, 1976).

In the investigation area both, Miocene sediments (i.e. the Hollenburg-Karlstetten) and late Pliocene to Pleistocene river terraces are widely covered with loess (Schnabel et al., 2002). Fink (1956) and Brandtner (1956) distinguish three different loess landscapes in Austria, each characterized by a specific type of loess-paleosol facies and precipitation regime during the Upper Pleistocene: (i) The wet loess landscape (northern alpine foreland from Upper Austria to St. Pölten) with a mean annual precipitation (MAP) of 700-800 mm, (ii) the transition zone (situated in the Kamp valley, the area of Krems and extending south to the Traisen valley) with 600-700 mm of MAP and (iii) the dry loess landscape (eastern part of Lower Austria) with <600 mm of MAP. The main difference in terms of loess-paleosol facies is the predominance of solifluction in the wet loess landscape, whereas in the dry loess landscape solifluction does not occur or is of minor significance (Brandtner, 1956). Langenlois is situated in the transition zone. According to Fink (1956), loess sequences of the transition zone are often characterised by thick loams, typically for the dry loess landscape, but are overprinted by solifluction during the initial stage of an ice age, resulting in thick, intensively coloured solifluction soils.

Along the southern margin of the Bohemian massif in Lower Austria (i.e. in the wider Krems/Langenlois region), lee sided loess accumulation was common during the Pleistocene. As outlined already, loess accumulation was interrupted periodically by pedogenesis during interglacials and interstadials and this climate-driven sedimentation pattern resulted in thick loess-paleosol sequences in that region. In this wider Krems/Langenlois region Havlíček et al. (1998) identified 12 pedocomplexes, 10 of which were assigned by him to the time interval from the Early to the Middle Pleistocene. Middle to Late Pleistocene loess-paleosol sequences were described by Haslinger et al. (2009) at the "red outcrop" located in the vicinity of Langenlois (Fig. 1C), but these authors did not attempt to correlate these loess and paleosol units to specific glacial and interglacial periods.

Thiel et al. (2011a, b, c), Terhorst et al. (2011) and Lomax et al. (2014) used luminescence dating to numerically constrain the depositional age of several loess-paleosol sequences and related phases of pedogenesis in the Krems/Langenlois region, and these findings are elaborated on in more detail in the following: Thiel et al. (2011b) dated a pedocomplex (the so-called "Paudorfer Bodenbildung") located in Paudorf, ~6 km south of Krems (Fig. 1B) and showed that this paleosol formed during the last Interglacial, i.e. the marine isotope stage (MIS) 5e, also known as Eem. Younger phases of loess accumulation occurred in the Krems/Langenlois region and were dated to the MIS 3 and the Last Glacial Maximum (LGM; e.g. Thiel et al. 2001a, b, c; Lomax et al., 2014). It has actually been suggested that two phases of loess accumulation occurred during the MIS 3 (Therhorst et al., 2011; Thiel et al., 2011a, c): an earlier phase that took place from ~57 ka to ~35 ka, followed by a later phase lasting from ~35 to ~28 ka. The earlier phase was observed in outcrops in Stratzing (~ 6 km southeast of Langenlois; Fig. 1B) and in the abandoned brickyard of Langenlois (Fig. 1C; Thiel et al., 2011c). The later MIS 3 depositional phase was only verified in the outcrop of Stratzing (Thiel et al., 2011a). The loess deposits from each of the MIS 3 phases contain cryogenic layers (sediments altered by freeze-thaw processes). Furthermore, cultural horizons (Upper Paleoltihic layers of the Aurignacien) were identified at each of those sites. LGM-loess has only been documented in few outcrops in the Krems-Langenlois area (e.g. Krems-Wachtberg; Lomax et al., 2014), which led to the assumption that a more recent erosional phase removed most of the LGM loess in that region (Terhorst et al., 2011). It is also noted that sediments covering the age range between ~55 ka and ~106 ka have not been reported for the Krems/Langenlois loess landscape so far, which has been explained by a long lasting and intensive erosional period (Terhorst et al., 2011; Havlíček & Holásek 1998).

3. Sampling and methodology

At the Loisium wine-world three sediment outcrops were logged, and structural geological features recorded in the course of this study. The outcrops Haimerl and Nidetzky (each log ~3-4 m in length) are part of the Loisium cellar complex, while the third outcrop (Steininger, log ~12.5 m in length) was exposed during construction work adjacent to the Loisium in spring and early summer 2017 only (Fig. 3). For logging and description of sediment lithofacies the classification scheme of Keller (1996) was applied.

In total 9 samples were collected for OSL-dating, two samples from the cellar wall Haimerl and 7 samples from the excavation pit Steininger. The cellar wall Nidetzky was heavily affected by faulting, hence no OSL samples were obtained from this outcrop. OSL sample preparation and dating was conducted at the OSL laboratory of the Institute of Geology, University of Innsbruck. Establishing a robust OSL chronology for the sediment successions of the Loisium wine-world was the focus of this

thesis. One sample of a charcoal was retrieved from the excavation pit Steininger. It was AMS radiocarbon dated by the Poznan Radiocarbon Laboratory in Poland.

Field work at the Loisium wine-world was conducted in collaboration with Reinhard Roetzel from the Geological Survey of Austria (GBA). The following sedimentological and mineralogical data, that were integrated into this thesis, were provided by the GBA: particle size distribution, bulk mineralogy and clay mineralogy. These data are based on 8 samples from the cellar wall Haimerl, 7 samples from the cellar wall Nidetzky and 11 samples from the excavation pit Steininger and were already presented in an unpublished report (Roetzel et al., 2018). Since the data is required for the description of the sedimentary logs and the follow-up discussion, it is summarized in chapter 4, while the detailed data is listed in the Annex – mineralogical and sedimentological results. The sedimentological methods are detailed in the following.

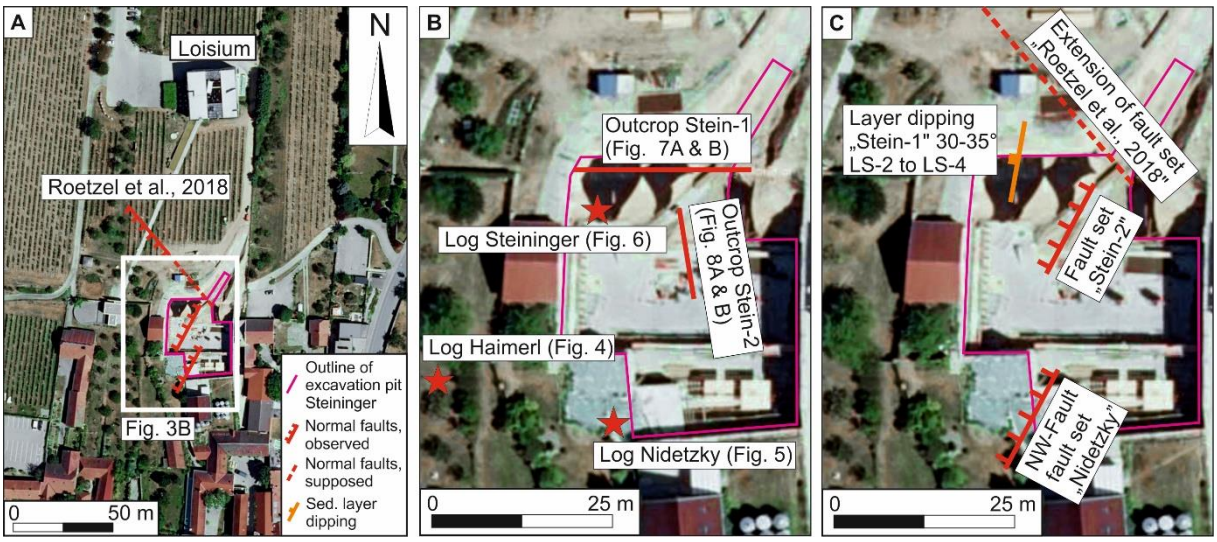

Fig. 3: A: Orthophoto of the Loisium site (NÖ atlas, 2021) with outline of the excavation pit Steininger and faults observed in this study and by previous authors (i.e. normal fault, recorded by Reinhard Roetzel during construction work in 2003 in the Loisium cellar complex). **B:** Steininger excavation pit with orientation of the outcrops Stein-1 and 2 and the position of the Loisium cellar outcrops and sediment logs Haimerl and Niedetzky. **C:** Observed and proposed faults at the Loisium site. Also indicated is the dip direction of sedimentary layers (units LS-1 to LS-4) in outcrop Stein-1 (details see text).

3.1. Particle size analysis

The particle size analysis was a combination of wet sieving for the grain size fraction >32 µm and settling analysis for finer fractions. For wet sieving, dried samples were pre-treated with hydrogen peroxide (H_2O_2; 15%) and disaggregated in an ultrasonic bath before they got sieved in steps of integer phi-numbers. A sub-sample of the <32 µm fraction was dried, sodium triphosphate (Na5P3O10; 0.5%) was added and dispersed in an ultrasonic bath and grain size distribution measured via a MICROMETRICS SEDIGRAPH III 5125. The grain size distributions for the coarse and the fine grain fractions were combined and the software *SEDPAK* was used to calculate the grain size distribution for the bulk sample (Malecki, 1985; Reitner et al., 2005). The samples were classified using the relative proportions of gravel, sand, silt, and clay according to Müller (1961) and Füchtbauer (1959). Conversion into weight percent was carried out based on the German norm DIN 4022. Additionally, mean, standard deviation and skewness of the particle size distribution were calculated.

3.2. Mineralogical analysis

For bulk mineralogy X-ray diffraction analyses (XRD) were conducted on powdered sub-samples via a PANalytical X'Pert Pro diffractometer and data analysed using the software *X'Pert Highscore*. For qualitative XRD analysis the data were matched with phase diagrams of the data base from the International Centre for Diffraction Data (ICCD). Semi-quantitative analyses of the individual mineral phases were carried out with the software *AutoQuan*.

3.3. Radiocarbon dating

Radiocarbon dating was applied on charcoal retrieved from loess. The sample was wrapped in aluminium foil, packed in sealable plastic bags and sent to the Poznan Radiocarbon Laboratory for dating via AMS (accelerator mass spectrometry). The chemical pre-treatment was done following Brock et al. (2010), applying HCL and NaOH to remove any contamination. The sample was then combusted in closed quartz tubes to produce CO_2. The CO_2 was reduced with hydrogen, using Fe powder as a catalyst. Finally, the carbon isotopic ratios ($^{14}C/^{12}C$ and $^{14}C/^{13}C$) of the sample were determined using an accelerator mass spectrometer (AMS). The calculated ^{14}C age was calibrated using the *OxCal* program.

3.4. Luminescence dating

Luminescence samples were collected using metal tubes, which were hammered into the freshly cleaned sediment outcrops. The sampling tubes were sealed with duct tape and opened under controlled red-light conditions in the laboratory, where the outermost (light-exposed) 2 cm of the sample material were removed. Sample preparation followed standard procedures (Wintle, 1997) and involved wet sieving to obtain the coarse-grained (63-212 µm diameter) quartz grains, followed by removal of carbonates and organics using hydrochloric acid (30% and 10%) and hydrogen peroxide (10 %). After etching, the samples were carried through magnetic separation and the non-magnetic fraction was density separated via sodium polytungstate solutions with densities of 2.70 g/cm^3 and 2.62 g/cm^3 to isolate quartz from the bulk sample. The quartz extracts were etched for 40 minutes in 40% hydrofluoric acid and subsequently washed in hydrochloric acid to remove eventual freshly precipitated fluorides. Finally, the samples were soaked in 34% hexafluorosilicic acid for three days to remove any remaining feldspar contamination that has not been destroyed with the hydrofluoric acid step and re-sieved to retain the target grain size fraction.

All OSL measurements were carried out either on Risø TL/OSL DA15 or a DA20 reader equipped with an Electron Tubes Ltd 9635Q photomultiplier tube and calibrated $^{90}Sr/^{90}Y$ beta sources (~0.1 Gy/s). Quartz aliquots were stimulated with blue (470 nm) LEDs and the signals were filtered through a 7.5 mm Hoya U-340 filter (i.e. detected in the near UV range). A convex quartz lens was placed in between the filter and the photomultiplier tube to optimize the signal intensity entering the photomultiplier tube. The coarse-grained quartz samples were mounted on stainless steel discs using a silicon spray for adhesion. The size of the spray masks for aliquot preparation varied between 1 and 3 mm in diameter, resulting in multi-grain discs each holding between 20 and 200 grains. The samples were measured using a modified Single-Aliquot Regenerative-Dose (SAR) protocol (Murray and Wintle, 2000, 2003). Dose recovery tests and a preheat plateau test were carried out on two samples (OSL-LOIS-7, OSL-LOIS-8) to optimize the SAR protocol. For dose recovery tests, multi grain aliquots were sun-bleached for at least 3 days. Preheat temperatures were systematically varied from 160°C to 300°C to determine suitable preheat conditions for dating.IR stimulation for 40 s at 40°C was executed prior

Table 1:
SAR protocol used in this study. This protocol was combined with an early background subtraction approach (Cunningham and Wallinga, 2010) and the post-IR blue quartz OSL signal used for dating. As regenerated doses (R1 to R6 in step 1) 0-530 Gy were used. In the first SAR cycle no regenerative dose was administered and the natural dose measured.

Step	Treatment
1	Dose
2	Preheat, 180°C, 10 s
3	IR stimulation, 40°C, 40 s
4	Blue LED stimulation, 125°C, 40 s
5	Test dose (16.5 Gy)
6	Preheat, 180°C, 10 s
7	IR stimulation, 40°C, 40 s
8	Blue LED stimulation, 125°C, 40 s
9	Bleach, blue LED, 290°C, 40 s
10	Return to step 1

to each blue OSL stimulation in order to eliminate contribution from feldspar inclusions that were not destroyed via etching. OSL signals were measured with blue LEDs at 125°C for 40 s. The size of the test dose was ~16.5 Gy. A hot-bleach with blue light for 40 s at 290°C at the end of each SAR cycle was introduced to minimize signal build-up during the measurement cycle. The measurement protocol is summarized in Table 1. Aliquots had to conform with the following quality criteria to be accepted for further analysis: (i) a test dose error ≤10%; (ii) recuperation ≤5% of the natural dose or an error overlapping with the 5% threshold; (iii) a recycling ratio consistent with unity at the 2σ error level; (iv) an initial OSL signal from the first test dose >3 times above background count; (v) the sensitivity-corrected natural OSL signal intercepts the dose-response curve below $2*D_0$, which is considered to be the threshold below which reliable De-estimates can be obtained (Wintle and Murray, 2006), and (vi) a dose response curve that could be Monte Carlo fitted (using 500 iterations). For data analysis, an early background subtraction (EBS) was chosen following Cunningham and Wallinga (2010), using the initial signal of 0-0.31 s and a background interval from 0.31 to 1.38 s (for more information check Annex – OSL basics and further details). An exponential function was used for fitting the SAR dose response curves. D_e estimation and overdispersion calculation were obtained via the central age model (CAM) of Galbraith et al. (1999).

For each sample, the radionuclide concentrations of Uranium, Thorium and Potassium were determined by a combination of alpha (on a Daybreak 583 alpha counter) and beta-counting (on a Risø GM25-5 beta counter). Radionuclide concentrations were converted into gamma and beta dose rates using the conversion factors of Stokes et al. (2003). The effect of grain size on beta attenuation and etch effect was considered according to Brennan (2003) and Brennan et al. (1991). Cosmic dose rates were calculated following Prescott & Hutton (1988) taking into account the latitude, longitude and altitude of the site. The field moisture as well as the saturated moisture content were determined for each sample. Since, the sediments of profile Steininger were freshly exposed during construction work, the values of the field water content were used for age calculations. For the two samples from profile Haimerl an average value from the loess samples of profile Steininger were used. Error margins of 5% were added to the field water content to consider variations of soil moisture through time.

4. Results

4.1. Description of sediment logs and outcrops

The sediment log Haimerl was recorded on a cellar wall situated in the wine cellars of the Loisium (Fig. 3 and 4). The base of the log lies at ~11 m below ground surface. The lower right corner of the cellar wall is composed of ~40 cm thick, stratified, greenish-grey, silty clays that are yellowish-brown spotted and free of carbonate (unit LH-1). The layers are inclined to the left (west) which is why LH-1 is not exposed in the left part of the cellar wall. LH-1 is overlain by 60-90 cm thick, yellowish-grey to

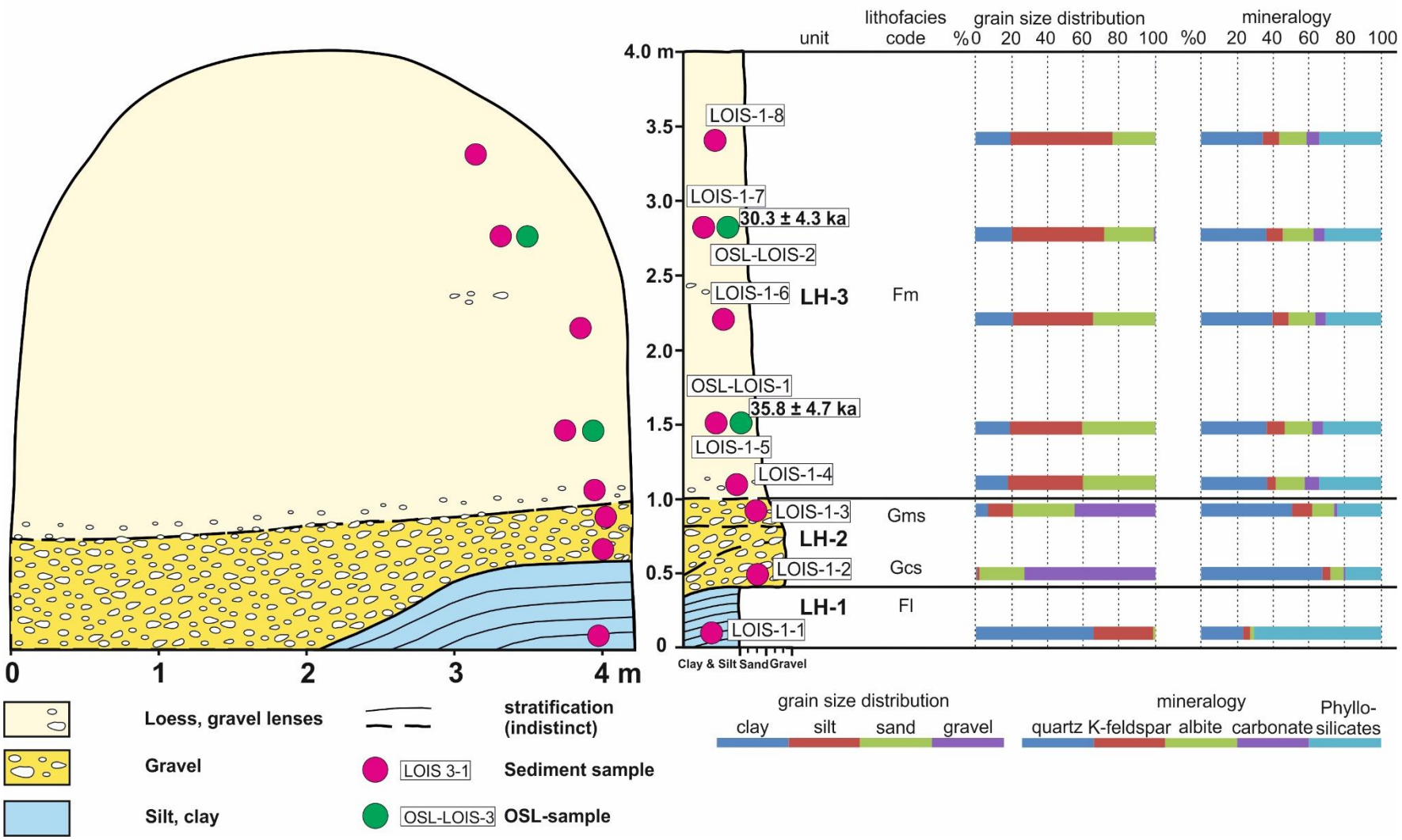

Fig. 4: Sketch and log of the cellar wall Haimerl with grain size distribution data and mineralogy. The position of the OSL samples and corresponding luminescence ages are indicated. The cellar wall is facing into southern direction, i.e. the reader's view is to the north.

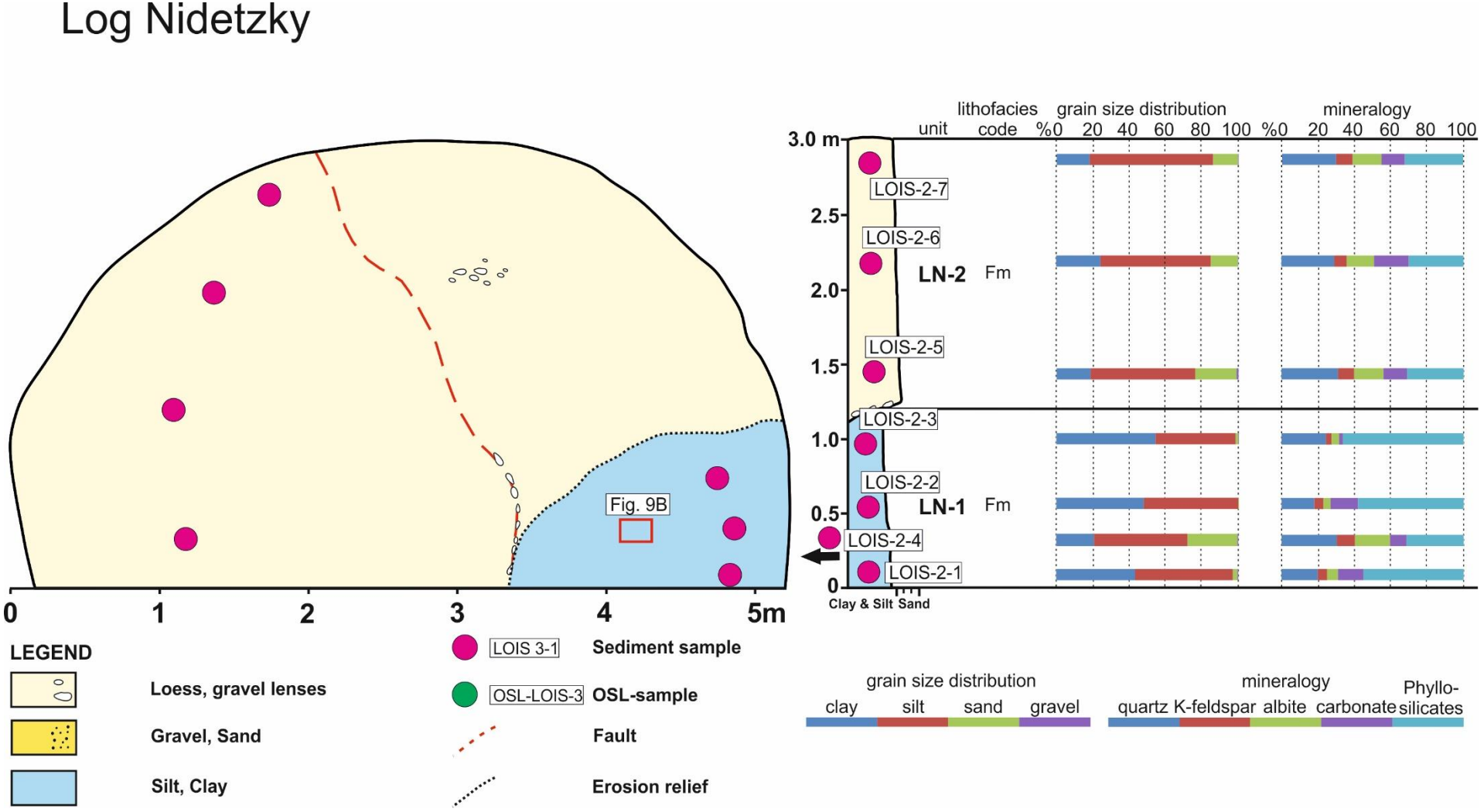

Fig. 5: Sketch and log of the cellar wall Haimerl with grain size distribution data and mineralogy. The position of the OSL samples and corresponding luminescence ages are indicated. The cellar wall is facing into southern direction, i.e. the reader's view is to the north.

brown gravels (LH-2) which are forming the base of the left part of the outcrop. These gravels show an indistinct stratification. The gravels are dominated by the medium to coarse gravel fraction and show a high sand content and fine fractions that are increasing up-section. The gravels of the unit LH-2 are well-rounded and mostly composed of quartz-rich, crystalline clasts (e.g. gneisses). The contact between unit LH-1 and 2 is partly exposed and on the clay-rich bedding surface of LH-1 striations are preserved, suggesting that the contact between both units is potentially tectonic in nature. The uppermost exposed unit of log Haimerl is a 3 m thick loess deposit (LH-3). The loess consists of yellowish brown, clayey silts. LH-3 contains also a significant proportion of fine sand that is decreasing up-section. The basal 20 cm of LH-3 exhibit scattered quartz components with a diameter of up to3 cm, while the rest of the LH-3 unit is homogenous, except for the occurrence of sporadic and isolated gravel lenses.

The cellar wall and sediment log Nidetzky is also located in the wine cellars of the Loisium, ~25 m east of log Haimerl (Fig. 3 and 5). Several faults cut through the cellar wall, with a major fault indicated in Fig. 5. On the lower right side of the wall, up to 120 cm thick fine-grained sediments (LN-1) are exposed. The sediments consist of blueish to greenish-grey clayey silts and silty clays that are yellowish-brown spotted. The carbonate content of this unit is comparatively high given the clay-rich nature of this sediment and LN-1 also contains calcite concretions with a diameter of up to 4 cm. A convex unconformity separates LN-1 from the loess unit LN-2 and the left part of the cellar wall Nidetzky is thus completely made up of LN-2 loess. This loess consists of clayey fine-sanded silts containing small, isolated gravel lenses. The carbonate content in LN-2 is slightly higher compared to the loess of log Haimerl (LH-3). Similar to the loess of LH-3 an upward fining trend can be recognized, but the sediment of LN-2 has a generally lower sand content.

The location Steininger is a ~12 m deep excavation pit. Within the pit, an E-W striking sediment wall (labelled outcrop Stein-1 in Fig. 3B and shown in Fig. 7), as well as a N-S striking sediment wall (labelled outcrop Stein-2 in Fig. 3B and shown in Fig. 8) were exposed and documented. In the excavation pit a detailed sediment log has been recorded too (Fig. 3B and 6). This log (log Steininger) is positioned in the eastern section of the outcrop Stein-1 and the log trace is also indicated in Fig. 7B.

Log Steininger is a ~12.5 m thick succession composed of fluvial sediments as well as loess and paleosols (Fig. 6). It is subdivided into 5 sedimentary units (LS-1 to 5) with 3 units (LS-2, LS-3 and LS-5) that are sub-divided into further subunits.

The base of the log is composed of stratified silty sands (LS-1), with some layers containing a significant amount of fine to medium gravel (see Annex – mineralogical and sedimentological results). The colour of the sediment is yellowish brown with intercalated brown, reddish brown and grey layers composed of the same type of silty sands.

LS-1 is overlain by a 140-160 cm thick unit labelled as LS-2a in Fig. 6. This unit is made up of greenish to blueish-grey clay that is laminated and also contains layers of silt. In the upper ~70 cm the subunit LS-2a transitions to subunit LS-2b in form of a succession of alternating 5-10 cm thick layers of silts and horizontally stratified fine to medium sands. LS-2b consists of 130 cm thick coarse to medium sands with a minor gravel component. The sands constitute 5-10 cm thick layers that show either wavy stratification or cross bedding. At ~4 m of the log an erosional channel occurs within the sands of LS-2b which was filled up with through cross bedded silty fine to medium sands and overlain by a layer of gravelly sand (top layer of LS-2b, Fig. 6). The gravel components contain well-rounded quartz as well as angular crystalline clasts. In units LS-1 and LS-2 only traces of carbonate were detected.

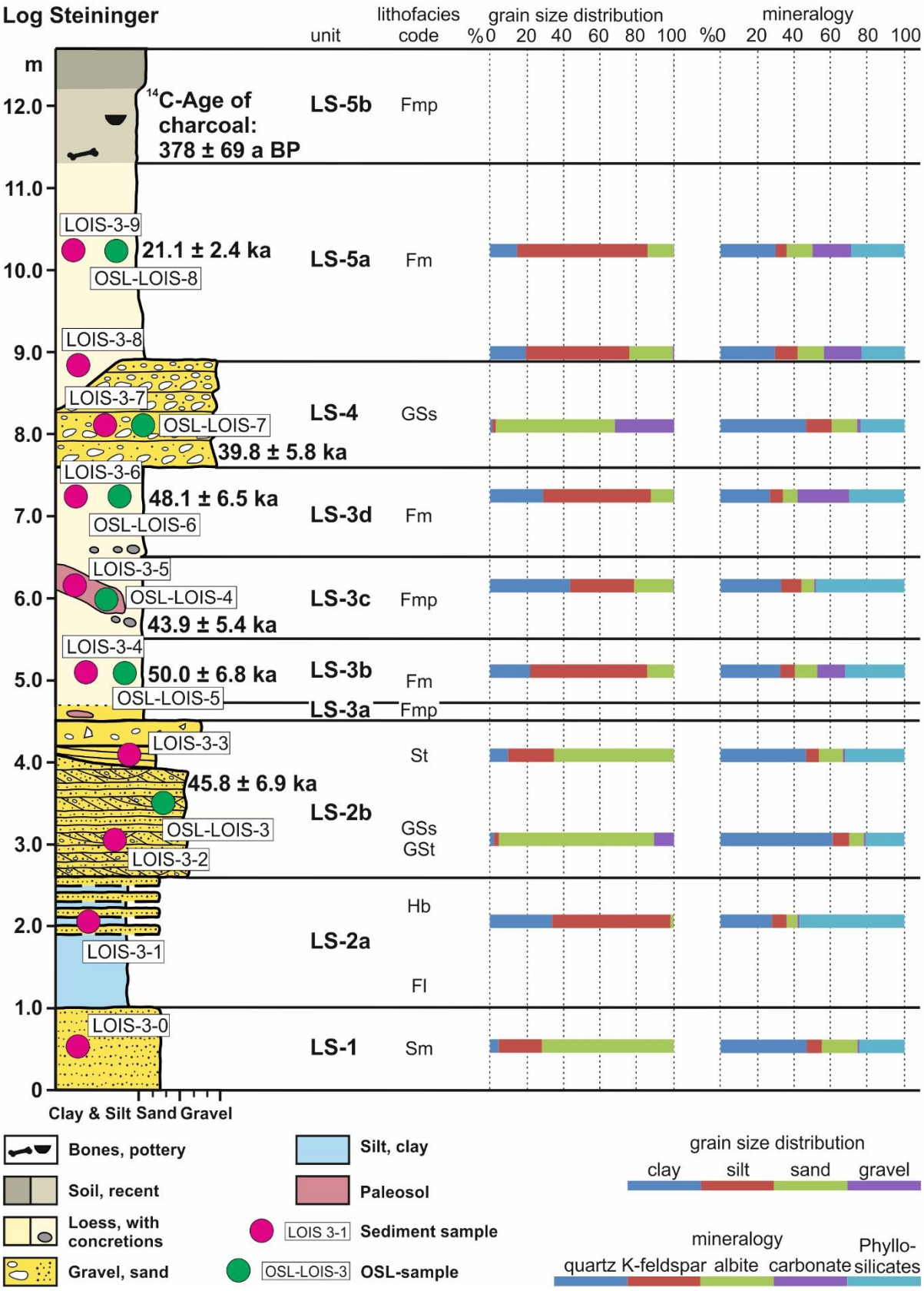

Fig. 6: Log of the northern wall of excavation pit Steininger (i.e. outcrop Stein-1) with grain size distribution data and mineralogy. The position of the OSL samples and corresponding luminescence ages are indicated.

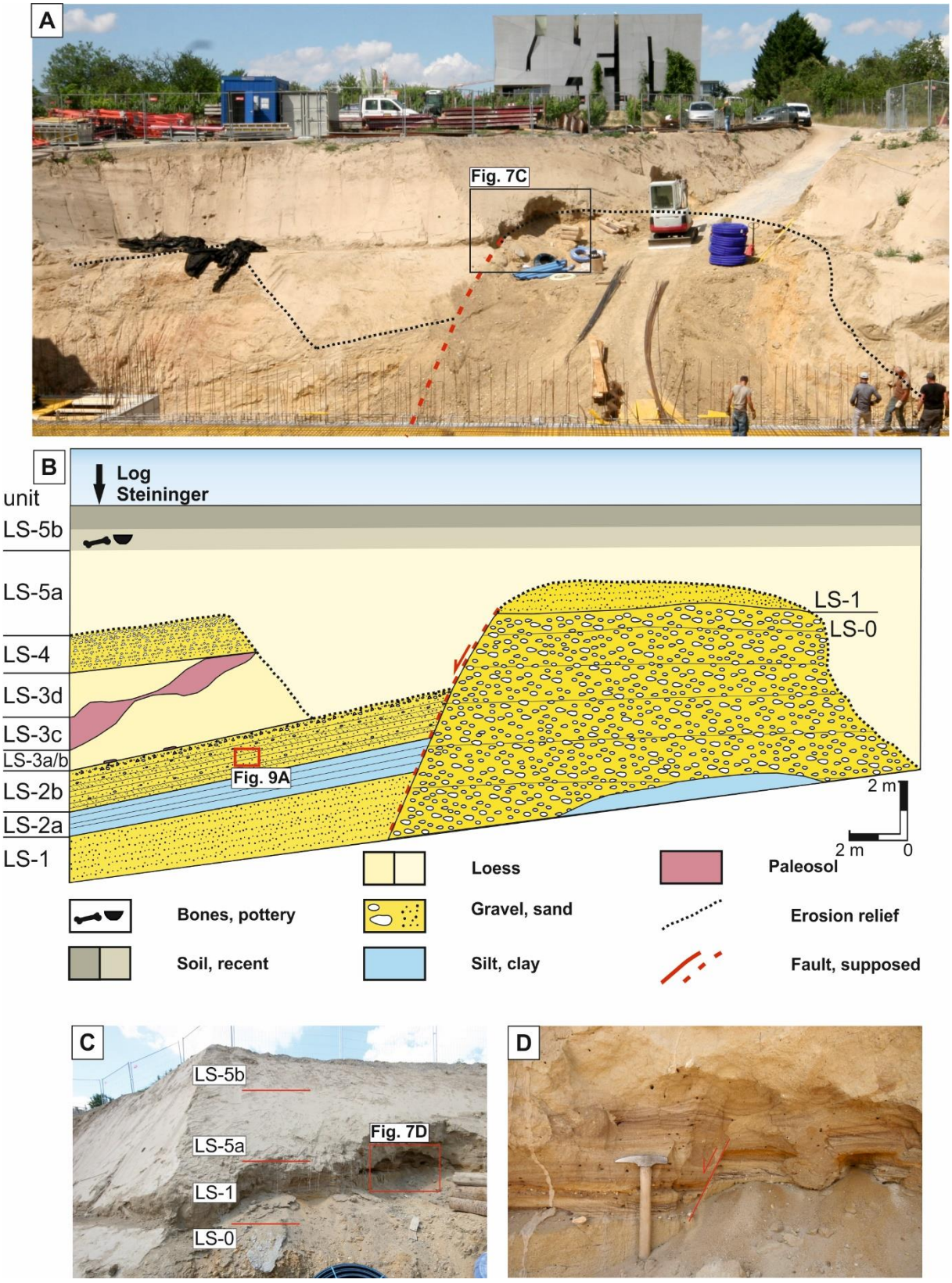

Fig. 7: Documentation of the outcrop Stein-1. **A:** Field image of the outcrop Stein-1 (i.e. northern wall of the excavation pit Steininger) with the erosion relief and a supposed normal fault indicated. **B:** Sketch of the outcrop Stein-1 with the position of the sediment log Steininger indicated. Note the erosion relief is levelled by sedimentary unit LS-5a. View is to the north. **C:** Field image of Stein-1 outcrop detail. Note that here the sedimentary units LS-0 and LS-1 occur ~3 m below ground surface and are overlain by loess unit LS-5a. View is to west-northwest. **D:** Fault within unit LS-1 with an apparent dip to the south.

The subsequent loess-paleosol succession LS-3 is subdivided into four subunits (Fig. 6). The basal subunit LS-3a is a 10-30 cm thick carbonate-free, greyish to yellowish brown silt and sandy silt that is reddish brown spotted and contains small, reddish-brown, silty lenses. Based on these sedimentological criteria (grain size, lack of carbonate content and colour) this unit is interpreted as a paleosol remnant. It is overlain by 60-80 cm thick loess (LS-3b) composed of yellowish-brown clayey to sandy silt with carbonate concretion in the upper part. The carbonate content of this loess is comparable with the loess of unit LN-2 of the log Nidetzky. The next sediment unit LS-3c comprises up to 1 m thick loess containing Ca-concretions with a maximum diameter of 10 cm. Within the loess up to 1.3 m long and 70 cm thick slabs of reddish-brown loam are intercalated (LS-3c). These slabs are inclined to the west and equivalent to subunit LS-3a interpreted as the erosional remnants of a paleosol. The loam that constitutes these reddish slabs of paleosol are depleted in carbonate and have a higher clay content compared to the encompassing loess. Subunit LS-3c is followed by LS-3d, which is an up to 110 cm thick layer of loess composed of sandy to clayey silts. At the base of LS-3d Ca-concretions 5-10 cm in diameter can be observed. Compared to LS-3a, this loess has a slightly higher clay fraction and a higher carbonate content.

The LS-3 loess-paleosol succession is followed by a ~130 cm thick layer of fluvial sediments labelled as sediment unit LS-4 (Fig. 6). This unit is composed of greyish-brown, medium to coarse sands with a high gravel content. The gravels are primarily angular to sub-rounded granites and gneisses and show imbrication.

The subsequent unit LS-5a is a yellowish-grey loess and has a thickness of ~240-300 cm. This loess is composed of clayey to sandy silt with a slightly higher carbonate content compared to subunit LS-3b. At the base of the subunit LS-5a the silt content is comparable to the loess units LS-3b and 3d. The silt content is increasing up-section and in the upper part of subunit LS-5a the coarse silt fraction attains ~50 weight% of the total sediment (compare Annex – mineralogical and sedimentological results).

The uppermost ~140 cm of the log are composed of another loess unit that is brownish-grey in colour and composed of sandy and clayey silt (unit LS-5b). Within this loess unit remnants of pottery and bone as well as tooth and charcoal fragments were retrieved from pit like structures in relatively shallow depths. For the charcoal a radiocarbon age of 378±69 a cal BP was obtained. The bone fragments were identified at the natural history museum of Vienna as a domestic cat (personal communication Dr. Ursula Göhlich). Unit LS-5b is covered by modern soil, which is a Tschernosem.

The sedimentary architecture within the excavation pit Steininger is complex and this complexity is outlined in more detailed in the following via the outcrop sketches Stein-1 (Fig. 7A and B) and Stein-2 (Fig. 8A and B). The correlation of sedimentary units between these two outcrops and the sediment log Steininger (Fig. 6) are established here too.

The outcrop Stein-1 is up to ~12 m in hight and has a width of ~30 m and the log Steininger is situated in the left (western) sector of this outcrop (Fig. 7B). In this western sector the sediment units LS-1 to LS-4 are tilted to the left (i.e. west). LS-3c has a higher inclination compared to the encompassing sediment, causing the overlying loess layer LS-3d to pinch out to the east. An erosional unconformity is confining the sediment units LS-3 and LS-4 and generated a pronounced erosional relief. This erosional relief is draped by loess of LS-5a, which causes direct contact between the loess of LS-5a and the gravel layer LS-2b.

In the central upper part of the outcrop Stein-1 at ~2 m below ground surface a sand unit occurs that has similar sedimentological characteristics as sediment unit LS-1 from log Steininger, i.e. fine to medium sands and gravelly sands with well-developed horizontal stratification and cross-bedding and colours that vary from yellowish brown to reddish brown and grey (Fig. 7D). These fluvial sediments

from the central upper part of the outcrop Stein-1 were thus correlated with the sediment unit LS-1 from the log Steininger (Fig. 6 and 7B). In the outcrop Stein-1 unit LS-1 has a thickness of ~70 cm and minor faults cut through this fluvial layer (Fig. 7D).

Further down-section in outcrop Stein-1 and directly below unit LS-1 coarse, well-rounded, yellowish to reddish brown gravels occur (Fig. 7C). This gravel unit comprises quartzites, quartz-rich crystalline and sandstone clasts and is interpreted as fluvial sediment and labelled LS-0 (Fig. 7B). In the deepest exposed part of LS-0, blueish-grey, silty clays are interbedded into this otherwise coarse-grained sediment (Fig. 7B). In this central part of the outcrop Stein-1 both fluvial units (i.e. LS-1 and LS-0) are confined by a convex unconformity and the resulting relief is levelled out by loess of unit LS-5a (Fig. 7B and 7C). This unconformity is partly erosive and partly tectonic in nature and described in more detail in section 4.2 below.

Outcrop Stein-2 was temporarily exposed along a N-S striking wall of the driveway that was used by the construction vehicles during excavation of the pit (Fig. 3; Fig. 8A). The left (northern) part of the outcrop was made up of layered silty fine to medium sand. The colour of this sand is yellowish brown with intercalated reddish brown and grey layers. To the right (south) these sands become gravelly. Stratigraphically and sedimentologically these sands and gravelly sands can be correlated with unit LS-1. In the northern sector of the outcrop Stein-2 (right part of Fig. 8A) coarse, well-rounded, yellowish to reddish brown gravels occur. These gravels were also exposed on the opposite side of the driveway, i.e. in outcrop Stein-1 (Fig. 3 and 7B), where they are in direct contact with the gravels of unit LS-0. Hence, the sandy and gravelly sediment units in outcrop Stein-2 were correlated with the sediment units LS-1 and LS-0 in outcrop Stein-1, respectively. The outcrop Stein-2 is also intensively affected by normal faulting, as outlined in more detail in section 4.2 below.

4.2. Tectonic structures

Various brittle tectonic observations were made in the outcrops of the Loisium wine-world and their general features are described in the following in more detail. Unfortunately, no detailed structural measurements of all fault orientations have been made due to the temporary nature of the outcrops, the rather unexpected encounter of intensive tectonic faulting in these outcrops and time constraints during sampling and logging. In addition, in several instances an exact measurement of fault orientation would not have been possible due to the unconsolidated nature of the deposits. Despite this lack of detailed measurements of fault orientation, the fault kinematic could be discerned well in many outcrops, because of the displacement of nicely visible marker horizons such differently coloured sands (e.g. Fig. 8). Hence, only a few of the fault orientations are based on measurements, while for other faults only the general orientation is indicated in the following and a schematic overview of this general picture of fault orientation and fault kinematics is provided in Fig. 9C and 3A.

In the cellar wall Haimerl fault striations are preserved on the contact surface between LH-1 and 2. The dip direction of this fault lineation was measured and is ~208/27 (lineation “Haimerl” in Fig. 9C).

The cellar wall Nidetzky exhibits two intersecting fault sets within the fine-grained sediments of unit LN-1, dipping ~298/85 and ~252/80, respectively (Fig. 9B and fault planes “Nidetzky” in Fig 9C). Minor displacement is observed along these faults, suggestive of normal fault kinematic. In addition, a fault dipping ~298/85 occurs in the central part of the Nidetzky cellar wall cutting through the loess layer LN-2. Gravels that occur as isolated gravel lenses within the loess LN-2 were dragged along this

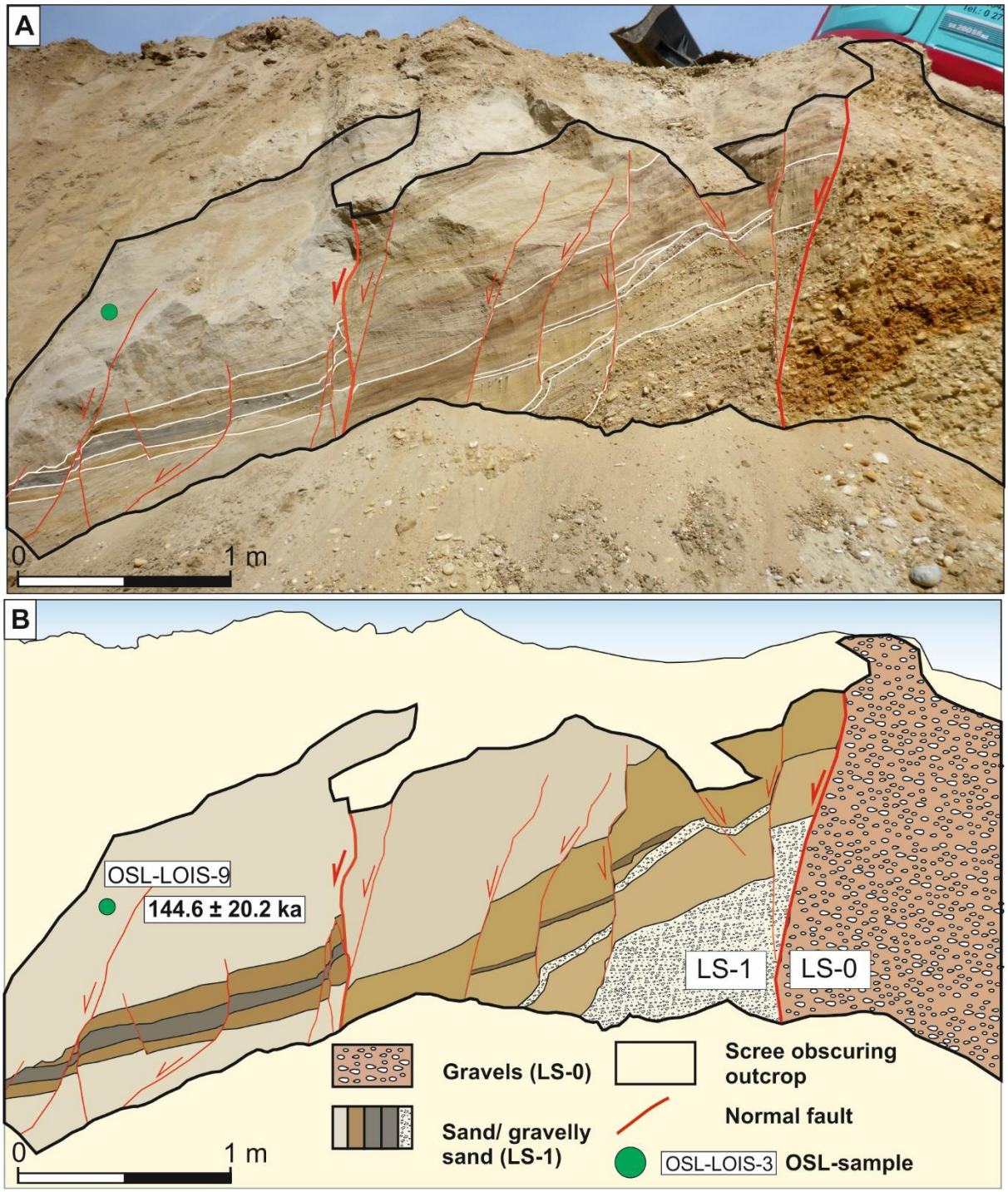

Fig. 8: Field image (**A**) and sketch of the sedimentary units and structures (**B**) of outcrop Stein-2 with the sampling position of OSL-LOIS-9. The outcrop is facing into western direction, i.e. the reader's view is to the east. Note the numerous NE-SW striking normal faults. Two major faults (compare text) are delineated as bold lines. The major fault on the right-hand side is acting as a border between the units LS-0 and LS-1. For exact location of the outcrop see Fig. 3B.

fault plane that presumably has a normal fault kinematic (Fig. 5). The offset could not be measured due to the absence of a marker horizon.

In the outcrop Stein-1 minor northwest and southwest dipping normal faults were recorded in the sediment units LS-1 (Fig. 7D) and LS-2b (Fig. 9A and fault planes "Stein-1" in Fig. 9C). Furthermore, units LS-1 to LS-4 are tilted and dipping gently west to northwest with ~280/30 to ~320/35 (left side of outcrop Stein-1; Fig. 7B and bedding planes "Stein-1" in Fig. 9C). A high angle normal fault is considered

to separate the sediment units LS-1 to LS-4 in the left part of this outcrop from the units LS-0 and LS-1 that are preserved in the central part of the outcrop (Fig. 7B; see section 5.3). Unfortunately, the fault could not be observed directly due to scree from the construction work that was obscuring the fault trace. However, using unit LS-1 as marker horizon, a displacement of ≥ 8.5 meters along a high-angle normal fault must be assumed (Fig. 7B). 12 meters further east from this high angle normal fault the units LS-0 and LS-1 are bounded by an erosional unconformity (i.e. right-hand side in Fig. 7B). Overall, in this central part of the outcrop Stein-1 it appears that the gravel and sand units LS-0 and LS-1 are forming a tectonic horst structure, albeit this horst is bounded by a high angle normal fault along its western end only (Fig. 7B).

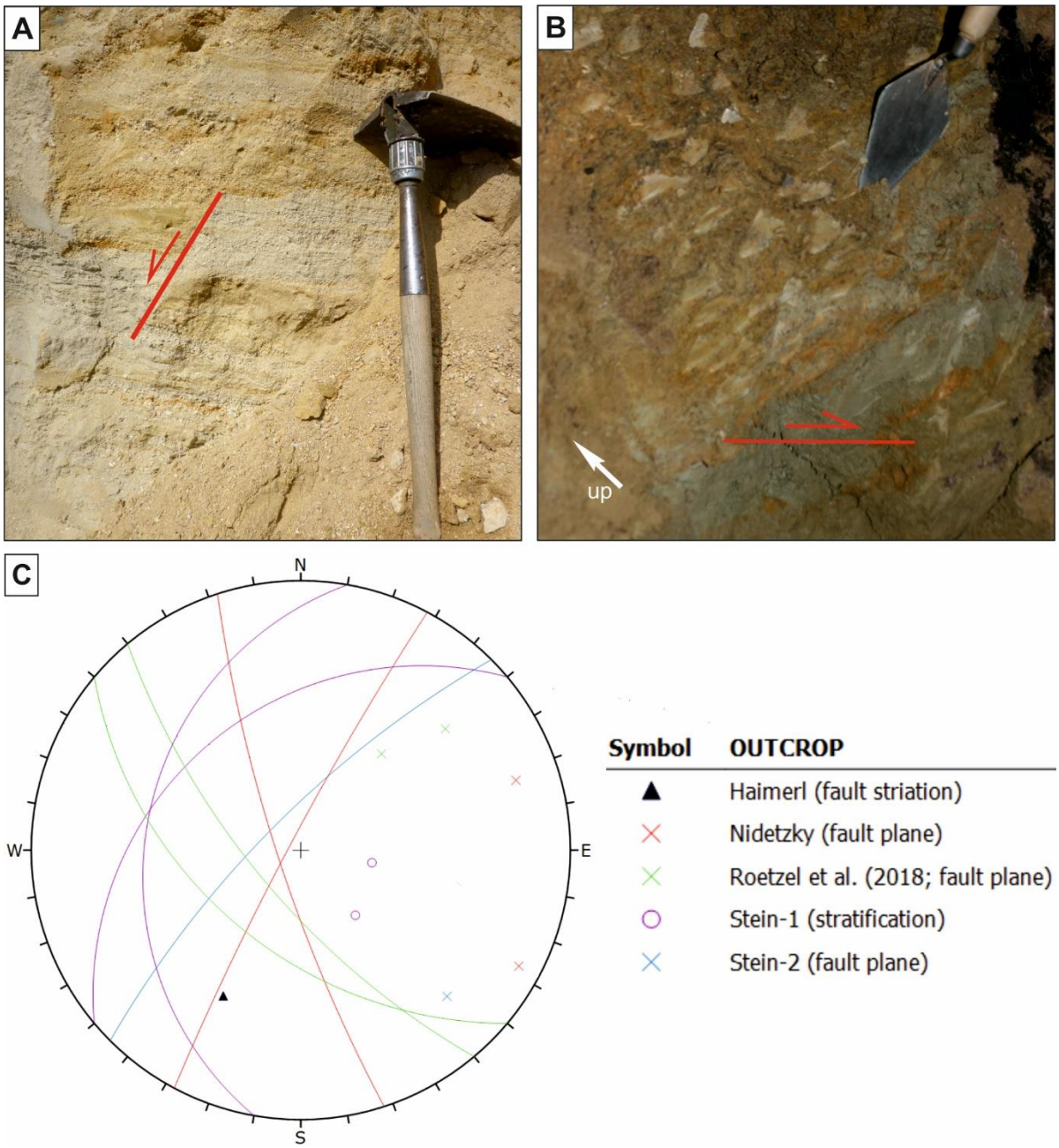

Fig. 9: A: Photo of a minor NE-SW striking normal fault within unit LS-2b in outcrop Stein-1. View is to the north. **B:** Photo of a minor normal fault within unit LN-1 in the outcrop Nidetzky (Fig. 5). View is to the west **C:** Stereonet with the approximate orientation of the normal faults (lines) and the corresponding poles of the fault planes (x). The black triangle indicates the orientation of the fault striation detected in outcrop Haimerl. Furthermore, the dip direction of the tilted sedimentary units LS-1 to LS-4 from outcrop Stein-1 are plotted too.

In the outcrop Stein-2 the sediment unit LS-1 of outcrop Stein-1 is exposed (Fig. 8). The sands of this unit are dissected by high-angle and partly conjugated normal faults (Fig. 8B). The exact dip direction and dip angle for these faults were not quantified, however, the general dip direction of these faults is estimated to be approximately northwest (315/75; fault planes "Stein-2" in Fig. 9C). Using the coloured LS-1 sand layers as marker horizons, the cumulative, measureable downward displacement over the outcrop width (~4 meters) amounts to ~2 m (Fig. 8B). Two faults in the outcrop Stein-2 indicate a displacement equal or higher than the height of the outcrop (≥ 2m), since marker horizons of the hanging wall could not be detected in the foot wall(bold marked faults in Fig. 8B). One of these faults separates the sands of unit LS-1 from the gravels of unit LS-0 (right fault in Fig. 8B). The other fault is exposed in the middle left part of the outcrop Stein-2 within sand unit LS-1 (left fault in Fig. 8B).

4.3. OSL dating

Nine samples were collected for OSL dating: two loess samples from log Haimerl and seven samples from log Steininger, comprising three loess samples, three samples from fluvial sand layers or lenses and one sample from a paleosol lens. For sampling positions see Figures 4, 6 and 8, respectively.

4.3.1 OSL Sample characteristics

Based on dose recovery tests, a temperature combination of 180°C/180°C for 10 s each was considered as most suitable for preheating during the SAR protocol. The dose recovery tests conducted with this preheat combination showed a measured/given dose ratio of 0.94 ± 0.11, an average recycling ratio of 0.99 ± 0.13 and a recuperation of 2.24 ± 2.20 % based on an EBS (early background

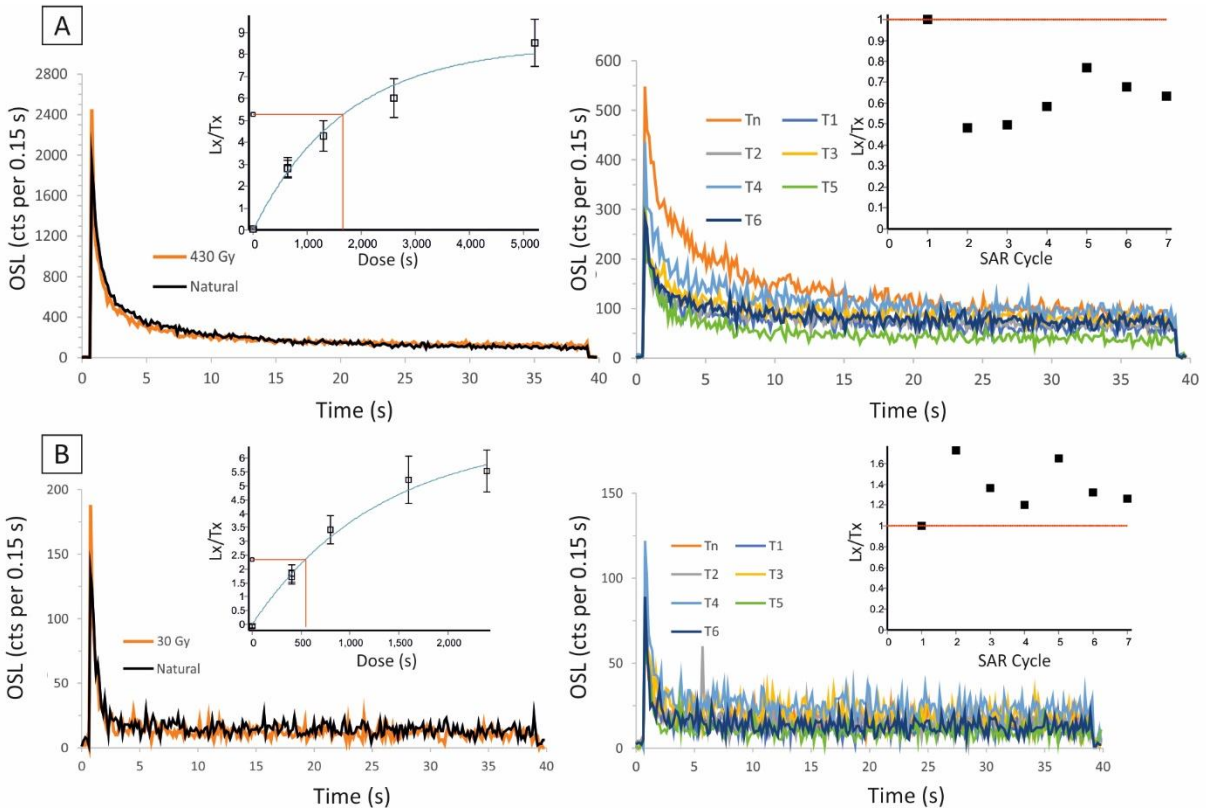

Fig. 10: OSL characteristics of a typical bright (**A**; OSL-LOIS-4) and a typical dim (**B**; OSL-LOIS-8) aliquot. On the left hand-side the OSL decay curves for the natural and a regenerated dose are shown together with the corresponding SAR dose response curve (inlet). On the right-hand side the decay curves of the test doses are depicted together with a plot of the Tx/Tn ratios (inlet).

subtraction) approach. With an LBS (late background subtraction) the same measurements yielded a measured/given dose ratio of 1.08 ± 0.07, an average recycling ratio of 0.99 ± 0.08 and a recuperation of 2.78 ± 1.98 %. The measurement protocol is shown in Table 1.

A characteristic feature of all samples is the relatively low signal intensity of the natural and regenerated OSL signals of individual aliquots, ranging from hundred to a few thousands of counts for dim and bright aliquots, respectively (Fig. 10).

Despite the low signal intensity of the Loisium OSL loess and fluvial samples, most aliquots show OSL shine-down curves with a fairly rapid decay that reaches background levels in the first ~5 to 10 seconds (Fig. 10). Where this rapid decay occurs within the initial few seconds of the OSL shine down curves, it can be safely assumed that the corresponding quartz aliquots are dominated by a fast OSL component (Li and Li, 2006). However, in several aliquots medium and even slow OSL components seem to be present too. This can be seen by OSL decay curves that reach background level only after OSL stimulation for several tens of seconds. The reason for such slowly decaying OSL shine-down curves is that the medium and slow OSL components have much lower decay rates compared to the fast component (compare Annex – OSL basics and further details). Another indication for the presence of a medium and/or slow OSL components and their detrimental effect on D_e estimation is a decreasing D_e-trend with increasing signal integration interval. This was demonstrated by Li and Li (2006) who concluded that a decrease of D_e-values with increasing stimulation time may occur due to a thermally unstable medium component (the latter is per definition not present in the natural signal), therefore causing De underestimation. These characteristics will not only yield lower D_e-values but also cause OSL age underestimation. A decrease of the D_e for an aliquot of sample OSL-LOIS-2 is illustrated in Fig. 11.

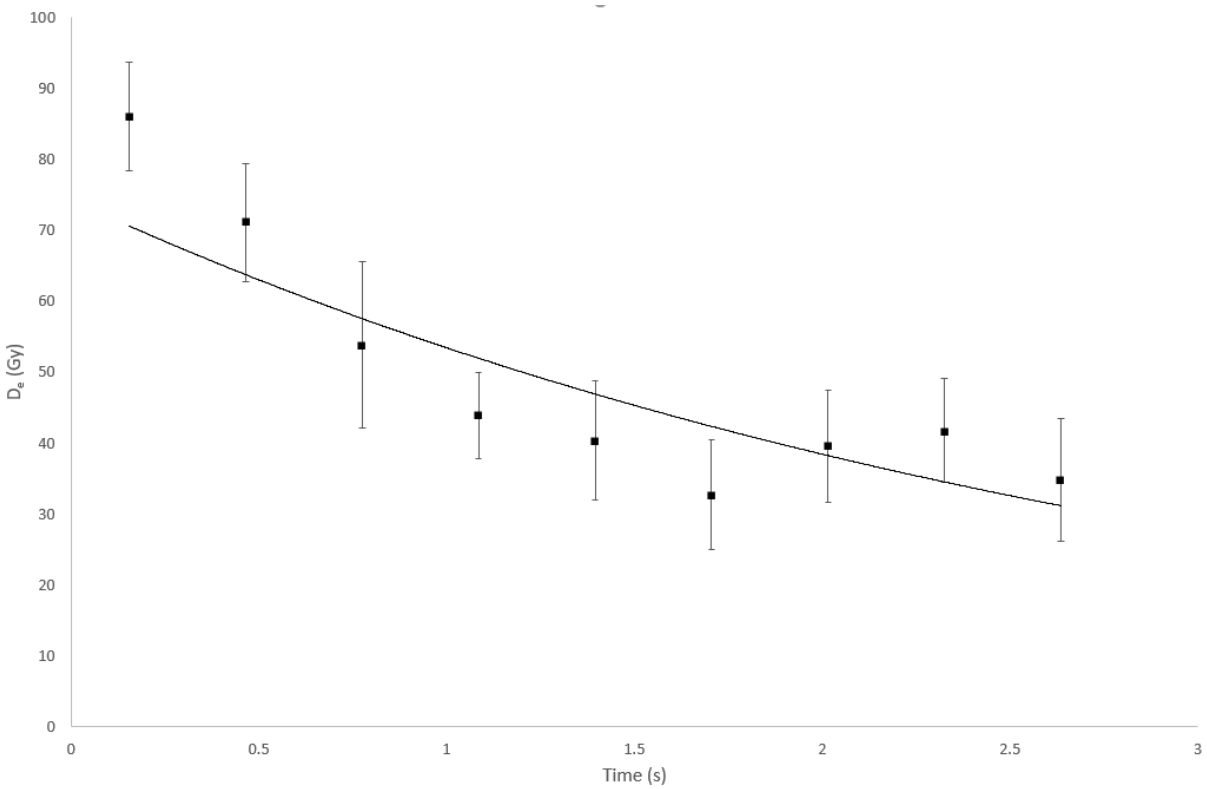

Fig. 11: $D_e(t)$ plot of an aliquot of sample OSL-LOIS-2 showing a decrease in D_e towards later integrals.

To maximise the contribution of the fast component on D_e and prevent De underestimation, an EBS approach was applied in this study (Cunningham and Wallinga, 2010). The effect of using an EBS compared to an LBS approach are higher De-values as well as a lower overdispersion for most of the samples (Fig. 12). However, ~60% of the samples had to be rejected with EBS while only ~45% were rejected with LBS. From the rejected aliquots analysed with EBS 56% were rejected based on the $2D_0$ criteria (i.e. their D_e values were higher than 2 times the D_0 threshold), for 28% of the rejected aliquots the test signal was too low compared to the background signal, 10% suffered from poor recycling ratios and only 1% from recuperation. 4% of the rejections were caused by the signal being too low or highly scattered regeneration points for which the SAR dose response curve could not be fitted using an exponential function. The detailed rejection statistics for each sample are provided in Annex – OSL results.

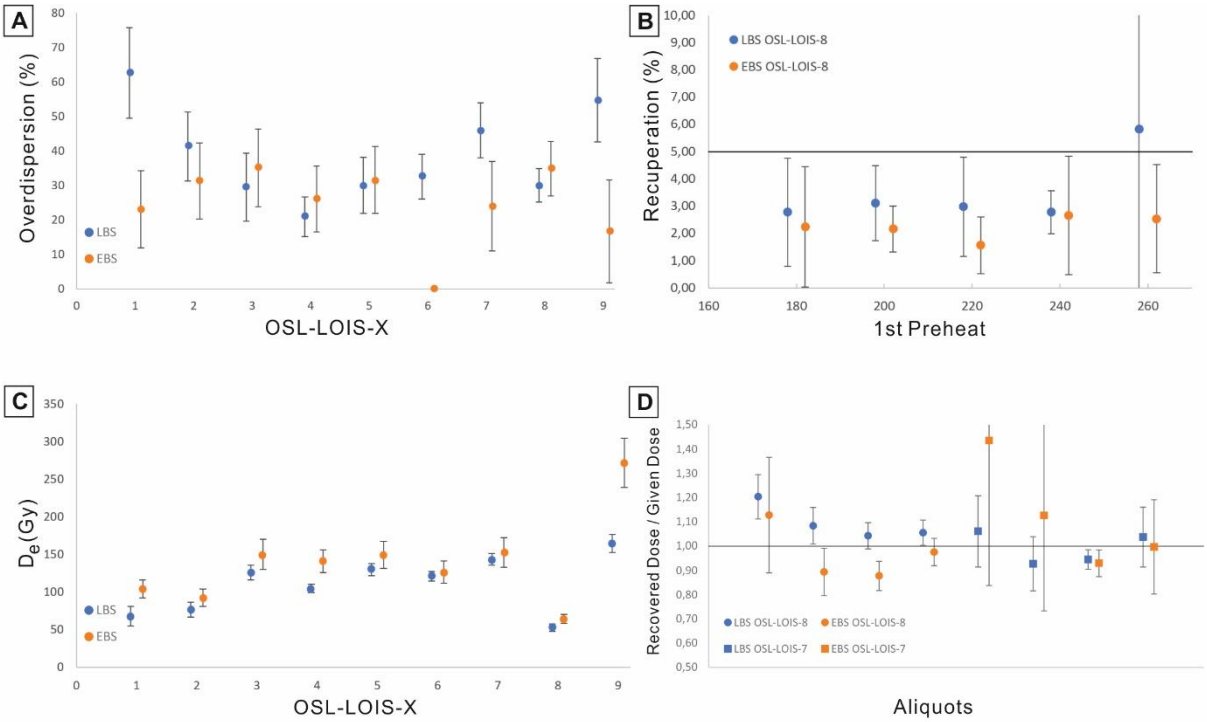

Fig. 12: Comparison of the performance of the SAR protocol using an EBS versus an LBS approach. **A:** Overdispersion values of the measured D_e for all samples (OSL-LOIS-1 to OSL-LOIS-9). **B:** Recuperation as a function of preheat temperature measured during the dose recovery test. **C:** D_e-values for all samples. **D:** Dose recovery ratio measured during the dose recovery test for four aliquots of sample OSL-LOIS-8 and four aliquots of sample OSL-LOIS-7. Note that an EBS allowed a given dose to be recovered more precisely and accurately compared to a LBS and also improved the overall stratigraphic coherency.

4.3.2 Age results

In Table 2 the D_e values of all 9 samples, their dose rates and the resulting optical ages are summarized. The D_e value for each sample was calculated with the central age model (CAM) and the corresponding overdispersion (OD) values are given Table 2 as well. The topmost loess unit (LS-5a) of Log Steininger (Fig. 6) shows an age of 21.1 ± 4.7 ka (OSL-LOIS-8). The underlying loess-paleosol-gravel succession LS-3a to LS-4, as well as the subsequent sand subunit LS-2b yielded ages between 39.8 ± 5.8 and 50.0 ± 6.8 ka (OSL-LOIS-3 to OSL-LOIS-7) that are within errors all consistent with each other. The fluvial sands that were sampled in the outcrop Stein-2 (sediment unit LS-1; Fig. 8A and B) are significantly older, i.e. they yielded an OSL age of144.6 ± 20.2 ka (OSL-LOIS-9). The OSL-samples that were taken from the loess of log Haimerl (sediment unit LH-3; Fig. 4) yielded ages of 35.8 ± 4.7 ka for the lower (OSL-LOIS-1) and 30.3 ± 4.3 ka for the upper sample (OSL-LOIS-2), respectively.

Table 2:
OSL samples, water content, radionuclide concentrations, dose rates, equivalent doses (De) and luminescence ages. Note that the De values are all based on the Central Age Model (CAM). n represents the number of aliquots accepted and nt the total number of aliquots measured.

Sample	Sed. unit	Sediment type	Water content (%)	n/nt	OD (%)	Th (ppm)	U (ppm)	K (%)	Cosmic (Gy kyr^{-1})	Dose rate (Gy/ka)	De (Gy)	Age (ka)
OSL-LOIS-1	LH-3	Loess	14.7 ± 5	10/24	23 ± 11	7.59 ± 0.34	3.22 ± 0.10	2.08 ± 0.08	0.06 ± 0.01	2.90 ± 0.18	104 ± 12	35.8 ± 4.7
OSL-LOIS-2	LH-3	Loess	14.7 ± 5	11/24	31 ± 11	9.63 ± 0.41	3.15 ± 0.12	2.12 ± 0.08	0.07 ± 0.01	3.05 ± 0.19	92 ± 11	30.3 ± 4.3
OSL-LOIS-3	LS-2b	Sand/Gravel	3.7 ± 5	10/24	35 ± 11	5.68 ± 0.21	1.12 ± 0.06	2.72 ± 0.08	0.09 ± 0.01	3.27 ± 0.22	150 ± 20	45.8 ± 6.9
OSL-LOIS-4	LS-3c	Paleosol	17.6 ± 5	11/24	26 ± 10	9.11 ± 0.33	3.45 ± 0.10	2.35 ± 0.09	0.09 ± 0.01	3.21 ± 0.20	141 ± 15	43.9 ± 5.4
OSL-LOIS-5	LS-3b	Loess	19.1 ± 5	9/24	32 ± 10	9.47 ± 0.32	3.51 ± 0.09	2.11 ± 0.08	0.08 ± 0.01	2.98 ± 0.18	149 ± 18	50.0 ± 6.8
OSL-LOIS-6	LS-3d	Loess	15.8 ± 5	6/48	0	9.40 ± 0.36	2.88 ± 0.10	1.68 ± 0.07	0.10 ± 0.01	2.62 ± 0.16	126 ± 15	48.1 ± 6.5
OSL-LOIS-7	LS-4	Gravel	2.2 ± 5	9/48	24 ± 13	5.10 ± 0.22	1.37 ± 0.06	3.20 ± 0.09	0.12 ± 0.01	3.84 ± 0.26	152 ± 20	39.8 ± 5.8
OSL-LOIS-8	LS-5a	Loess	9.3 ± 5	25/48	35 ± 8	10.30 ± 0.27	3.02 ± 0.08	1.82 ± 0.08	0.14 ± 0.01	3.05 ± 0.19	64 ± 6	21.1 ± 2.4
OSL-LOIS-9	LS-1	Sand/Gravel	2.5 ± 5	8/24	17 ± 15	3.96 ± 0.19	1.51 ± 0.06	1.21 ± 0.05	0.09 ± 0.01	1.88 ± 0.13	272 ± 33	144.6 ± 20.2

5. Discussion

5.1. Optical ages

The 7 OSL-ages from the excavation pit Steininger range from 21.1 to 144.6 ka in age and are in correct chronostratigraphic order (Fig. 6 and 8B; Table 2). The 2 OSL samples from the cellar Wall Haimerl are ca. 30.2 and 35.8 ka in age and – on the outcrop scale – are also in chronostratigraphic order (or at least overlap within error; Fig. 4; Table 2).

The OD values for these 9 OSL samples range from 0% to 35% (Table 2). Many single-grain OSL studies have reported OD values for well bleached sediment samples (e.g. well-bleached aeolian deposits) that are on the order of ~20% (Jacobs et al., 2003; 2006; Olley et al., 2004a, b; Galbraith et al., 2005). However, also significantly higher OD values of up to 40% have been obtained for single grain OSL D_e distributions from well-bleached, unmixed settings (Carr et al., 2007; Demuro et al., 2013; Arnold and Roberts, 2009). For single grain measurements OD values of 20%, or even 25% are often considered as a threshold representing a single- well bleached dose population (Duller, 2008b; Arnold and Roberts, 2009). Since aliquot sizes were small in the current study (20-200 grains per disc) and because quartz from the study site is characterized by relatively low initial signal intensities of a few hundred to thousand counts (with some aliquots even showing no signal at all), it can be assumed that only a few grains per disc contributed to the measured luminescence of an individual aliquot. In the current study the OSL measurements were not conducted on a single-grain level, yet, with the small-aliquot approach followed here, we can rule out large averaging effects of OSL signals. Actually, for aliquots holding only a few tens of grains per discs, pseudo-single grain resolution might be achieved.

The OSL samples from the Loisium wine-world have low signal intensities, causing poor counting statistics during OSL signal detection, ultimately translating into slightly larger errors on D_e estimates and OSL ages than are typical for OSL dating. Typical OSL age uncertainties range from 5 to 10%, while in the current study the relative age uncertainties between ~10 and 14% are typical (Table 2). In consequence, also the uncertainties on the OD values that are calculated from the CAM D_e distributions are relatively high (Table 2).

Considering these relatively large errors on the OD values, almost all samples conform to the 20% OD threshold for well bleached samples, and all samples would confirm with this threshold if an OD value of 25% OD would be chosen. The exceptions are the loess samples OSL-LOIS-5 (OD 32±10%; unit LS-3b) and OSL-LOIS-8 (OD 35±8%; unit LS-5) and the fluvial sample OSL-LOIS-3 (OD 35±11%, unit LS-2b). Generally speaking, this scatter in D_e-values can be caused by different factors such as dose rate heterogeneity, partial bleaching, post-depositional mixing or intrinsic factors such as aberrant OSL behaviour. Numerous studies have shown that fluvial sediments, such as OSL-LOIS-3, can suffer from

partial bleaching (e.g. Murray et al., 1995). Partial bleaching in fluvial settings is the result of limited sunlight exposure of the sediment grains during transport due to the rapidity of the fluvial transport and burial processes in combination with the attenuation of light through the water column (Berger, 1990). Partial bleaching can result in D_e, hence, age overestimation. If partial bleaching is affecting fluvial sample OSL-LOIS-3 (unit LS-2b), it can be supposed that this process is neglectable and did not cause any age overestimation, because (i) no age inversion in the sediment sequence is observed, and (ii) the age of 45.8±6.9 ka of sample OSL-LOIS-3 is concordant with the ages of the overlying loess units LS 3 (i.e. loess LS-3b to d: samples OSL-LOIS-5, 4 and 6; fluvial unit LS-4: sample OSL-LOIS-7; compare Fig. 6, Table 2), suggesting rapid deposition of both units around that time. Hence, it is argued that the CAM OSL age of 45.8±6.9 ka for sample OSL-LOIS-3 taken from the fluvial unit LS-2b is accurate and that the concordant OSL ages of the units LS-2b, LSS-3 and LS-4 reflect rapid deposition of this ~9 thick succession during MIS 3.

For the two loess samples with an OD value beyond the 20-25% threshold for well bleached samples (i.e. OSL-LOIS-5 and OSL-LOIS-8 from the units LS-3b and LS-5, respectively; Fig. 6, Table 2), partial bleaching is not supposed to be a problem, because it can be arguably assumed that during aeolian transport, sediments were exposed to sufficient sunlight to remove any trapped charge from the quartz grains. Hence, other causes should be considered for these elevated OD values, including (i) geological processes that can cause mixing of younger and older sediment units and/or (ii) intrinsic processes, such aberrant OSL properties of some aliquots. Both sedimentary units from which these two OSL samples have been retrieved (i.e. LS-3a and LS-5) are overlain by horizons that indicate soil formation (i.e. paleosol unit LS-3b, top-soil unit LS-5b; Fig. 6). Sample OSL-LOIS-8 from unit LS-5a, was retrieved in relative proximity to the topsoil (~1 m below topsoil unit LS-5B), and bioturbation due to intense long-time agriculture and deep-rooting vine grapes could be an explanation for the above-average OD value of this sample. Bioturbation cannot be invoked for sample OSL-LOIS-5, because it is overlain by the paleosol unit LS-3c that is of approximately the same age as the sediment unit LS-3b from which sample OSL-LOIS-5 has been retrieved (Fig. 6). Another process that might have caused post-depositional mixing and thus affecting sample OSL-LOIS-5 is solifluction which was observed only within the LS-3 succession (see section 5.2). Yet – again – if the stratigraphy and chronology is considered, this would have only caused mixing of similar aged sediments, and thus only partly explain the elevated OD value of this sample. It is thus suggested that dose rate heterogeneity on the micro level (particularly of the beta dose rate e.g. due to the presence of calcite concretions and coatings of quartz grains or the presence and uneven spatial distribution of isolated hot spot minerals such as feldspar) and/or an aberrant OSL behaviour of some aliquots that were not rejected via the quality assurance criteria outlined above, are the most likely causes for the OD value of 32±10% for sample OSL-LOIS-5.

In conclusion the shape of the D_e distributions and their OD values for the majority of OSL samples supports the usage of a CAM for D_e calculation (Table 2). For the three samples with above average OD values (i.e. OSL-LOIS-3: 35±11%; OSL-LOIS-5: 32±10% and OSL-LOIS-8: 35±8%) other processes than partial bleaching are invoked in order to explain these elevated OD values, namely: dose rate heterogeneity and/or aberrant OSL behaviour of some aliquots (in the case of sample OSL-LOIS-3 and OSL-LOIS-5) and bioturbation (sample OSL-LOIS-8). Therefore, also for these samples, it is a fair approximation to use the CAM D_e value of each of these sample for age calculation. Furthermore, the accordance of the optical ages obtained via this approach with known periods of loess deposition in the vicinity of the study area (as outlined below), suggests that the OSL chronology for the Loisium site is robust.

5.2. Sedimentary successions and log correlation

5.2.1 Early Pleistocene fluvial gravels (unit LS-0)

The study site reveals a sedimentary succession that formed via aeolian and fluvial deposition. Several studies from the area around Langenlois describe loess or loess-paleosol successions that are Late Pleistocene in age (e.g. Terhorst et al., 2011; Thiel et al., 2011a, b, c), only few outcrops with loess covering middle to early Pleistocene fluvial gravels and sands exist (e.g. Piffl, 1959; Zöller et al., 1994; Fladerer et al., 2005; Fig. 2). At the Loisium site the stratigraphically lowermost unit is formed by the gravels of unit LS-0, exposed in the outcrops Stein-1 and 2, respectively (Fig. 7 and 8). No OSL samples have been extracted from this coarse-grained sediment unit. With a composition of quartz and crystalline components and a matrix of brown sands, as well as the absence of carbonate, LS-0 has significant similarities with the Danube terrace gravels of the Hochstrassberg terrace, described by Piffl (1959; Gobelsburger Niveau; Fig. 2). Correlating the gravel unit LS-0 with the Hochstrassberg terrace is also supported by the fact that unit LS-0 and the terrace gravels are both situated at an altitude of ~230 m a.s.l. The sandstones or marlstones within LS-0 might originate from the Palaeozoic sediments of the Zöbing formation that is preserved just north of the study site, indicating an influence of the river Kamp that drains the region north of Langenlois (Fig. 2). Piffl, 1959 estimated the Hochstrassberg terrace level to be early Pleistocene in age, based on its morpho-stratigraphic position in the wider Krems-Langenlois area. The overlying sands of unit LS-1 have an optical age of ~145 ka and are thus significantly younger. If the gravel unit LS-0 is equivalent to the Hochstrassberg terrace gravels and the assignment of the Hochstrassberg terrace to the Early Pleistocene is correct, a significant hiatus in between both units must be assumed (Fig. 13).

5.2.2 Riss Glacial sedimentation (fluvial sediment succession LS-1)

With an optical age of 144.6±20.6 ka of sample OSL-LOIS-9 the deposition of the fluvial sediment succession LS-1 can be assigned to the MIS 6 (Riss glacial; Fig. 8B and 13). The lithological composition of the fluvial components suggests a large catchment area within the Bohemian massif, thus, unit LS-1 is supposed to be deposited by the river Kamp. No sediments are exposed of the subsequent periods MIS 5 and 4 in the excavation pit Steininger or the Loisium cellar complex (Fig. 13). An erosional unconformity on top of unit LS-1 indicates an erosional phase which might have removed any deposits of these time periods. Tectonic processes, which are documented as normal faults within units LS-0 and LS-1 (Fig. 8), are supposed to have intensified or even facilitated the formation of that erosional relief.

The rest of the sediment succession investigated at the Loisium site is dated into significantly younger time intervals (Fig. 13). The details regarding chronostratigraphic relation and the paleoenvironmental significance of individual sediment units are outlined in the following. Here, it is just noted that (i) the stratigraphically higher units LS-2 to LS-4 exposed in log Steininger (Fig. 6) and the related outcrop Stein-1 (Fig. 7) are overlapping within error and have a weighted mean age of 45.3±4.0 ka, placing them into the MIS 3 and (ii) the loess units LH-3 (log Haimerl; OSL-LOIS-1 and 2; Fig. 4) and LS-5 (OSL-LOIS-8; Fig. 6) are even younger and were, according to their OSL ages, deposited at the end of the MIS 3 and during the LGM, respectively (Fig. 13).

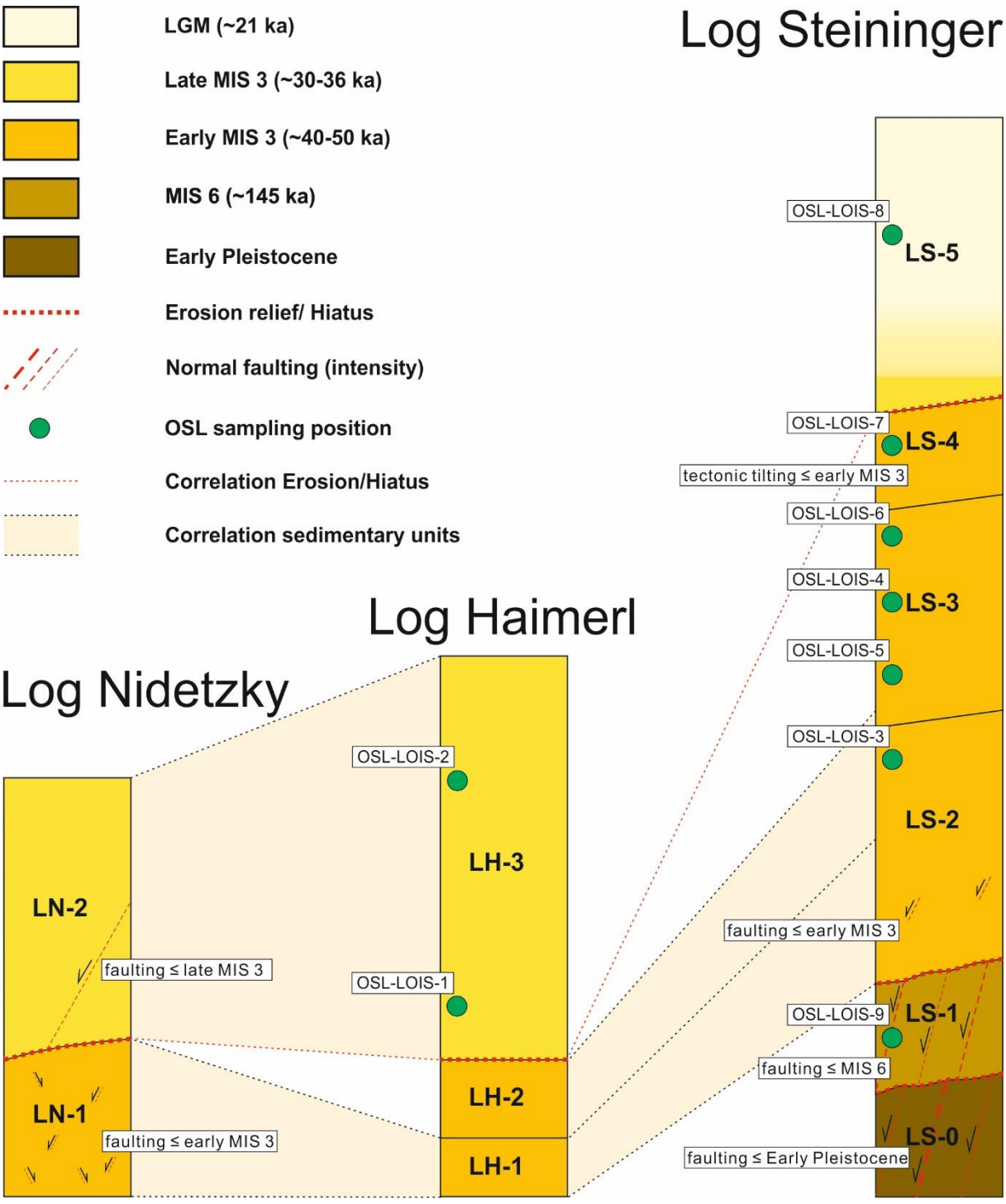

Fig. 13: Schematic chrono- and lithostratigraphic correlation of the sedimentary units and their unconformities (compare Figs. 3, 4, 5 and 6 for sediment logs). The colour-coding indicates the age of the sediment units and is based on luminescence dating (i.e. MIS 6, 3 and LGM units) or lithostratigraphic correlation with the Early Pleistocene Hochstrassberg Danube terrace gravels. For unit LS-5 a colour gradient from bright yellow to pale yellow has been chosen to indicate a possible continuous loess deposition from late MIS 3 to the LGM (see text for details). Also, the faulting intensity is schematically depicted in this figure. Note that the logs are not drawn to scale to facilitate correlation.

5.2.3 Early sedimentation phase during MIS 3 (units LS-2 to 4; LN-1; LH-1 and 2)

In this section sediment units from the earlier depositional phase of MIS 3 are examined and all litho- and chronostratigraphic correlations are made and discussed that fall into this time period.

As outlined above (section 4.1.), the fine-grained sediment unit LS-2a that was deposited on top of LS-1 can be correlated stratigraphically with the fine-grained units LH-1 in log Haimerl and LN-1 in log Nidetzky, based on their granulometric and mineralogical properties (Fig. 4, 5, 6 and 13). The only significant difference lies in the carbonate content. While LH-1 is carbonate-free and LS-2a contains only traces of calcite, the clays of log Nidetzky reveal upward decreasing carbonate concentrations from 15 to 2 wt.%. This is presumably the result of secondary carbonate solution within the uppermost parts of the layer. Correlation of these three fine-grained sediment units can also be established based on their similar depth below the ground surface of ~11 m. No OSL-samples were extracted from either of these units (LS-2a, LH-1 and LN-1).

The next stratigraphically higher unit is LS-2b, which has an OSL age of ~46 ka (Fig. 6). The continuous sedimentary transition of LS-2a into LS-2b suggests that both sedimentary units are of similar age, i.e. belong into the MIS 3. Consequently, the fine-grained sediment units LH-1 and LN-1 of the logs Haimerl and Nidetzky that correlate with unit LS-2a in the log Steininger should have been deposited during MIS 3 too (Fig. 13).

Another stratigraphic correlation between the sediment units in the log Steininger and the log Haimerl can be established. The fluvial gravel and sand units LS-2b (log Steininger; Fig. 6) and LH-2 (log Haimerl; Fig. 4) are correlated based on their (i) same stratigraphic position, (ii) similar depth below the ground surface (~10 m) and (iii) identical facies (Fig. 13). However, the mineralogy divers slightly between both units (Fig. 3 and 5), which is attributed to the variable granulometry that is a typical phenomenon in fluvial deposits. Unit LS-2b is sand-dominated, thus, has a higher content of phyllosilicates and contains less quartz and feldspar whereas unit LH-2 is more gravelly and mineralogically thus quartz and feldspar dominated. Interestingly, no equivalent to these two fluvial sediment units is present in log Nidetzky (Fig. 5).

In the log Steininger a further fluvial unit exits, i.e. the gravel unit LS-4 (Fig. 6). Sedimentologically these gravels cannot be correlated with any of the other gravel layers of the Loisium site. Although the grain size distribution and mineralogy of LS-4 are comparable with the fluvial sediments LH-2 of log Haimerl (Fig. 4), these gravel units differ from each other in terms of the lithological composition of the coarser gravel components. Unit LH-2 contains well-rounded quartz-rich components with only a few gneiss lithoclasts, while unit LS-4 is composed of poorly rounded local granite-gneisses that are weathered more intensively compared to unit LH-2. The gravels of LS-4 were thus most likely deposited by the local river Loisbach (Fig. 1).

Five loess units were identified in the various outcrops of the Loisium site, namely LN-2 in the cellar wall Nidetzky (Fig. 5), LH-3 in cellar wall Haimerl (Fig. 4), and LS-3b, 3d and 5a in the excavation pit Steininger – outcrop Stein-1 (Fig. 6).

In the sediment log Steininger the stratigraphically lowermost loess succession is LS-3 (Fig. 6). The loess dates into the early part of the MIS 3, i.e. the OSL ages of the units LS-3b, c and d range from ~50 to 48 ka (Fig. 6 and 13). Unit LS-3c is interpreted as reworked soil sediments that developed during a short interstadial with warmer and more humid climatic conditions compared to the time periods during which loess accumulated (compare section 4.1). The reddish-brown slabs of paleosol are sandwiched into the loess units LS-3b and d. These loess units contain Ca-concretions that are

interpreted as remnants of a Ca-horizon from the former soil (i.e. LS-3c). LS-3c is tilted at 13-17° relatively to the other sediment units, suggesting that the paleosol formed on a pre-existing topographic relief (Fig. 7B). The observation that this paleosol is not continuous but only preserved as isolated slabs of loam swimming in a matrix of loess indicates that an additional process caused fragmentation. Gravity driven slope processes such as soil creep are the most plausible explanation for the observed soil fragmentation, and it is likely that this mass wasting process occurred under permafrost conditions (solifluction) during the subsequent cooling phase that also caused deposition of the loess unit LS-3d. Importantly, and despite the remnant nature of this paleosol encountered in unit LS-3c, the presence of such a well-developed soil suggests that the MIS 3 loess succession at the Loisium site also records a prolonged interstadial.

Remnants of a paleosol can also be found in subunit LS-3a (Fig. 6). The reddish spotted loam of the subunit LS-3a might indicate a second, older interstadial dating into early MIS 3 (Fig. 13). It is speculated that another soil horizon previously existed and was thinned out and fragmented via periglacial processes during subsequent stadial conditions.

5.2.4 Regional comparison of early MIS 3 sedimentation patterns

In the brickyard of Langenlois ~1 km southwest of the Loisium (Fig. 1C) Thiel et al. (2011c) encountered a loess deposit that has been IRSL dated by these authors to ~55-35 ka using feldspars as dosimeters (their profile LB 5). Thiel et al. (2011c) also pointed out that (i) apart from 3 cryosol horizons, no distinct paleosol was discernable within this ~5 m thick and 55-35 ka old loess package and (ii) the LGM loess was lacking altogether in the brickyard Langenlois. These findings contrast with the observations made at the Loisium site, where (i) the MIS 3 loess does contain a paleosol, albeit erosionally fragmented and (ii) the LGM loess is preserved in the form of a ~3m thick aeolian cover sheet (see section 5.2.6). Although the MIS 3 loess packages in the Langenlois brickyard and the Loisium are thick (i.e. ~5 and ~3 m in the brickyard and the Loisium, respectively) and thus the temporal resolution of these sediment successions relatively high, the precision on the individual IRSL and OSL ages is too low to allow for an exact chronostratigraphic correlation of individual layers between both sites or to resolve individual MIS 3 stadials and interstadials.

However, despite this insufficient chronological resolution a tentative correlation between specific sediment units of both sites, based on sedimentological criteria might be attempted. It is suggested that the paleosol unit LS-3c of the Loisium site and the unit LB 5/12 of the Langenlois brickyard can be correlated. Although soil formation was not observed in the unit LB 5/12 the following similarities between both units exist that support such a tentative correlation (i) the inclination of the layer, (ii) evidence for permafrost formation (cryosol on top of LB 5/12, fragmentation of LS-3c) subsequent to the soil formation, and (iii) higher contents of clay and sand, and lower values of silt in both unit LS-3c and LB 5/12 compared to the loess into which these units are integrated (Thiel et al., 2011c; Fig. 6).

5.2.5 Late sedimentation phase during MIS 3 (unit LH-3)

In this section sediment units from the earlier depositional phase of MIS 3 are examined.

The two OSL samples from the loess unit LH-3 of log Haimerl yielded ages of ~35.8±4.7 and 30.3±4.3 ka, respectively and thus fall into the final stage of the MIS 3 (Fig. 4 and 13). Loess from the final phase of the MIS 3 was dated in numerous sites within the area of Krems and Langenlois, e.g. in Langenlois (Thiel et al., 2011c), Stratzing (Thiel et al., 2011a), Göttweig-Aigen (Thiel et al, 2011b), and at the Wachtberg site in Krems (Lomax et al., 2014; Fig. 1B). The widespread distribution of late MIS 3 loess indicates intense loess deposition during that period, as already stated by Terhorst et al. (2011). As far as the stratigraphic situation in the log Haimerl is concerned, late MIS 3 loess (unit LH-3, OSL

dated) is lying on top of the early MIS 3 gravels (LH-2, chronostratigraphically correlated with the OSL dated sediment unit LS-2 in log Steininger; Fig. 13). This implies that in log Haimerl the loess succession LS-3 and the LS-4 gravels are absent, which is argued with an erosional phase during MIS 3 (see section 5.2.8; Fig. 13).

5.2.6 Sedimentation during the LGM

In this section, sedimentation during the LGM is examined. The LGM is defined as the time period with the largest ice extent during the last glaciation. It is necessary to distinguish between the global LGM and local last glacial maxima. Global LGM can be constrained to 26.5 to 19 ka by sea level lowstand (Clark et al., 2009). In the Eastern Alps very cold climate prevailed between 31 and 21 ka BP, yet glacial maximum wasn't reached until 24 ka BP and lasted 3000-4000 years (Van Husen, 1997).

The youngest loess exposed at the study site is unit LS-5a (Fig. 6). It was OSL-dated to ~21 ka and thus accumulated during the LGM (Fig. 13). Unit LS-5a is characterised by a distinct grain size distribution, i.e. it is silt dominated (total silt content ~71 wt.%; Fig. 6) with a coarse silt fraction of ~50 wt.% of the total sample (Annex – mineralogical and sedimentological results). These are the highest silt concentrations in all investigated loess units at the Loisium site.

In the Krems-Langenlois area the absence of the LGM loess was demonstrated in various sites by OSL/TL-dating (e.g. Paudorf & Göttweig-Furth, Zöller et al., 1994; Stratzing, Thiel et al., 2011a; Langenlois, Thiel et al., 2011c; Fig. 1B) and micromorphological investigations (e.g. in the north-western Weinviertel area (~30 km north-east of Langenlois; Havliček et al., 1998). Only few sites exhibit LGM loess (e.g. the Wachtberg site in Krems, Lomax et al., 2014). The paucity of LGM loess at the south-eastern margin of the Bohemian massif (i.e. the Krems-Langenlois area) has been explained via extensive Upper Pleistocene erosion in this region (Havliček et al., 1998; Thiel et al., 2011c). The presence of LGM loess in log Steininger is thus unique for this region and suggests local preservation of these loess deposits during peak glacial conditions at the study site.

A correlation of the loess unit LN-2 of log Nidetzky (Fig. 5) is difficult. On the one hand, chronological data is not available for LN-2. On the other hand, grain size distribution and mineralogy vary within the outcrop and show similarities with either of the other investigated loess units of the study site (Fig. 4, 5 and 6). However, distinctive patterns can be pointed out: (i) grain size distribution indicates an upwards decreasing sand content, and (ii) the loess was deposited on top of an erosional relief (i.e. LN-1; Fig. 13). Both patterns were also demonstrated for the loess unit LH-3 in outcrop Haimerl, thus correlation of unit LN-1 with the loess unit LH-3 seems appropriate (Fig. 13).

The same situation of loess deposition on top of an erosional relief and an upwards decreasing sand content was observed for loess unit LS-5a (Fig. 6 and 7B). Anyways, late MIS 3 loess (such as the LH-3 unit) was not encountered in log Steininger (Fig. 6 and 13). This might be the result of the OSL sampling resolution that was too coarse to resolve an MIS 3 loess layer. If so, there might have been continuous loess sedimentation from late MIS 3 to the LGM, as observed at the Wachtberg situated ~11 km southwest of the Loisium site by Lomax et al. (2014; Fig. 13). Alternatively, erosional processes might have removed the MIS 3 loess layer within log Steininger, which did not affect LH-3 since the latter was preserved in an erosional channel.

5.2.7 Holocene soil formation

The topsoil layer LS-5b (Fig. 6) formed during the Holocene and was classified as a Tschernosem according to the soil classification scheme of the Austrian soil science society (Fink, 1969). In this topsoil remnants of pottery and bones of a domestic cat were found. These observations and charcoal with a calibrated 14C-age of 378±69 cal BP indicates recent anthropogenic pedoturbation of the topmost meter of this topsoil layer.

5.2.8 Erosional processes

Several erosional features and hiati were observed within the outcrops of the study site and suggest different erosional phases that affected the depositional setting. These unconformities are shown in Fig. 13 and discussed in this section.

The oldest hiatus is observed in the excavation pit Steininger (Stein-1 and 2) where unit LS-0 (correlated with the Early Pleistocene) is overlain by the sand unit LS-1 (OSL dated to MIS 6; Fig. 13). Thus, an erosional event during, or previous to MIS 6 must have removed any other deposits of the Early to Middle Pleistocene.

A second hiatus is present in between LS-1 (MIS 6) and LS-2a (MIS 3; Fig. 6). The absence of sediments indicates an erosional phase which might have removed any deposits of MIS 4 and 5. This erosional event matches the sediment pattern of the Krems-Langenlois region, where the absence of sediments between ~55 ka and ~106 ka was registered in several sites (e.g. Stratzing (Thiel et al., 2011a), Paudorf and Göttweig-Aigen (Thiel et al., 2011b)) and was linked with long lasting and intensive erosion processes (Terhorst et al., 2014).

An erosional unconformity can be recognised in the outcrop Stein-1 (Fig. 7B), where the fluvial-aeolian succession LS-1 to LS-4 is incised down to LS-2b and this erosional relief is levelled out with loess from the LGM (unit LS-5a). This erosional event must have occurred subsequent to ca. 40±6 ka, i.e. after deposition of the OSL dated unit LS-4. If the hypothesis of continuous sedimentation from late MIS 3 to LGM is pursued, the erosional relief of Stein-1 can be correlated with the hiatus of log Haimerl between LH-2 and LH-3 (compare section 5.2.5; Fig. 13). The erosional event that occurred subsequent to ~40 ka might have caused the sharp erosional unconformity in the Nidetzky outcrop too and probably removed any fluvial material equivalent to unit LS-2b that might have been present in the Nidetzky area originally (Fig. 5).

5.3. Neotectonic activity

Several tectonic features were observed within the Quaternary sediments of the study site, including high angle normal faults and fault striation (Fig. 7, 8 and 9). Furthermore, also the tilting of the sedimentary succession LS-1 to LS-4 in outcrop Stein-1 could have a tectonic origin too (Fig. 7 and 9). Tectonic faults were already encountered in the corridors linking the Loisium vine shop with the Haimerl cellar during construction work in 2003. There, normal faults dipping 230/70 and 220/50 (i.e. steeply towards south-west) were observed by R. Roetzel (Roetzel et al., 2018; Fig. 3A and C and fault planes “Roetzel et al., 2018” in Fig. 9C).

We suggest a tectonic rather than a gravitational origin of these structures for the following reasons: (i) karst features were described for the Hollenburg Karlstetten formation (e.g. smaller caves in Rohrendorf; Kobloch, 1980) and subsurface carbonate dissolution could cause local sagging

phenomena. There is a possibility that the Loisium site is underlain by the Hollenburg Karlstetten formation, rather than the crystalline basement of the Bohemian massif (Fig. 2). However, such dissolution and sagging processes would rather cause circular doline-like structures that are not compatible with the spatial distribution and orientation of the observed faults. A karst origin for the Loisium faults and for the large-scale tilting of entire sediment succession are therefore excluded; (ii) the Loisbach river is bounding the investigation site in the south. This small river is incised into the quaternary sediments by ~10 m. River bank and valley slope instabilities could cause localized south-facing translational or rotational faults. Again, the orientation of the Loisium faults and tilting of the sedimentary layers (see Fig. 9C) are clearly incompatible with such a gravitational mass wasting scenario.

In outcrop Stein-2 normal faulting occurred in the old gravels and sands of units LS-0 and LS-1 (Fig. 8 and fault planes "Stein-2" in Fig. 9C). A major normal fault dipping northwest is separating LS-0 from LS-1 (indicated with a red thick line in Fig. 8B). Numerous normal faults occur in unit LS-1 and cause a cumulative minimum offset of 2 m (Fig. 8). This offset displaces the unit LS-0 from LS-1 and fragmented unit LS-1 causing its stepwise displacement towards northwest.

In the outcrop Stein-1 faulting was not directly observed within units LS-0 and LS-1 but is strongly suggested since unit LS-1 and the underlying unit LS-0 are exposed ~3 m below ground surface in the central part of outcrop Stein-1, whereas ~10 m to the west unit LS-1 was recorded ~11.5 m below ground surface in sediment log Steininger (Fig. 7). Thus, a major high-angle normal fault with an offset of >8.5 m is proposed to separate the fluvial LS-0 and LS-1 sediments from the central part of the outcrop Stein-1 to the west (Fig. 7A & B). This fault is indicated in red in Fig. 7B and not directly observed but based on stratigraphic considerations. The fault is assigned to the south-west dipping fault set. This is suggested since the fault lies in the extension of the south-west dipping faults observed by Roetzel et al. (2018; Fig. 3A & C, fault planes "Roetzel et al (2018)" in Fig. 9). Furthermore, the outcrop Stein-1 lies ~10 m north of the faults in outcrop Stein-2 (stepwise displacing units LS-0 and LS-1 downward towards northwest; Fig. 3 & 8) and the south-western dip direction could explain the reoccurrence of LS-0 and LS-1 in outcrop Stein-1 close to the ground surface (Fig. 14).

Also, the sediment unit LN-1 of the cellar wall Nidetzky reveals normal faults dipping in south-western direction (Fig. 9B and fault planes "Nidetzky" in Fig. 9C). It is supposed that the north-west dipping faults and the south-west dipping faults form a conjugated fault set which generated a local depression in excavation pit Steininger where sediment units LS-2 to LS-4 were deposited into (Fig. 14).

A similar situation was documented in Gobelsburg ~2 km south of the study site by Piffl (1959). He described continuous downward displacement of gravels of the Gobelsburger level (i.e. the Early Pleistocene Hochstrassberg terrace) in south-western direction with younger loess sediments overlying the offset gravels in the southwestern extension of the outcrop, but made no further description of the tectonic structures or deduced tectonic processes or kinematics from these outcrops.

The depositional age of the fluvial unit LS-0 has been tentatively assigned to the Early Pleistocene based on lithostratigrahic correlation, while LS-1 has been OSL dated to MIS 6 (Fig. 13). Normal faulting appears to affect fluvial units LS-0 and LS-1 more intensively than other sedimentary units at the Loisium site. The number of faults and the absolute displacement in these two units is an order of

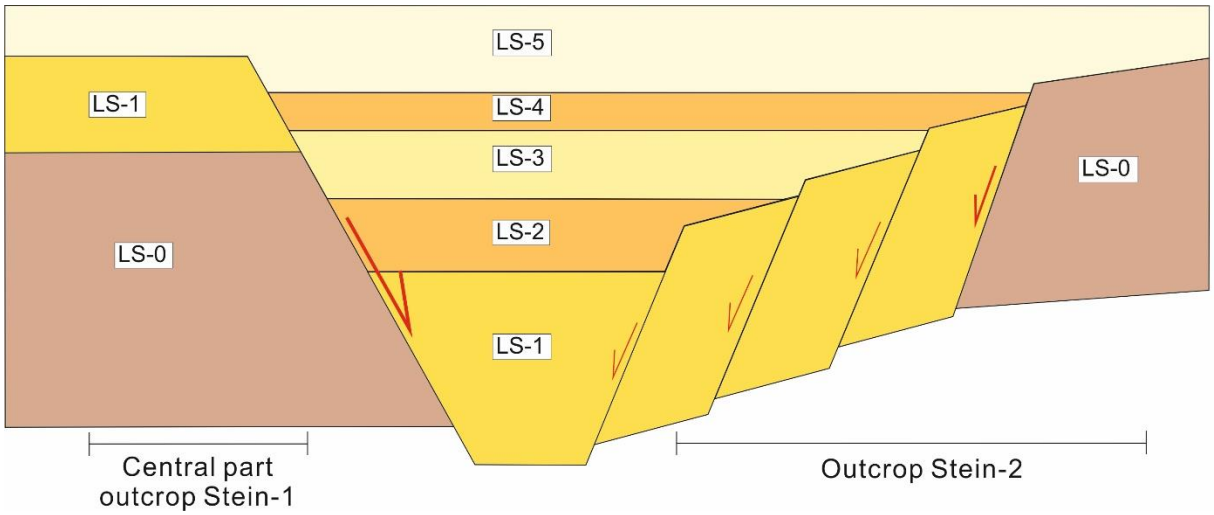

Fig. 14: Sketch of a north-south profile through the outcrop Stein-2 and the central part of outcrop Stein-1 (the reader's view is to the east). Note the tectonic depression formed by conjugated faulting of sediment units LS-0 and LS-1 and backfilled by sediment units LS-2 to LS-5. The offset of the faults is comparatively indicated.

magnitude larger than in other sediment units further up-section (Fig. 13); i.e. for these two units ≥8.5 m of displacement are observed in outcrop Stein-1 (Fig. 6A & B) and >2 m in outcrop Stein-2 (Fig. 7).

The overlying early MIS 3 units LS-2 and LN-1 reveal only minor normal faulting (scattered faults with up to 5-10 cm of displacement; Fig. 9A and 13). A fault within unit LN-2 (late MIS 3 deposit) indicates higher displacement of a few dm through up-dragged gravel components (Fig. 5). However, determination of exact offset values for the fault remains impossible due to the absence of marker horizons.

The stratigraphically upwards decreasing effect of tectonism suggests that faults did not arise from a single event, but from continuous tectonic activity over a prolonged period of time. However, establishing the exact displacement values, faulting history and earthquake recurrence rates from the current set of observations remains difficult for several reasons. Firstly, constraining these tectonic structures in time is challenging, since direct dating of these faults is not possible. Furthermore, on some faults we likely observe the cumulative slip from several seismic faulting events, which is probably particularly true for those faults with very large (m-scale) displacement (SW dipping fault in outcrop Stein-1 (Fig. 7A & B) and NW dipping faults in outcrop Stein-2 (Fig. 8)). It is actually very unlikely for the tectonic setting of the Loisium site (i.e. at the margin of the Bohemian massif) that such very large displacements result from a single rupturing event, because this would imply incredibly large earthquake magnitudes. It is more likely that these large displacements are the combined result of multiple slipping events and an eventually additional unknown aseismic component. Deciphering these coseismic from post-seismic slipping components along these faults cannot be easily resolve with our current set of observations.

Despite these difficulties, (and assuming coseismic displacement), the age of the faulted layers can be interpreted as a maximum age for the tectonic activity causing these faults (Fig. 13). Since loess of log Nidetzky (LN-2) is correlated with unit LH-3 (Fig. 13), faults within LN-2 suggest neotectonic activity at the Loisium site subsequent to 30.3±4.3 ka. The tilting of the fluvial-aeolian succession (LS-1 to LS-4; Fig. 7A & B) is best explained as the effect of tectonic extension and subsidence. Thus, tectonic processes must have continued after the deposition of the gravel layer LS-4 (~40 ka). Younger tectonic structures could not be detected at the study site.

It appears likely that the DDF operates as the regional tectonic structure that is controlling normal faulting of the sedimentary units in the study area (Fig. 15). Although, the region of Langenlois appears to be tectonically inactive on a first sight, brittle deformation and subsidence of buildings and the natural ground surface actually suggest ongoing movement along the DDF also in recent history (Roštínský et al., 2013; Figdor & Scheidegger, 1977). The geological map (Fig. 2) shows that the main fault line of the DDF is trending NE-SW and splitting into two fault segments ~7 km north-east of the town of Zöbing. These two fault branches disappear under quaternary sediments just before the village of Langenlois (Fig. 2). The main as well as these secondary fault branches all reveal a sinistral strike-slip kinematic (Fig. 2). A direction change of the northern fault branch from NE-SW to N-S could cause strike-slip transtension in the Langenlois region and form a pull-apart basin in the study area. The model of a pull-apart basin is schematically presented in Fig. 15 and the possible trace of this northern sub-branch of the DDF is depicted in Fig. 2 (dashed red line). If this model of a pull-apart basin induced by fault segmentation and strike-slip transtension in the Langenlois area is correct, the faults observed at the study site would best be interpreted as a set of conjugated antithetic normal faults relative to the DDF (Fig. 9C and 14). However, more investigation on different outcrops in the Krems-Langenlois region are required to verify the tectonic model of a pull-apart basin. Not only the quaternary sediments, but also the Miocene sediments of the Hollenburg-Karlstetten formation and the basement rocks of the Bohemian massif should exhibit evidence for the proposed model.

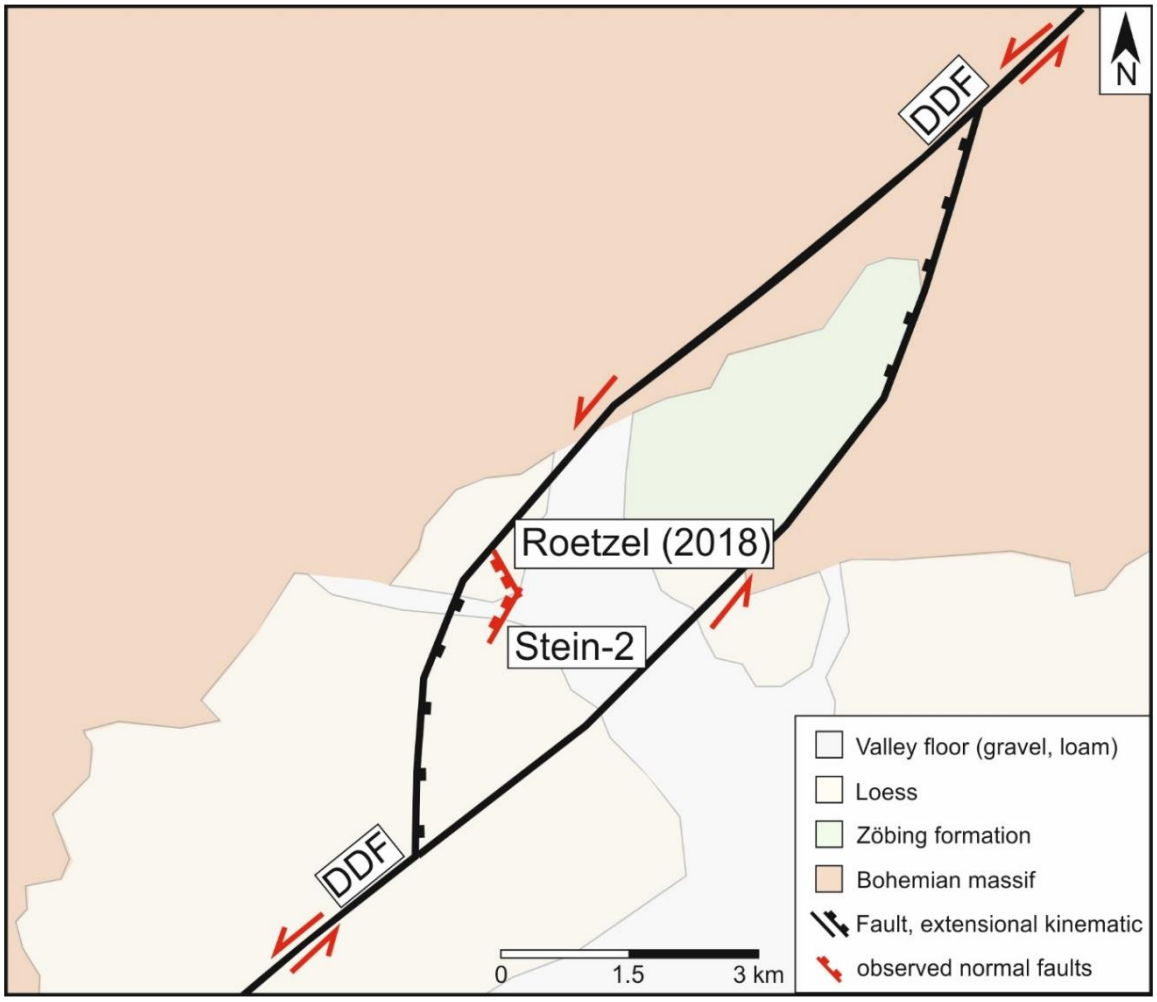

Fig. 15: Sketch of a pull-apart basin in the Langenlois area. The normal faults observed at the study site are indicated in the figure (not drawn to scale).

Summary and conclusions

In this study sediments exposed in the cellar walls of the Loisium wine-world and temporarily accessible during construction work in an adjacent excavation pit were investigated. Mineralogical and sedimentological analyses, as well as OSL-dating of quartz were conducted which allowed correlation of sedimentary units across different outcrops and sediment logs of the study site. Furthermore, chronostratigraphic correlations with loess layers in the vicinity of Langenlois described by other authors in previous studies have been attempted too.

The sediment succession at the Loisium site reveals alternating episodes of fluvial and aeolian deposition as well as periods of pedogenesis. Erosional phases formed unconformities. Tectonic faulting might have amplified the relief locally and thus enhanced erosional and depositional processes. Such, at least partly fault-related depressions were back-filled with younger sediments and created a complex and laterally highly variable sediment pattern in the Loisium area.

OSL dating revealed 3 main periods of loess deposition dated to the LGM (~21 ka) and to the late (~30-36 ka) and early MIS 3 (~48-50 ka), respectively. These phases of loess accumulation are in accordance with phases for loess deposition established for several sites in the wider Krems-Langenlois area, including an IRSL dated loess sequence in the Langenlois brickyard, situated just a few km south of the study site. The early MIS 3 loess unit at the study site shows a well-developed paleosol, which has been affected by solifluction and is thus only preserved as fragmented slabs. Correlation of the MIS 3 sediments with a sediment succession in a brickyard just south of Langenlois suggests that these aeolian phases are not restricted to the sediments of the study site but had at least local extents.

The loess-paleosol succession of the Loisium site overlies fluvial sediments which were OSL dated to MIS 6 (~145 ka). MIS 3 and 6 sediments at the study site are resting on fluvial gravels, which were correlated with the Danube terraces of the Hochstrassberg. This terrace has been assigned to the Early Pleistocene by Piffl (1959).

Normal faults were recorded in the lower stratigraphic units (Early Pleistocene to late MIS 3) and reveal a stepwise displacement towards northwest and southwest. Within the outcrops a total displacement of >12.5 meters was observed, which is interpreted as the combined result of multiple slipping events. Intensity of faulting is high in the Early Pleistocene to Middle Pleistocene units (LS-0 and LS-1) and appears to decrease up-section (i.e. early and late MIS 3 units). Together with west to northwest tilting of the early MIS 3 sediments (LS-2 to LS-4), they document continuous tectonic activity lasting from the early Pleistocene to at least ~30 ka. The normal faults observed in the cellar wall of the Loisium and the excavation pit are interpreted as a conjugated set of antithetic normal faults that are kinematically linked to the sinistral Diendorf strike-slip fault. It is suggested that the splitting of the DDF northwest of the town of Zöbing induces a transtensional strike-slip regime and forms a pull-apart basin in the Langenlois area.

The data generated in the course of this study provide genuine insights into the quaternary tectonic activity of the DDF. Although only few and very localized chronological and structural data was retrieved in this study, it provides a first step in deciphering the complex tectonic setting of the Langenlois area and allows to propose a model of a pull-apart basin. To specify the related tectonic kinematics more data of the region is needed to reliably constrain the corresponding stress field and reconstruct movements along the branches of the DDF.

References

Aitken, M.J., 1998. An Introduction to Optical Dating: The Dating of Quaternary Sediments by the use of Photon-stimulated Luminescence. Oxford University Press, Oxford, 267 pp.

Arnold, L.J. & Roberts, R.G., 2009. Stochastic modelling of multi-grain equivalent dose (D_e) distributions: Implications for OSL dating of sediment mixtures. Quaternary Geochronology 4, 204-230.

Bailey, R.M., 2003. Paper II: The interpretation of measurement-time-dependent single-aliquot equivalent-dose estimates using predictions from a simple empirical model. Radiation Measurements 37, 685-691.

Bailey, R.M., Smith, B.W. & Rhodes, E.J., 1997. Partial bleaching and the decay form characteristics of quartz OSL. Radiation Measurements 27, 123-136.

Berger, G.W., 1990. Effectiveness of natural zeroing of the thermoluminescence in sediments. Journal of Geophysical Research 95, 12,375– 12,397.

Bøtter-Jensen, Andersen, C.E., Duller, G.A.T. & Murray, A.S., 2003. Developments in radiation, stimulation and observation facilities in luminescence measurements. Radiation Measurements, 37, 535-541.

Bøtter-Jensen, L., Duller, G.A.T., Murray, A.S. & Banerjee, D., 1999. Blue light emitting diodes for optical stimulation of quartz in retrospective dosimetry and dating. Radiat. Prot. Dosim. 84, 335-340.

Brandtner, F., 1954. Jungpleistozäner Löß und fossile Böden in Österreich. Eiszeitalter und Gegenwart, 4 (5), 49–82.

Brandtner, F. 1956. Lößstratigraphie und paläolithische Kulturabfolge in Niederösterreich und den angrenzenden Gebieten (Zugleich ein Beitrag zur Frage der Würmgliederung). E&G - Quaternary Sci. J., 7, 127-175.

Brennan, B.J., 2003. Beta dose to spherical grains. Radiat. Meas., 37, 299-303.

Brennan, B.J., Lyons, R.G. & Phillips, S.W., 1991. Attenuation of alpha particle track dose for spherical grains. Int. J. Rad. Appl. Instrum. D, 18, 249-253.

Brock, F., Higham, T., Ditchfield, P. & Bronk Ramsey, C., 2010. Current pretreatment methods for AMS radiocarbon dating at the Oxford radiocarbon accelerator Unit (Orau). Radiocarbon, 52, 103-112.

Buylaert, J.-P., Jain, M., Murray, A.S., Thomsen, K.J., Thiel, C. & Sohbati, R., 2012. A robust feldspar luminescence dating method for Middle and Late Pleistocene sediments. Boreas, 41, 435-451.

Carr, A.S., Bateman, M.D. & Holmes, P.J., 2007. Developing a 150 ka luminescence chronology for the barrier dunes of the southern Cape, South Africa. Quaternary Geochronology 2, 110-116.

Clark, P.U., Dyke, A.S., Shakun, J.D., Carlson, A.E., Clark, J., Wohlfarth, B., Mitrovica, J.X., Hostetler, S.W. & McCabe, A.M., 2009. The Last Glacial Maximum. Science 325, 710-714.

Cordier, S., Adamson, K., Delmas, M., Calvet, M. & Harmand, D., 2017. Of ice and water: Quaternary fluvial response to glacial forcing. Quaternary Science Reviews, 166, 57-73.

Cunningham, A.C. & Wallinga, J., 2010. Selection of integration time intervals for quartz OSL decay curves. Quat. Geochronol. 5, 657-666.

Demuro, M., Arnold, L.J., Froese, D.G. & Roberts, R.G., 2013. OSL dating of loess deposits bracketing Sheep Creek tephra beds, northwest Canada: Dim and problematic single-grain OSL characteristics and their effect on multi-grain age estimates. Quaternary Geochronology 15, 67-87.

Duller, G.A.T., 2008. Luminescence Dating: Guidelines in Using Luminescence Dating in Archaeology. English Heritage, Swindon.

Duller, G.A.T., 2008. Single-grain optical dating of Quaternary sediments: why aliquot size matters in luminescence dating. Boreas, 37, 589-612.

Einwögerer, T., Friesinger, H., Händel, M., Neugebauer-Maresch, C. & Simon, U., 2006. Upper Palaeolithic infant burials. Decorations on the bodies of newborns indicate that they were probably important in their community. Nature 444, 285.

Frechen, M., Oches, E.A. & Kohfeld, K.E., 2003. Loess in Europe - mass accumulation rates during the last glacial period. Quaternary Science Reviews 22, 1835-1857.

Figdor, H. & Scheidegger, A.E., 1977. Geophysikalische Untersuchungen an der Diendorfer Störung. Verh. Geol. B.-A. 1977, 243-270.

Fink, J., 1954. Die fossilen Böden im österreichischen Löß. Quartär 6, 85–108.

Fink, J., 1956. Zur Korrelation der Terrassen und Lösse in Österreich. E&G - Quaternary Sci. J., 7, 49-77.

Fink, J., 1969. Nomenklatur und Systematik der Bodentypen Österreichs. Mitteilungen der Österreichischen Bodenkundlichen Gesellschaft, Heft 13.

Fink, J., 1976. Exkursion durch den österreichischen Teil des nördlichen Alpenvorlandes und den Donauraum zwischen Krems und Wiener Pforte. Erweiterter Führer zur Exkursion aus Anlass der 2. Tagung der IGCP-Projektgruppe "Quaternary Glaciations in the Northern Hemisphere. Mitteilungen der Kommission für Quartärforschung der Österreichischen Akademie der Wissenschaften 1, 1-113.

Fink, J. & Kukla, G. J., 1977. Pleistocene climates in central Europe: At least 17 interglacials after the Olduvai Event. Quaternary Research 7 (3), 363-371.

Fladerer, F.A., Havlíček, P., Roetzel, R., Salcher, T., Smolíková, L. & Tuzar, J., 2005. Der Steppenwisentfund (Bison priscus) von Langenlois-Buriweg, Niederösterreich - Paläontologische und pleistozänstratigrafische Untersuchungen. Mitt. Komm. Quartärforsch. Österr. Akad. Wiss., 14, 29-40., 14, 29-40, Wien.

Fuchs, W., 1972. Tertiär und Quartär am Südostrand des Dunkelsteiner Waldes. Jb. Geol. Bundesanst., 115, 205-245, Wien.

Fuchs, W., Grill, R., Matura, A. & Vasicek, W., 1984. Geologische Karte der Republik Österreich 1:50.000, Blatt 38, Krems, Wien (Geol. Bundesanst.).

Füchtbauer, H., 1959. Zur Nomenklatur der Sedimentgesteine. Erdöl und Kohle, 12/8, 605-613, Hamburg.

Galbraith, R.F., Roberts, R.G., Laslett, G.M., Yoshida, H. & Olley, J.M., 1999. Optical dating of single and multiple grains of quartz from Jinmium rock shelter, northern Australia: part I, experimental design and statistical models. Archaeometry, 41, 339-364.

Galbraith, R.F., Roberts, R.G. & Yoshida, H., 2005. Error variation in OSL palaeodose estimates from single aliquots of quartz: a factorial experiment. Radiation Measurements 39, 289-307.

Götzinger, G., 1936. Das Lößgebiet um Göttweig und Krems an der Donau. Führer für die Quartär-Exkursionen in Österreich. Geologische Bundesanstalt, Wien, pp. 1-11.

Grill, R., 1957. Aufnahmen 1956 auf den Blättern Krems an der Donau (38), Obergrafendorf (55) und St. Pölten (56). Verhandlungen der Geologischen Bundesanstalt 1957, 29-32.

Haslinger, E., Smoliková, L., Havliček, P., Roetzel, R., Heinrich, M., Holásek, O., Vachek, M. & Ottner, F., 2009. Pedological and geochemical investigations at the "Red Outcrop" of Langenlois (Lower Austria). E&G Quaternary Science Journal 58 (2), 135–147.

Havliček, P., Holasek, O., Smoliková, L. & Roetzel, R., 1998. Zur Entwicklung der Quartärsedimente am Südostrand der Böhmischen Masse in Niederösterreich. Jahrbuch der Geologischen Bundesanstalt Wien 141, 51-71.

Hintersberger, E., Decker, K., Lomax, J. & Lüthgens, C., 2017. Implications from palaeoseismological investigations at the Markgrafneusiedl Fault (Vienna Basin, Austria) for seismic hazard assessment. Nat. Hazards Earth Syst. Sci., 18, 531-553.

Höck, V., 1999. Das Kristalline Grundgebirge. Der geologische Bau des Grundgebirges. In: Steininger F.F., Erdgeschichte des Waldviertels, 2. Aufl. Schriftreihe des Waldviertler Heimatbundes, 38, 37-60.

Huntley, D.J., Godfrey-Smith, D.I. & Thewalt, M.L.W., 1985. Optical dating of sediments. Nature, 313, 105-107.

Jacobs, Z., Duller, G.A.T. & Wintle, A.G., 2006. Interpretation of single grain D_e distributions and calculations of D_e. Radiation Measurements 41, 264-277.

Jacobs, Z. & Roberts, R.G., 2007. Advances in Optically Stimulated Luminescence Dating of Individual Grains of Quartz from Archeological Deposits. Evolutionary Anthropology 16, 210-223.

Jacobs, Z., Wintle, A.G. & Duller, G.A.T., 2003. Optical dating of dune sand from Blombos Cave, South Africa: I – multiple grain data. Journal of Human Evolution 44, 599-612.

Jain, M., Murray, A.S. & Bøtter-Jensen, L., 2003. Characterisation of blue-light stimulated luminescence components in different quartz samples: implications for dose measurement. Radiation Measurements 37, 441-449.

Keller, B., 1996. Lithofazies-Codes für die Klassifikation von Lockergesteinen. Mitteilungen der Schweizerischen Gesellschaft für Boden- und Felsmechanik (Publications de la Sociiété de Mécanique des Sols et des Roches) 132, 1-8.

Knobloch, G., 1980. Die Konglomerathöhle im Saubühel (6845/54) und ein neues „Höhlengebiet“ bei Krems. Höhlenkundliche Mitteilungen, 36. Jg., 98-100.

Kohfeld, K.E. & Harrison, S.P., 2003. Glacial-interglacial changes in dust deposition on the Chinese Loess Plateau. Quaternary Science Reviews 22 (18-19), 1859-1878.

Li, B. & Li, S.H., 2006. Comparison of D_e estimates using the fast component and the medium component of quartz OSL. Radiation Measurements 41, 125-136.

Lisiecki, L.E. & Raymo, M.E., 2005. A Pliocene-Pleistocene stack of 57 globally distributed benthic $\delta^{18}O$ records. Paleoceanography 20, PA1003, doi:10.1029/2004PA001071

Lomax, J., Fuchs, M., Preusser, F. & Fiebig, M., 2014. Luminescence based loess chronostratigraphy of the Upper Palaeolithic site Krems-Wachtberg, Austria. Quaternary International 351, 88-97.

Malecki, G., 1985. SEDPAK. – Software-Entwicklung der Geologischen Bundesanstalt, Wien.

Meyer, H.-H. & Kottmeier, C., 1989. Die atmosphärische Zirkulation in Europa im Hochglazial der Weichsel-Eiszeit – Abgeleitet von Paläowind-Indikatoren und Modellsimulationen. E&G Quaternary Science Journal, 39, 10-18

Miall, A.D., 1977. A review of braided river depositional environment. Earth Science Reviews, 13, 1-16.

Müller, G., 1961. Das Sand-Silt-Ton Verhältnis in rezenten marinen Sedimenten. – Neues Jahrbuch für Mineralogie, Monatshefte, 1961, 148-163, Stuttgart.

Murray, A.S., Olley, J.M. & Caitcheon, G.G., 1995. Measurement of equivalent doses in quartz from contemporary water-lain sediments using optically stimulated luminescence. Quaternary Science Reviews 14, 365– 371.

Murray, A.S. & Wintle, A.G., 2000. Luminescence dating of quartz using an improved single-aliquot regenerative-dose protocol. Radiat. Meas. 32, 57-73.

Murray, A.S. & Wintle, A.G., 2003. The single aliquot regenerative dose protocol: potential for improvements in reliability. Radiat. Meas. 37, 377-381.

Neugebauer-Maresch, C., 1989. Zum Neufund einer weiblichen Statuette bei den Rettungsgrabungen an der Aurignacien-Station Stratzing/Krems-Rehberg, Niederösterreich. Germania 67, 551-559.

Nigst, P.R., Haesaerts, P., Damblon, F., Frank-Fellner, C., Mallol, C., Viola, B., Götzinger, M., Niven, L., Trnka, G. & Hublin, J.-J., 2014. Early modern human settlement of Europe north of the Alps occurred 43,500 years ago in a cold steppe-type environment. Proc. Natl. Acad. Sci. Unit. States Am. 111, 14394-14399.

Noll, M., Leitner-Wild, E. & Hille, P., 1994. Thermoluminescence dating of loess deposits at Paudorf, Austria. Quaternary Geochronology (Quaternary Science Reviews) 13, 473-476.

Olley, J.M., Pietsch, T. & Roberts, R.G., 2004. Optical dating of Holocene sediments from a variety of geomorphic settings using single grains of quartz. Geomorphology 60, 337-358.

Pécsi, M. & Richter, G., 1996. Löss. Herkunft, Gliederung, Landschaften. Zeitschrift für Geomorphologie, N.F., Supplementband 98.

Piffl, L., 1959. Eine altpleistozäne Schotterflur um Langenlois. Verhandlungen der Geologischen Bundesanstalt 1959, 132-140.

Piffl, L., 1976. Contribution in: Fink, J. (eds.): Erweiterter Führer zur Exkursion aus Anlass der 2. Tagung der IGCP-Projektgruppe "Quaternary Glaciations in the Northern Hemisphere. Mitteilungen der Kommission für Quartärforschung der Österreichischen Akademie der Wissenschaften 1, 113.

Prescott, J.R. & Hutton, J.T., 1994. Cosmic ray contributions to dose rates for luminescence and ESR dating: large depths and long-term time variations. Radiat. Meas. 23 (1), 497-500.

Pye, K., 1995. The nature, origin and accumulation of loess. Quaternary Science Reviews, 14 (7-8), 653-667.

Pye, K. & D. Sherwin, 1999. Loess. In: Goudie, A.S., Livingstone, I. & Stokes, S., 1999. Aeolian environments, sediments and landforms. John Wiley & Sons, Chichester.

Reitner, H., Malecki, G. & Roetzel, R., 2005. SEDPACWIN – SEDPACMAC Characterization of sediments by grainsize analysis. Gephysical Research Abstracts, 7, EGU General Assembly Vienna, 24.-29. April 2005, Wien.

Rhodes, E.J., 2011. Optically Stimulated Luminescence Dating of Sediments over the Past 200,000 Years. Annu. Rev. Earth Planet. Sci. 39, 461-488.

Rixhon, G., Briant, R.M., Cordier, S., Duval, M., Jones, A. & Scholz, D., 2017. Revealing the pace of river landscape evolution during the Quaternary: recent developments in numerical dating methods. Quaternary Science Reviews 166, 91-113.

Roberts, H.M., 2008. The development and application of luminescence dating to loess deposits: a perspective on the past, present and future. Boreas, Vol. 37, 483–507.

Roetzel, R., 1996. Bericht 1994/1995 über geologische Aufnahmen im Tertiär und Quartär mit Bemerkungen zur Tektonik am Diendorfer Störungssystem auf Blatt 22 Hollabrunn. Jahrbuch der Geologischen Bundesanstalt 139 (3), 286-295.

Roetzel, R., Meyer, M. & Wimmer-Frey, I., 2018. Endbericht über geologische und geochronologische Untersuchungen der Ablagerungen in den Kellern der Weinerlebniswelt Loisium und der Baugrube Steininger in Langenlois. Unpublished Report Geologische Bundesanstalt, Universität Innsbruck, Wien.

Schnabel, W., Fuchs, G., Matura, A., Roetzel, R., Scharbert, S., Krenmayr, H.G., Egger, J., Bryda, G., Mandl, G.W., Nowotny, A. & Wessely, G., 2002. Geologische Karte von Niederösterreich 1:200.000. Verlag der Geologischen Bundesanstalt, Wien.

Singarayer, J.S. & Bailey, R.M., 2003. Further investigations of the quartz optically stimulated luminescence components using linear modulation. Radiation Measurements 37, 451-458.

Singarayer, J.S. & Bailey, R.M., 2004. Component-resolved bleaching spectra of quartz optically stimulated luminescence: preliminary results and implications for dating. Radiation Measurements 38, 111-118.

Smolíková, L., 2003. Bericht 2002 über 875 Mikromorphologie, Typologie und Stratigraphie quartärer Böden vom Buriweg in Langenlois auf Blatt 38 Krems. Jahrbuch der Geologischen Bundesanstalt 143 (3), 506–507.

Smolíková, L. & Havliček, P., 2007. Bericht 2005 und 2006 über mikromorphologische Untersuchungen von quartären Böden im Gebiet des unteren Kamptales auf den Blättern 21 Horn und 38 Krems. Jahrbuch der Geologischen Bundesanstalt 147 (3-4), 682–683.

Sprafke, T., 2016. Löss in Niederösterreich – Archiv quartärer Klima- und Landschaftsveränderungen. Würzburg University Press, Würzburg, 253 pp.

Steffen, D., Preusser, F. & Schlunegger, F., 2009. OSL quartz age underestimation due to unstable signal components. Quaternary Geochronology, 4, 353-362.

Steinhauser, P., Meurers, B. & Brückl, E., 1987. Geophysikalische Untersuchung des Molasseschelfs im Raum Röschitz. Geophysikalischer Forschungsbericht 23, Institut für Meteorologie und Geophysik Universität Wien.

Steininger, F.F., 1999. Erdgeschichte des Waldviertels, 2. Aufl. Schriftreihe des Waldviertler Heimatbundes, 38.

Stevens, T., Buylaert, J.-P., Thiel, C., Újvári, G., Yi, S., Murray, A.S., Frechen, M. & Lu, H., 2018. Ice-volume-forced erosion of the Chinese Loess Plateau global Quaternary stratotype site. Nature communications, 9 (983), 1-12.

Stokes, S., Ingram, S., Aitken, M.J., Sirocko, F., Anderson, R. & Leuschner, D., 2003. Alternative chronologies for Late Quaternary (Last Interglacial-Holocene) deep sea sediments via optical dating of silt-sized quartz. Quaternary Science Reviews, 22, 925-941.

Terhorst, B., Kühn, P., Damm, B., Hambach, U., Meyer-Heintze, S. & Sedov, S., 2014. Paleoenvironmental fluctuations as recorded in the loess-paleosol sequence of the Upper Paleolithic site Krems-Wachtberg. Quat. Int. 351, 67-82.

Terhorst, B., Thiel, C., Peticzka, R., Sprafke, T., Frechen, M., Fladerer, A.F., Roetzel, R. & Neugebauer-Maresch, C., 2011. Casting new light on the chronology of the loess/paleosol sequences in Lower Austria. Quaternary Sci. J., 60, 270-277.

Thiel, C., Buylaert, J.-P., Murray, A., Terhorst, B., Hofer, I., Tsukamoto, S. & Frechen, M., 2011a. Luminescence dating of the Stratzing loess profile (Austria) — testing the potential of an elevated temperature post-IR IRSL protocol. Quaternary International 234, 23-31.

Thiel, C., Buylaert, J.-P., Murray, A.S., Terhorst, B., Tsukamoto, S. & Frechen, M., 2011b. Investigating the chronostratigraphy of prominent palaeosols in Lower Austria using post-IR IRSL dating. E&G Quaternary Science Journal 60, 137–152.

Thiel, C., Terhorst, B., Jaburová, I., Buylaert, J.-P., Murray, A.S., Fladerer, F.A., Damm, B., Frechen, M. & Ottner, F., 2011c. Sedimentation and erosion processes in Middle to Late Pleistocene sequences exposed in the brickyard of Langenlois/Lower Austria. Geomorphology 135, 295-307.

Van Husen, D., 1997. LGM and late-glacial fluctuations in the Eastern Alps. Quaternary International 38/39, 109-118.

Van Husen, D., 2000. Geological processes during the Quaternary. Mitteilungen der Österreichischen Geologischen Gesellschaft, 92, 135-156.

Van Husen, D. & Reitner, J.M., 2011. Klimagesteuerte Terrassen- und Lössbildung auf der Traun-Enns-Platte und ihre zeitliche Stellung (Das Profil Wels/Aschet). Mitt. Komm. Quartärforsch. Österr. Akad. Wiss., 19, 1-11.

Vasicek, W. & Steininger, F.F., 1999. Die Landschaftsgeschichte des Waldviertels und des westlichen Weinviertels vom Jungpaläozoikum bis heute. Jungpaläozoikum von Zöbing. In: Steininger F.F., Erdgeschichte des Waldviertels, 2. Aufl. Schriftreihe des Waldviertler Heimatbundes, 38, 63-72.

Wallbrecher, E., Brandmayr, M., Handler, R., Loizenbauer, J., Mader-Bacher, F. & Platzer, R., 1993. Konjugierte Scherzonen in der südlichen Böhmischen Masse: Variszische und alpidische kinematische Entwicklungen. Projekt S4713. Mitt. Österr. Min. Ges., 138, 237-252. Wien.

Wallner, G., Wild, E., Aref-Azar, H., Hille, P. & Schmidt, W.F.O., 1990. Dating of Austrian loess deposits. Radiation Protection Dosimetry 34, 69-72.

Weissl, M., Hintersberger, E., Lomax, J., Lüthgens, C. & Decker, K., 2017. Active tectonics and geomorphology of the Gaenserndorf Terrace in the Central Vienna Basin (Austria). Quaternary International 451, 209-222.

Wintle, A.G., 1997. Luminescence dating: laboratory procedures and protocols. Radiat. Meas. 27 (5), 760-817.

Wintle, A.G. & Murray, A.S., 2006. A review of quartz optically stimulated luminescence characteristics and their relevance in single-aliquot regeneration dating protocols. Radiat. Meas. 41, 369-391.

Zöller, L., Oches, E.A. & McCoy, W.D., 1994. Towards a revised chronostratigraphy of loess in Austria with respect to key sections in the Czech Republic and in Hungary. Quaternary Geochronology (Quaternary Science Reviews) 13, 465-472.

Annex

OSL dating – basics and further details

Optically stimulated luminescence (OSL) dating is a chronological method, used to determine the time since the burial of mineral grains in sediments. Its age range spans from just a few years to several hundreds of thousands of years (Jacobs & Roberts, 2007). The method utilizes light emissions from quartz and feldspar generated by photosensitive effects. As two of the most abundant minerals in the earth crust are used, OSL dating has a wide applicability on quaternary sediment. The method is based on radioactive decay of isotopes of elements such as uranium, thorium and potassium. A small proportion of the emitted energy by this decay is stored within the structure of the proximate crystals. Electrons within the crystal get excited and raised to the conduction band. From there they can be trapped at sites within the crystal structures, where they are normally forbidden to reside, but where they can be stored because of defects within the structure, at so called trapping centres (Fig. 1; Duller, 2008a). Brief heating at 200°C - 400°C, or few seconds of daylight exposure causes certain electron trap populations to get emptied to a low level, effectively resetting the OSL dating clock (Rhodes, 2011). After reburial of the grain, the energy starts to slowly build up again. A useful analogy is that of a rechargeable battery (Fig. 2; Duller, 2008a). For dating, unbleached sedimentary material gets bleached under controlled conditions. A common approach for measuring the luminescence of quartz is stimulation with blue LEDs and filtering the luminescence signal with a U-340 filter to detect the near ultraviolet spectrum by the photomultiplier tube (PMT). On the one hand, this emission spectrum has proven as one of the most suitable and stable through geological time, on the other hand confining of the measured spectrum is essential to ensure that no stimulation light is recorded by the PMT. The light intensity measured is proportional to the absorbed energy. Thus, the total dose absorbed in the natural environment, which is referred to as the equivalent dose, or D_e, can be calculated by the laboratory luminescence measurements. D_e is measured in the SI unit Gray (Gy; 1 Gy = 1 J*kg^{-1}). For estimating D_e, measurements are carried out on single grains or small aliquots.

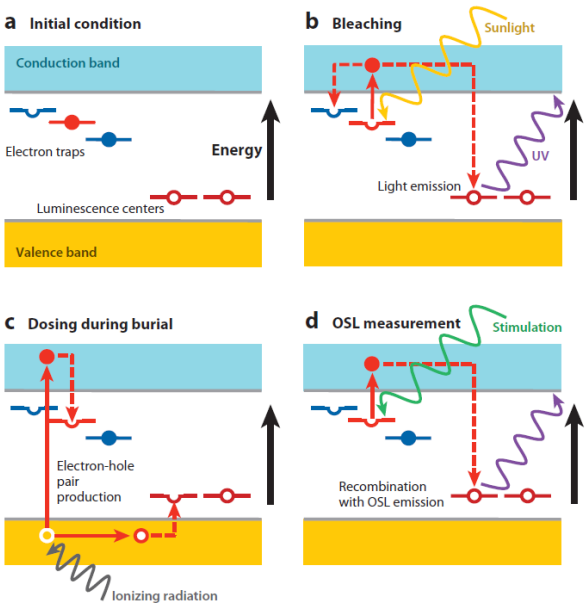

Fig. 1: Sample band gap energy model of optically stimulated luminescence (OSL). Illustration by Rhodes (2011).

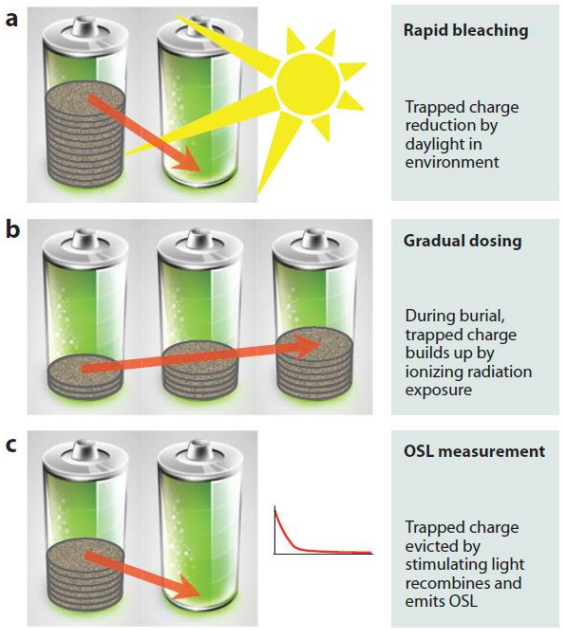

Fig. 1: The rechargeable battery forms a useful analogy to optically stimulated luminescence dating. Illustration by Rhodes (2011).

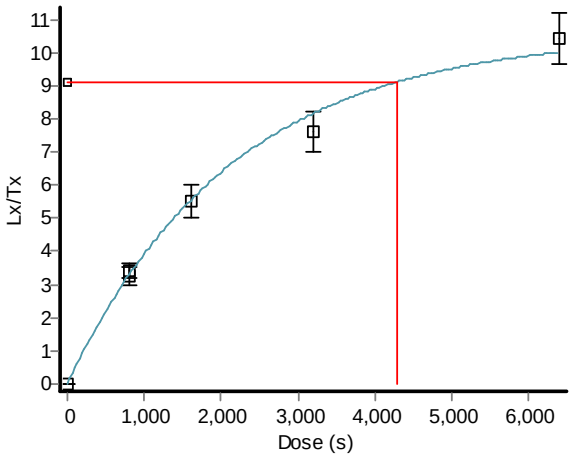

Fig. 3: Dose response curve by plotting the ratio Lx/Tx as a function of the laboratory dose.

Several measurement cycles are executed. The first measurement cycle determines the intensity of the natural luminescence. For the next cycle, a known laboratory dose (regeneration dose) is applied and measured. This step is repeated with varying doses to get different dose responses of the OSL signal. Luminescence sensitivity of the aliquot – the amount of light it emits for each unit of radiation to which it is exposed – changes depending on the laboratory procedures undertaken (Duller, 2008a). To correct this effect, a fixed radiation dose (test dose) is given and measured immediately after the natural and every regenerative-dose OSL measurement. The sensitivity corrected luminescence signal results from the ratio of the OSL signal from each natural and regenerative-dose measurement to the following sensitivity measurement. This ratio is used to construct a growth curve (dose response curve) by plotting it as a function of the laboratory dose (Fig. 3). Now, De can be calculated by projecting the measured natural signal onto the dose response curve. Before each OSL measurement, the sample is preheated to a fixed temperature in order to remove unstable signal components from shallow traps, so that the OSL signal comes only from electrons that would have been stored safely through the burial period.

Depending on the sample characteristics and the sedimentation setting, the aliquot size is varied. Larger aliquots containing thousands of grains yield higher luminescence intensities but are averaging the result in case of incomplete bleaching – when traps were not completely emptied during the transportation process. In settings where partial bleaching is likely, small aliquots are used for measurement to identify variation in D_e-values. If the deviation is high, partial bleaching is assumed and standard analysis would lead to an age overestimation. In this case, single-grain OSL measurement is undertaken. Typically, different De-populations can be determined, and the minimum equivalent dose population is used for age calculation.

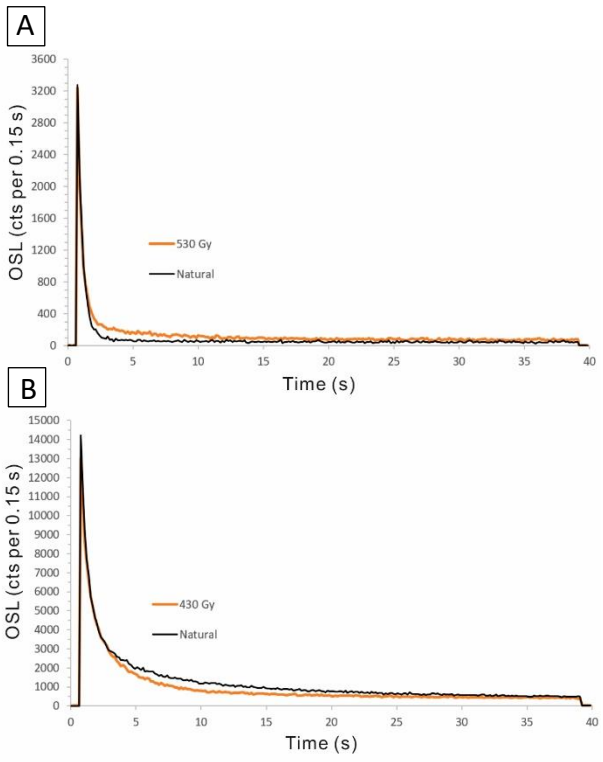

Fig. 4. Exponentially decreasing luminescence signals (shine-down curves). **A:** Aliquot dominated by the fast component with a rapid signal decay within the first seconds. **B:** Aliquot with a significant medium component and a wider decay curve.

The luminescence signal is decreasing exponentially with stimulation time. Thus, the signal is recorded as an exponential curve – the so-called shine-down curve (Fig. 4). It was found that the signal is made up of different exponential components originating from different traps and/or recombination centres (e.g. Bøtter-Jensen et al., 1999; Jain et al., 2003). Simplified, these components can be differentiated in a fast, medium and slow component (Bailey et al., 1997). Each

component has different characteristics regarding bleaching, thermal stability, sensitivity change, recuperation, saturation, etc. (Steffen et al., 2009; Singarayer and Bailey, 2003; 2004). It was found out, that samples with a dominant fast component are the most suitable for dating. Aliquots dominated by the fast component show a rapid decay of the signal within the initial 0-0.4 s after applying light stimulation (Fig. 4a; Li and Li, 2006). Aliquots with a significant contribution of the medium and/or slow component show much wider shine-down curves and may yield inaccurate equivalent doses (Fig. 4b; Li and Li, 2006; Steffen et al., 2009). This can be caused by partial bleaching due to a lower decay rate and thereby more unfavourable bleaching properties of the later components. Age underestimation can be a concern, if the ratio between the fast and medium component changes through the course of the SAR protocol (e.g. Jain et al., 2003; Li and Li, 2006; Steffen et al., 2009). It is supposed that this is due to a thermally unstable medium component which has been eroded in the natural signal (Li and Li, 2006; Steffen et al., 2009). An easy test to detect a problematic medium component is the use of a $D_e(t)$ plot (e.g. Bailey 2003; Steffen et al., 2009). With an ideal sample, D_e should not depend on the signal integration interval, whereas a falling D_e value towards the later intervals may indicate an unstable medium component (Li and Li, 2006; Steffen et al., 2009). To tackle this problem, Cunningham & Wallinga (2010) introduced the early background subtraction (EBS) approach. The standard practice is to subtract the late background (last few seconds of the stimulation time; LBS) from the initial integral of the decay curve. With an EBS, the time interval of the background subtraction immediately follows that of the integrated initial signal (Fig. 5) to maximise the proportion of fast component in the net signal (Cunningham & Wallinga, 2010). Using this method, Cunningham & Wallinga (2010) could achieve results showing less thermal transfer, less recuperation, tighter D_e distributions and more aliquots with D_e in line with the expected D_e than using the alternative late-background time intervals.

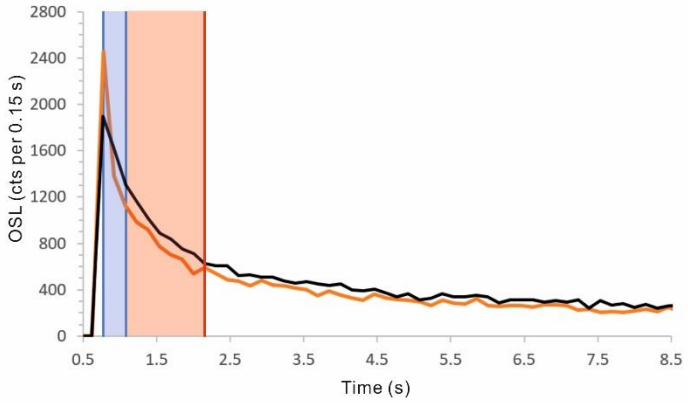

Fig. 5. Integration intervals used for the EBS attempt. The blue area marks the signal interval, the red area represents the background interval.

The second component required for luminescence age estimation is the dose rate. It is the amount of energy received by the sample each year from the radiation in the environment surrounding the measured material (Gy/year). Main components contributing to the dose rate are alpha particles, beta particles and gamma rays which originate from naturally occurring elements. A small contribution derives from cosmic rays (typically less than 10%) (Rhodes, 2011). The dose provided from radioactive elements can be measured either by measuring the concentration of U, Th and K to calculate the radiation dose or by directly counting the emission of radiation. Emission counting can be carried out on small, homogenous sub-samples in the laboratory, or directly in the field by gamma spectrometry. The advantage of in situ measurement is that the gamma dose rate is accurately captured, even if there is heterogeneity in the radiation field (Duller, 2008a).

If both components, D_e and the dose rate, are measured, the luminescence can be calculated by the equation: $age\ (years) = \frac{equivalent\ dose\ (De)(Gy)}{dose\ rate\ (\frac{Gy}{year})}$. Errors of the luminescence age normally range from 5 to 10 %, including both random and systematic sources of error (Duller, 2008a).

The luminescence signal of quartz is made up of individual signal components originating from different traps and/or recombination centres (Steffen, 2009). Each signal component has different characteristics regarding bleaching, thermal stability, sensitivity change, recuperation, saturation, etc (Wintle and Murray, 2006).

Mineralogical and sedimentological results

Results of the mineralogical analyses from Roetzel et al. (2017) for logs Haimerl (LOIS-1-X), Nidetzky (LOIS-2-X) and Steininger (LOIS-3-X).

Sample	Clay (wt. %)	Silt (wt. %)				Sand (wt. %)				Gravel (wt. %)			
	<2 µm	2-6.3 µm	6.3-20 µm	20-63 µm	Total	63-200 µm	0.2-0.63 mm	0.63-2 mm	Total	2-6.3 mm	6.3-20 mm	20-63 mm	Total
LOIS-1-1	65.3	17.0	11.2	5.3	33.5	0.4	0.6	0.2	1.2	0.0	0.0	0.0	0.0
LOIS-1-2	0.5	0.5	0.6	0.6	1.7	2.8	14.1	7.9	24.8	8.7	34.4	29.9	73.0
LOIS-1-3	6.9	3.2	4.8	5.8	13.9	9.9	15.5	8.8	34.2	7.6	18.1	19.4	45.1
LOIS-1-4	17.9	7.9	14.7	19.0	41.6	22.6	14.9	2.8	40.3	0.2	0.0	0.0	0.2
LOIS-1-5	19.0	8.3	12.7	19.2	40.2	25.0	13.2	2.3	40.5	0.3	0.0	0.0	0.3
LOIS-1-6	21.0	8.4	14.6	21.5	44.5	19.8	12.2	2.2	34.2	0.3	0.0	0.0	0.3
LOIS-1-7	20.5	8.8	17.8	24.4	51.1	16.0	9.2	2.3	27.5	0.9	0.0	0.0	0.9
LOIS-1-8	19.5	8.4	18.1	30.2	56.6	14.0	8.1	1.6	23.6	0.3	0.0	0.0	0.3
LOIS-2-1	43.2	19.8	18.9	15.1	53.8	1.4	0.8	0.4	2.5	0.5	0.0	0.0	0.5
LOIS-2-2	48.0	23.2	20.7	8.0	51.9	0.04	0.04	0.02	0.1	0.0	0.0	0.0	0.0
LOIS-2-3	54.6	18.5	15.0	10.5	44.0	0.9	0.3	0.1	1.4	0.03	0.0	0.0	0.03
LOIS-2-4	20.7	8.2	16.5	26.7	51.4	17.0	8.2	2.3	27.5	0.5	0.0	0.0	0.5
LOIS-2-5	18.7	9.5	18.3	29.7	57.5	13.8	6.9	2.1	22.8	1.0	0.0	0.0	1.0
LOIS-2-6	24.2	12.2	18.4	30.0	60.6	10.6	3.5	0.8	14.8	0.3	0.0	0.0	0.3
LOIS-2-7	18.2	10.1	20.5	37.1	67.8	9.1	3.5	1.1	13.7	0.3	0.0	0.0	0.3
LOIS-3-0	4.8	3.5	6.0	14.0	23.4	67.4	4.4	0.01	71.8	0.0	0.0	0.0	0.0
LOIS-3-1	33.9	11.0	25.4	27.7	64.2	1.6	0.3	0.02	1.9	0.0	0.0	0.0	0.0
LOIS-3-2	2.1	0.5	0.6	1.5	2.7	10.1	44.4	29.8	84.3	9.2	1.7	0.0	10.9
LOIS-3-3	9.8	4.2	6.0	14.9	25.1	33.5	29.0	2.6	65.1	0.1	0.0	0.0	0.1
LOIS-3-4	21.8	7.8	18.5	37.4	63.6	9.4	4.8	0.4	14.5	0.0	0.0	0.0	0.0
LOIS-3-5	43.6	4.2	10.2	20.4	34.8	9.9	7.8	3.6	21.2	0.4	0.0	0.0	0.4
LOIS-3-6	28.8	10.2	16.3	32.1	58.5	7.0	3.7	1.6	12.3	0.3	0.0	0.0	0.3
LOIS-3-7	1.2	0.5	0.5	1.0	2.0	5.1	37.4	22.2	64.7	14.9	12.8	4.6	32.2
LOIS-3-8	19.4	8.2	16.7	31.3	56.2	13.9	7.4	2.3	23.6	0.7	0.0	0.0	0.7
LOIS-3-9	14.8	6.5	14.6	49.7	70.8	9.1	3.4	1.6	14.2	0.2	0.0	0.0	0.2

Results of the sedimentological analyses from Roetzel et al. (2017) for logs Haimerl (LOIS-1-X), Nidetzky (LOIS-2-X) and Steininger (LOIS-3-X).

Sample	Minerals							Clay minerals					
	Quartz	K-Feldspar	Albite	Biotite	Muscovite	Calcite	Dolomite	Illite	Chlorite	Kaolinite	Smektite	Vermiculite	Total
LOIS-1-1	23	4	2	1	19	0	0	5	4	2	37	2	71
LOIS-1-2	74	5	8	4	2	1	0	1	2	1	3	9	12
LOIS-1-3	50	11	12	3	5	1	1	1	4	1	9	1	25
LOIS-1-4	37	5	16	0	12	3	5	3	5	3	10	2	35
LOIS-1-5	36	10	15	0	8	2	4	3	5	2	13	1	32
LOIS-1-6	40	9	15	1	9	2	4	5	5	3	7	1	30
LOIS-1-7	36	9	17	3	8	2	4	6	6	3	5	0	32
LOIS-1-8	34	9	15	0	11	3	4	3	8	3	7	2	34
LOIS-2-1	20	5	6	2	14	10	4	7	6	2	21	3	55
LOIS-2-2	18	5	4	3	15	10	5	10	5	5	19	1	58
LOIS-2-3	24	3	4	2	17	2	0	6	4	3	30	3	66
LOIS-2-4	30	10	19	2	7	5	4	1	8	3	9	1	31
LOIS-2-5	31	9	16	3	9	6	7	1	8	4	5	1	32
LOIS-2-6	29	7	15	1	9	10	9	3	5	5	6	1	30
LOIS-2-7	30	9	16	1	9	6	7	2	9	3	7	1	31
LOIS-3-0	46	8	19	2	6	1	0	4	4	2	5	1	25
LOIS-3-1	28	8	6	5	12	1	0	3	4	7	24	2	57
LOIS-3-2	61	9	8	5	6	1	0	7	1	1	1	0	22
LOIS-3-3	46	7	13	1	6	1	0	9	1	4	10	1	32
LOIS-3-4	32	8	12	3	5	11	4	2	4	3	14	1	33
LOIS-3-5	33	11	7	3	7	1	0	7	3	4	23	1	48
LOIS-3-6	27	7	8	2	7	19	9	6	3	4	7	1	29
LOIS-3-7	47	14	14	5	2	2	0	9	1	3	3	1	23
LOIS-3-8	29	12	14	1	5	13	7	1	5	2	7	2	23
LOIS-3-9	30	6	14	2	10	11	10	4	6	3	3	1	29

OSL Results

OSL-LOIS-1

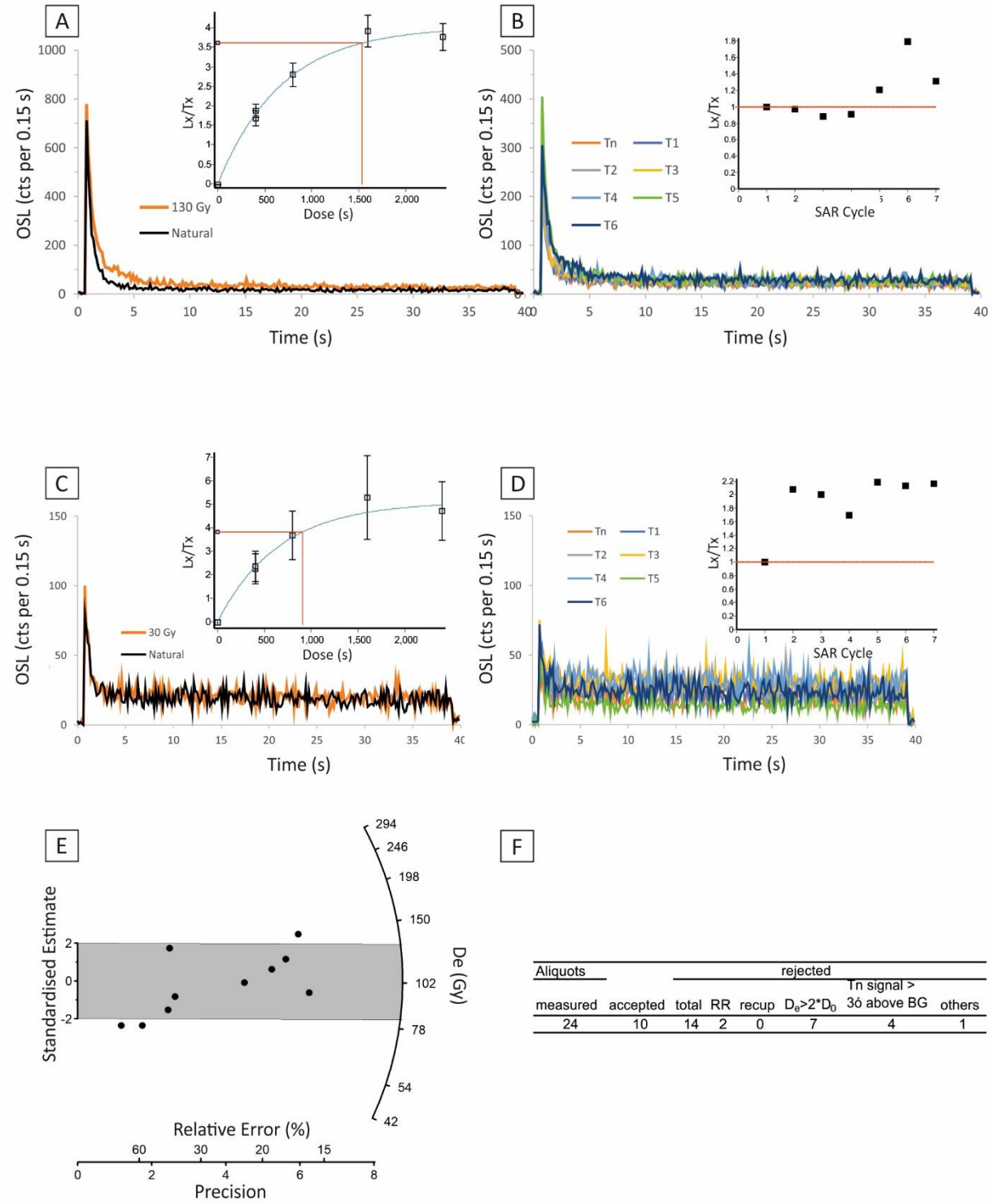

Aliquots		rejected					
measured	accepted	total	RR	recup	D_e>2*D_0	Tn signal > 3ó above BG	others
24	10	14	2	0	7	4	1

OSL dating results of sample OSL-LOIS-1. **A:** OSL decay curves and SAR dose response curves of a typical bright aliquot. **B:** Decay curves of the test doses with Tx/Tn ratios of the same bright aliquot. **C:** OSL decay curves and SAR dose response curves of a typical dim aliquot. **D:** Decay curves of the test doses with Tx/Tn ratios of the same dim aliquot. **E:** Single aliquot De distribution. **F:** Table with the number of accepted and rejected aliquots for the sample. RR = recycling ratio, recup = recuperation. For rejection criteria see main document chapter 3.4.

OSL-LOIS-2

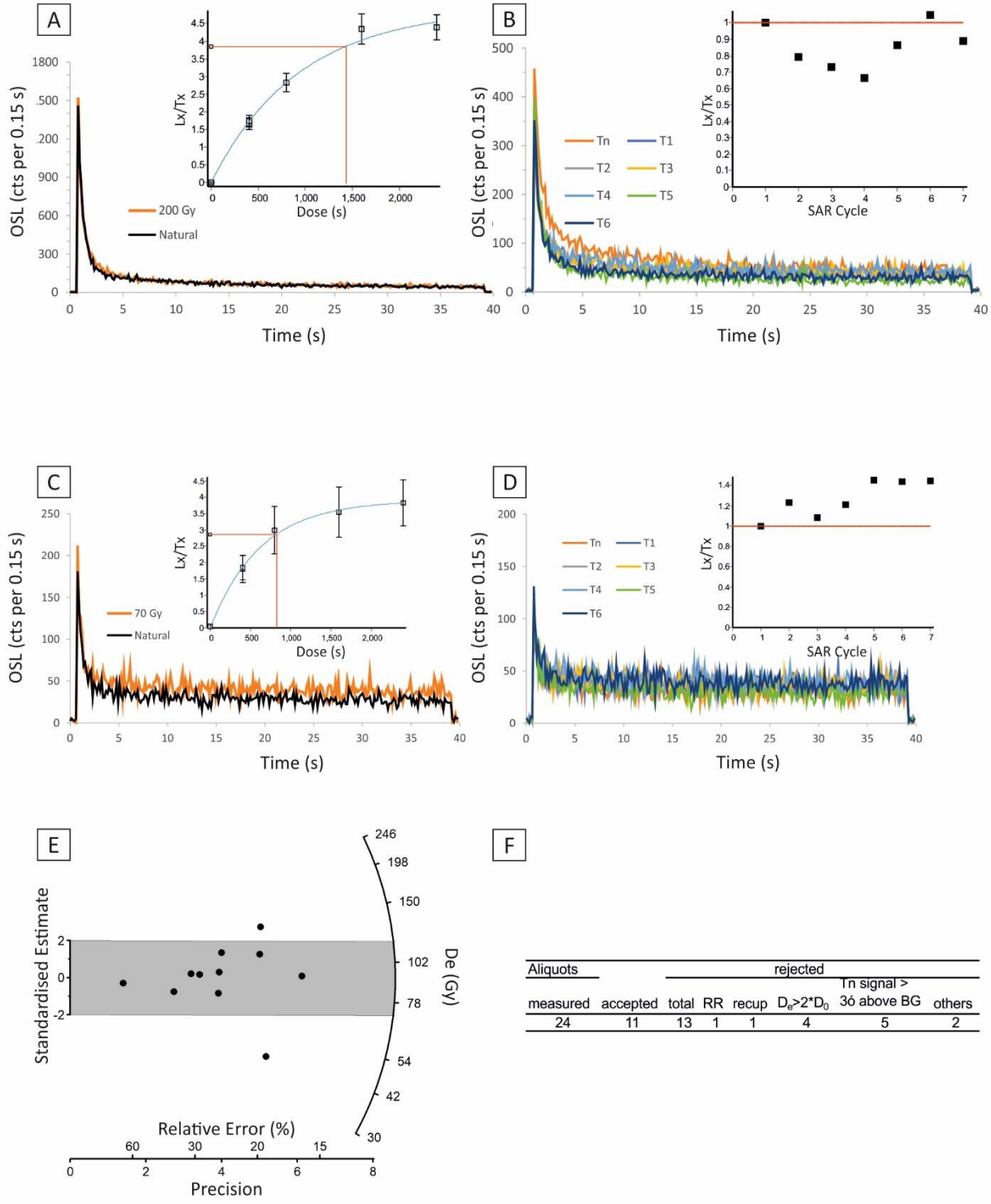

Aliquots		rejected					
measured	accepted	total	RR	recup	D_e>2*D_0	Tn signal > 3ó above BG	others
24	11	13	1	1	4	5	2

OSL dating results of sample OSL-LOIS-2. **A:** OSL decay curves and SAR dose response curves of a typical bright aliquot. **B:** Decay curves of the test doses with Tx/Tn ratios of the same bright aliquot. **C:** OSL decay curves and SAR dose response curves of a typical dim aliquot. **D:** Decay curves of the test doses with Tx/Tn ratios of the same dim aliquot. **E:** Single aliquot De distribution. **F:** Table with the number of accepted and rejected aliquots for the sample. RR = recycling ratio, recup = recuperation. For rejection criteria see main document chapter 3.4.

OSL-LOIS-3

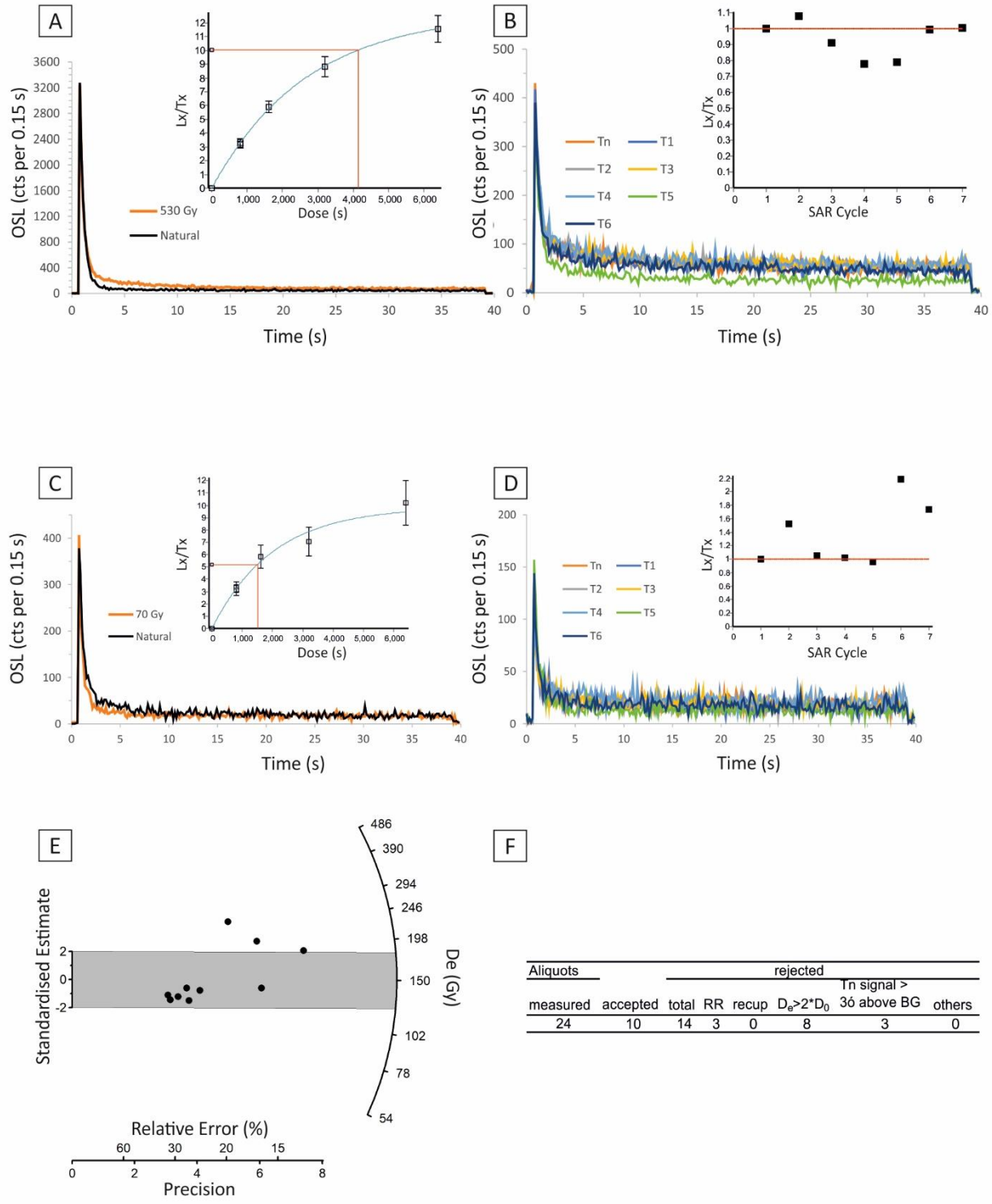

Aliquots		rejected					
measured	accepted	total	RR	recup	D_e>2*D_0	Tn signal > 3ó above BG	others
24	10	14	3	0	8	3	0

OSL dating results of sample OSL-LOIS-3. **A:** OSL decay curves and SAR dose response curves of a typical bright aliquot. **B:** Decay curves of the test doses with Tx/Tn ratios of the same bright aliquot. **C:** OSL decay curves and SAR dose response curves of a typical dim aliquot. **D:** Decay curves of the test doses with Tx/Tn ratios of the same dim aliquot. **E:** Single aliquot De distribution. **F:** Table with the number of accepted and rejected aliquots for the sample. RR = recycling ratio, recup = recuperation. For rejection criteria see main document chapter 3.4.

OSL-LOIS-4

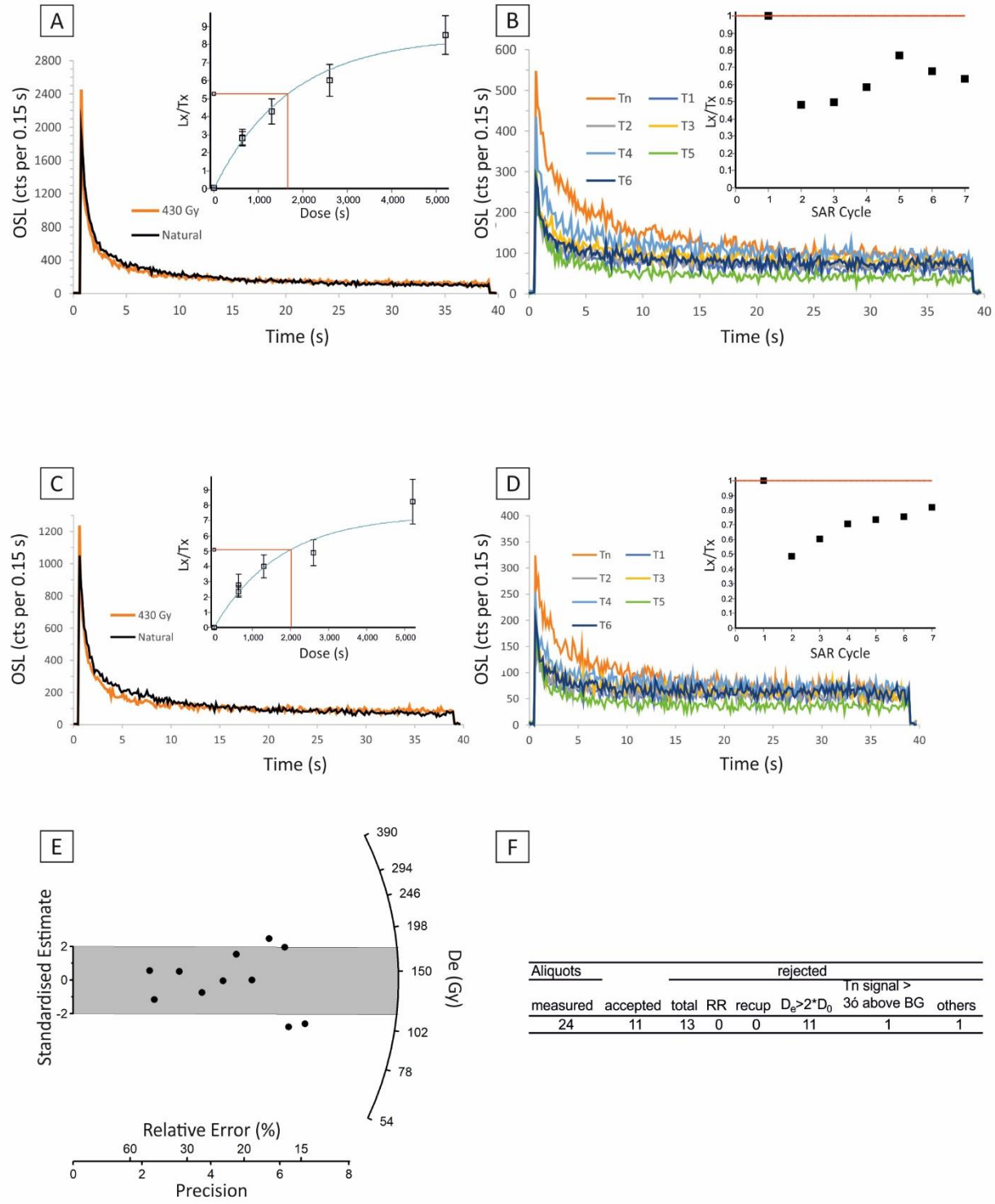

Aliquots		rejected					
measured	accepted	total	RR	recup	D_e>2*D_0	Tn signal > 3ó above BG	others
24	11	13	0	0	11	1	1

OSL dating results of sample OSL-LOIS-4. **A:** OSL decay curves and SAR dose response curves of a typical bright aliquot. **B:** Decay curves of the test doses with Tx/Tn ratios of the same bright aliquot. **C:** OSL decay curves and SAR dose response curves of a typical dim aliquot. **D:** Decay curves of the test doses with Tx/Tn ratios of the same dim aliquot. **E:** Single aliquot De distribution. **F:** Table with the number of accepted and rejected aliquots for the sample. RR = recycling ratio, recup = recuperation. For rejection criteria see main document chapter 3.4.

OSL-LOIS-5

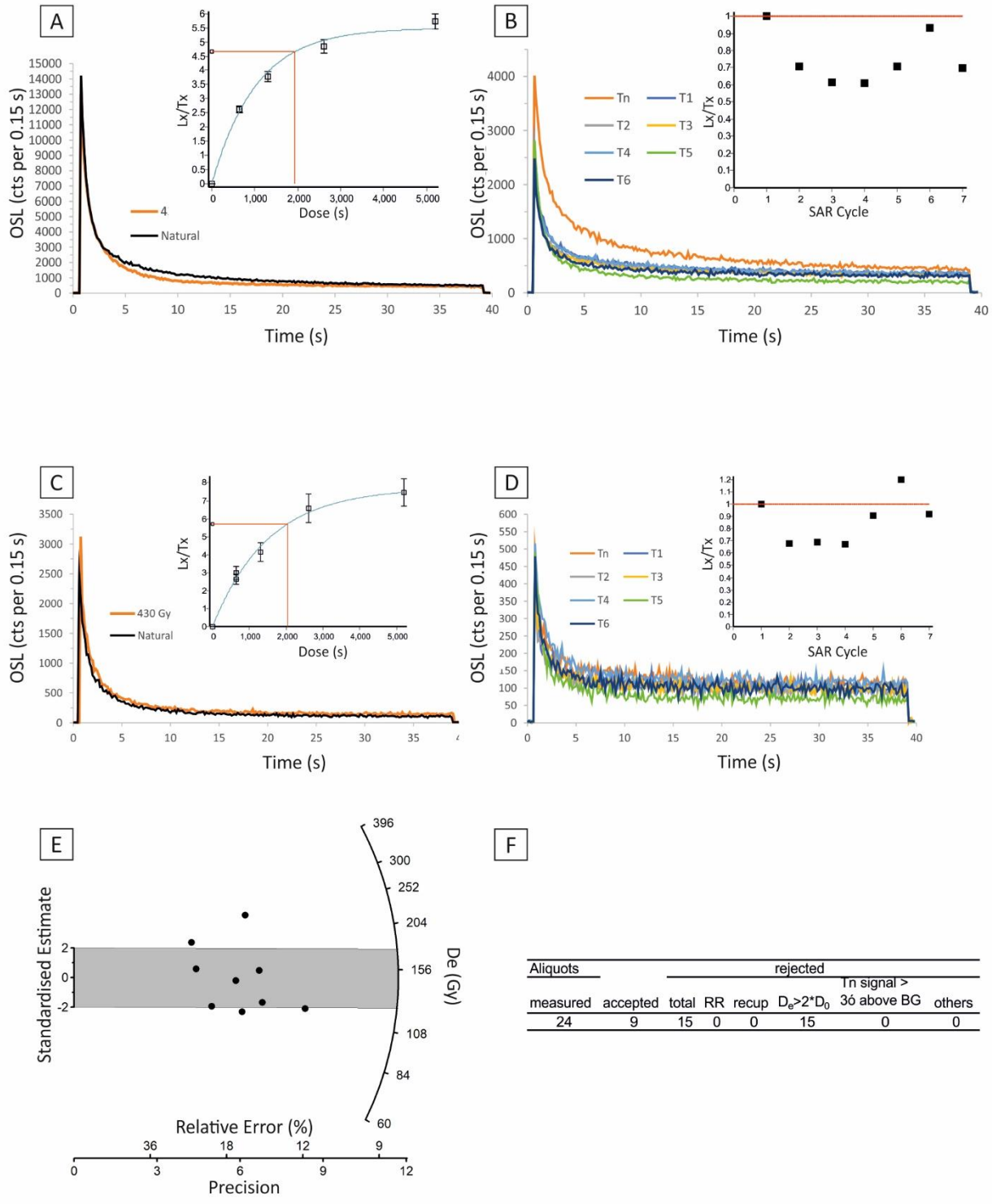

Aliquots		rejected					
measured	accepted	total	RR	recup	$D_e>2*D_0$	Tn signal > 3ó above BG	others
24	9	15	0	0	15	0	0

OSL dating results of sample OSL-LOIS-5. **A:** OSL decay curves and SAR dose response curves of a typical bright aliquot. **B:** Decay curves of the test doses with Tx/Tn ratios of the same bright aliquot. **C:** OSL decay curves and SAR dose response curves of a typical dim aliquot. **D:** Decay curves of the test doses with Tx/Tn ratios of the same dim aliquot. **E:** Single aliquot De distribution. **F:** Table with the number of accepted and rejected aliquots for the sample. RR = recycling ratio, recup = recuperation. For rejection criteria see main document chapter 3.4.

OSL-LOIS-6

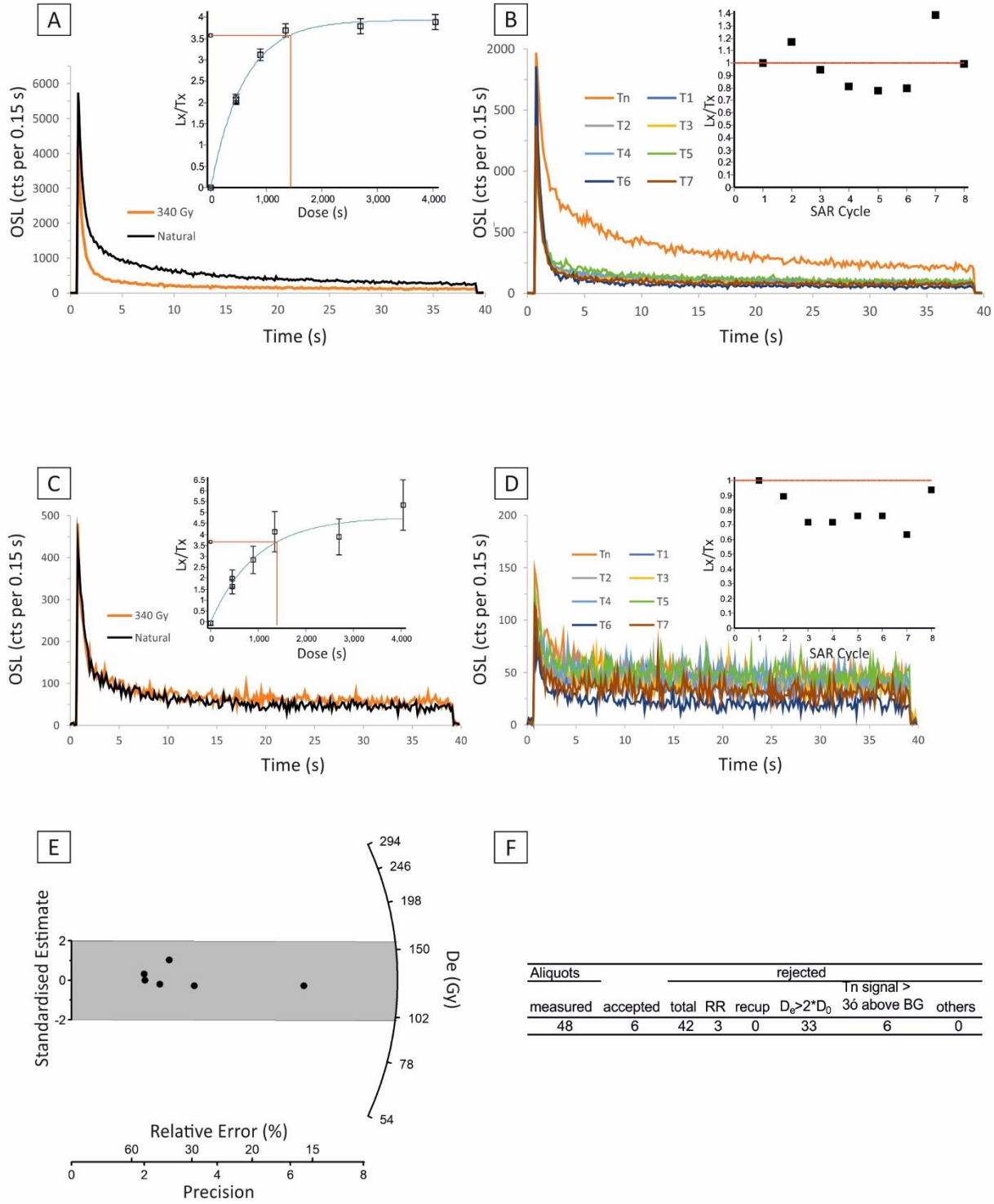

Aliquots		rejected					
measured	accepted	total	RR	recup	$D_e>2*D_0$	Tn signal > 3ó above BG	others
48	6	42	3	0	33	6	0

OSL dating results of sample OSL-LOIS-6. **A:** OSL decay curves and SAR dose response curves of a typical bright aliquot. **B:** Decay curves of the test doses with Tx/Tn ratios of the same bright aliquot. **C:** OSL decay curves and SAR dose response curves of a typical dim aliquot. **D:** Decay curves of the test doses with Tx/Tn ratios of the same dim aliquot. **E:** Single aliquot De distribution. **F:** Table with the number of accepted and rejected aliquots for the sample. RR = recycling ratio, recup = recuperation. For rejection criteria see main document chapter 3.4.

OSL-LOIS-7

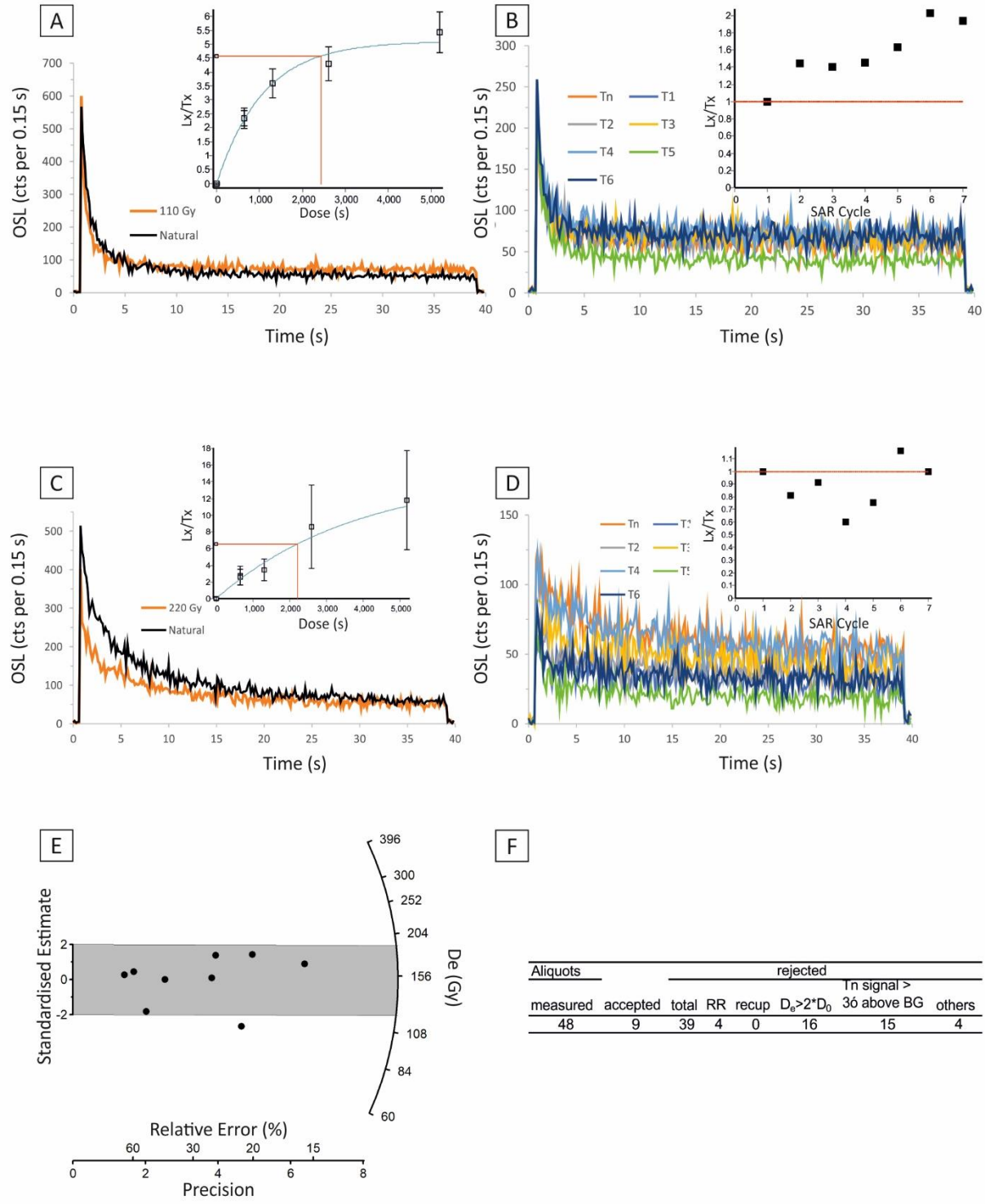

Aliquots		rejected					
measured	accepted	total	RR	recup	D_e>2*D_0	Tn signal > 3ó above BG	others
48	9	39	4	0	16	15	4

OSL dating results of sample OSL-LOIS-7. **A:** OSL decay curves and SAR dose response curves of a typical bright aliquot. **B:** Decay curves of the test doses with Tx/Tn ratios of the same bright aliquot. **C:** OSL decay curves and SAR dose response curves of a typical dim aliquot. **D:** Decay curves of the test doses with Tx/Tn ratios of the same dim aliquot. **E:** Single aliquot De distribution. **F:** Table with the number of accepted and rejected aliquots for the sample. RR = recycling ratio, recup = recuperation. For rejection criteria see main document chapter 3.4.

OSL-LOIS-8

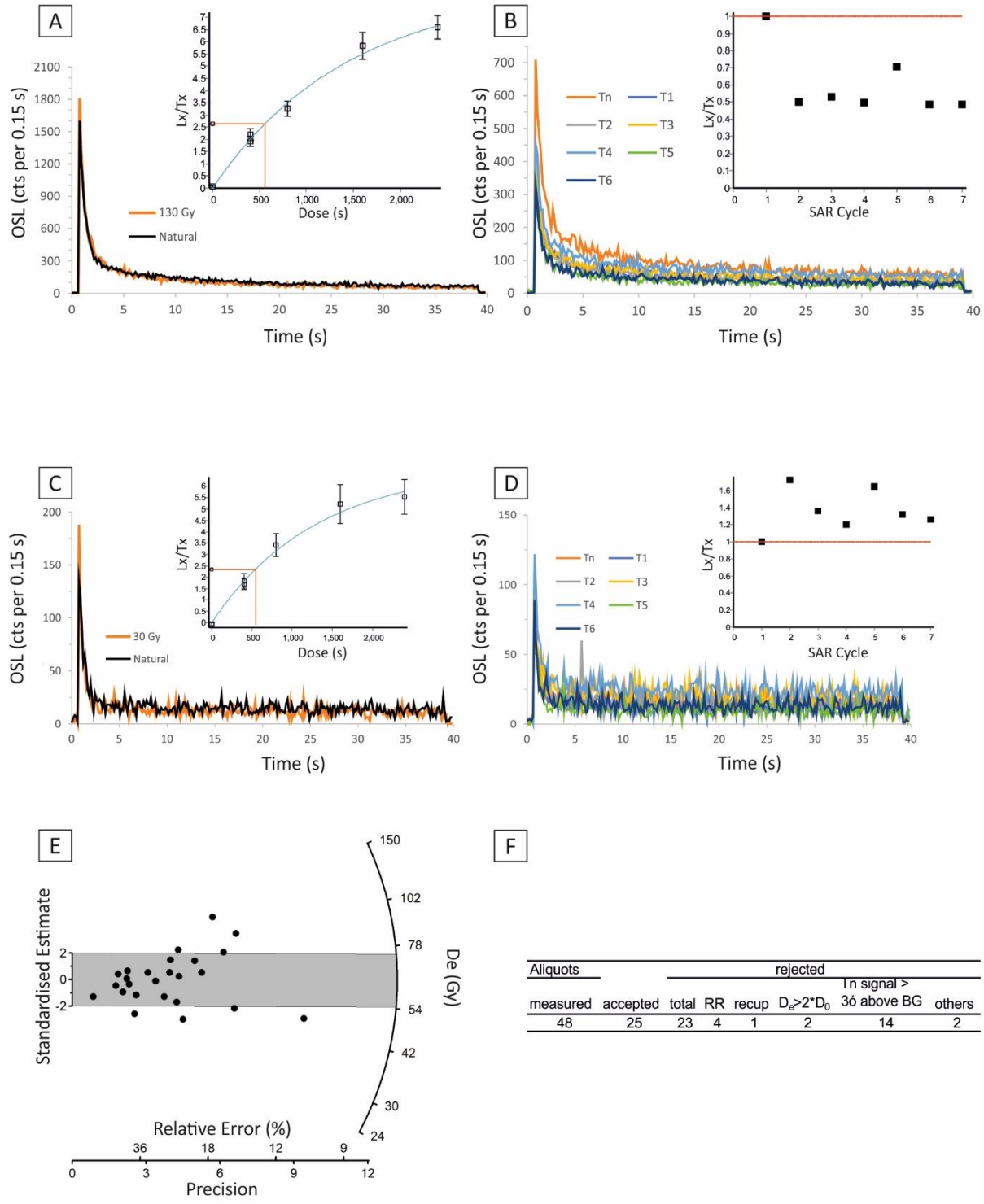

Aliquots		rejected					
measured	accepted	total	RR	recup	D_e>2*D_0	Tn signal > 3ó above BG	others
48	25	23	4	1	2	14	2

OSL dating results of sample OSL-LOIS-8. **A:** OSL decay curves and SAR dose response curves of a typical bright aliquot. **B:** Decay curves of the test doses with Tx/Tn ratios of the same bright aliquot. **C:** OSL decay curves and SAR dose response curves of a typical dim aliquot. **D:** Decay curves of the test doses with Tx/Tn ratios of the same dim aliquot. **E:** Single aliquot De distribution. **F:** Table with the number of accepted and rejected aliquots for the sample. RR = recycling ratio, recup = recuperation. For rejection criteria see main document chapter 3.4.

OSL-LOIS-9

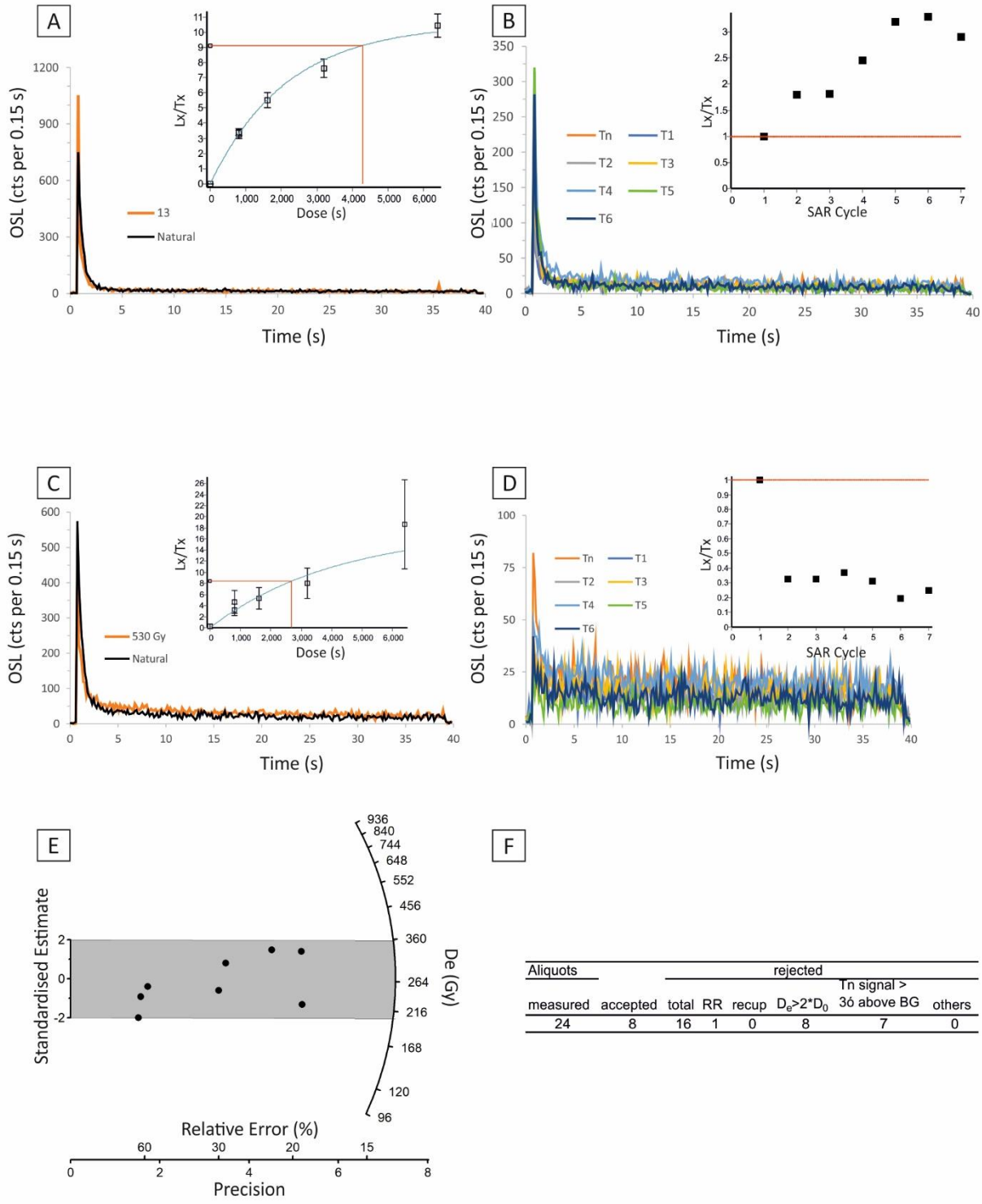

Aliquots		rejected					
measured	accepted	total	RR	recup	D_e>2*D_0	Tn signal > 3ó above BG	others
24	8	16	1	0	8	7	0

OSL dating results of sample OSL-LOIS-9. **A:** OSL decay curves and SAR dose response curves of a typical bright aliquot. **B:** Decay curves of the test doses with Tx/Tn ratios of the same bright aliquot. **C:** OSL decay curves and SAR dose response curves of a typical dim aliquot. **D:** Decay curves of the test doses with Tx/Tn ratios of the same dim aliquot. **E:** Single aliquot De distribution. **F:** Table with the number of accepted and rejected aliquots for the sample. RR = recycling ratio, recup = recuperation. For rejection criteria see main document chapter 3.4.